THE UNIVERSITY OF HULL

Energy Maximization of Control for a Point Absorber Wave Energy Converter

being a thesis submmited for the degree of Doctor of Philosophy
in the University of Hull

by

Doudou Li

MSc in Electronics and Communication Engineering (SMU, China)

BEng in Electronic and Information Engineering (SAU, China)

May 2024

Acknowledgements

First of all, I should give the deepest thanks to my supervisor Prof. Ron J. Patton for guiding me to walk through my PhD journey. He is a wise man with all kinds of inspiring ideas and he has his special academic perspective based on his long life research experience. Though he is full of humor in his daily life, he has an extremely rigorous and serious attitude towards academic research and various matters. I am impressed a lot by his rigorous critical thinking, deep insight and broad knowledge. In addition, I am appreciative of Prof. Ron for his numerous patient discussions.

I would show thanks to my second supervisor Prof. Jim Gilbert for giving me some ideas on improving my research work during the progress meeting. I would also like to say thanks to Prof. Bingyong Guo from Northwestern Polytechnical University and Dr. Shuoshi from Shangdong Electric Power Research Institute for their helpful discussions and suggestions. I am also thankful the colleagues including Dr. Mustafa Abdelrahman, and Yongjie Zhao in the Hull University.

Finally, best wishes and special gratitude to my beloved parents, who always love me and encourage me to keep on going forward.

Abstract

To date, one of the main challenges and requirements in wave energy technologies is to design energy-maximising control for a wave energy converter (WEC) device to achieve the energy maximization production, so as to reduce the levelized cost of energy (LCoE). Hence, this study starts from the numerical modelling of a 1:20 scaled Wavestar-prototype device based on the open source WEC-SIMulator (WEC-Sim) benchmark, which is developed by the National Renewable Energy Laboratory (NREL) and Sandia National Laboratories (Sandia).

Next, a hierarchical tracking structure is selected as the core idea of this study and it contains two different parts. The first high-level part includes the wave excitation moment (WEM) estimation and the determination of the optimal reference signal. Four simple but effective robust methods are considered to design WEM estimators using some practical ways with low computation complexity, such as (i) Unknown Input Observer (UIO) with linear matrix inequality (LMI), (ii) Luenberger observer (LO) with LMI, (iii) LO with pole-placement, and (iv) Adaptive sliding mode observer (ASMO). On the other hand, the Extended Kalman Filter (EKF) can perform well in estimating the instantaneous amplitude and frequency of WEM for optimal reference calculation.

The second low-level part is to design energy-maximising controller. For example, a mixed LQR/H_∞ control and sliding mode control (SMC) based on model-following tracking strategy (continuous-time modelling), model-predictive control (MPC) velocity tracking with Gaussian Process (GP) models (discrete-time modelling) are proposed, respectively. The designed tracking system can provide a near-resonance operation for the PAWEC device to achieve maximizing energy capture. Finally, a comparison study is done between the MPC and robust control methods in order to give some discussions and analysis about the robustness and optimality of the PAWEC control system with and without added matched disturbance tests, in terms of absorbed energy, extracted energy, extracted power and power take-off (PTO) moment, etc.

The simulation results show that ASMO gives best performance demonstrating low estimation delay, owing to fast sliding mode response property. ASMO has strong robustness and best all-round performance. LO-PP method has the simplest structure and is very attractive in real applications. The mixed LQR/H_∞ control and SMC methods can provide strong robustness for PAWEC system. But the main problem of robust Model-Following is large negative power in energy conversion. The approach of MPC tracking is one of the best methods in this PhD study. It can provide PAWEC system with good robustness and solve control input constraint properly.

The proposed novel tracking control methods (a) a robust Model-Following or (b) a robust MPC framework can help PAWEC system to achieve robustness enhancement and maintain maximized energy conversion efficiency with modelling uncertainty considered as a matched disturbance.

Table of Contents

List of Figures

List of Tables

List of Abbreviations and Symbols

Abbreviations

AE	Average Error
ASMO	Adaptive Sliding Mode Observer
AR	Autoregressive
BAC	Bayesian Actor-Critic
BEM	Boundary Element Method
BS	Bretschneider Sprectrum
CCC	Complex Conjugate Control
CFD	Computational Fluid Dynamics
CoB	Centre of buoyancy
CoE	Cost of Energy
CoG	Centre of gravity
DRL	Deep Reinforcement Learning
DOF	Degree of Freedom
DP	Dynamic Programming
DQN	Deep Q-Network
EKF	Extended Kalman Filter
GP	Gaussian Processing
GPML	Gaussian Process for Machine Learning
HHT	Hilbert-Huang Transform
HAWT	Half-Range Chebyshev Fourier
IRF	Impulse Response Function
KF	Kalman Filter
LCoE	Levelized Cost of Energy

LMI	Linear Matrix Inequality
LQG	Linear Quadratic Gaussian
LQR	Linear Quadratic Regulator
LMI	Linear Matrix Inequality
LO	Luenberger Observer
LTI	Linear Time-Invariant
MPC	Model Predictive Control
MHE	Moving Horizon Estimation
NREL	National Renewable Energy Laboratory
NRMSA	Normalized Root-Mean-Square Accuracy
NMPC	Nonlinear Model Predictive Control
OWC	Oscillating Water Column
OWS	Oscillating Wave Surge
O&M	Operation and Maintenance
PP	Pole Placement
PTO	Power Take-Off
PAWEC	point absorber wave energy converter
PAPR	Peak-to-Average Power Ratio
PM	Pierson-Moskowitz
QP	Quadratic Programming
RL	Reinforcement Learning
SM	Spectral Mixture
SMO	Sliding Mode Observer
SMC	Sliding Mode Control
SWL	Still Water Line
TEO	Teager Energy Operator
WEF	Wave Excitation Force
WEM	Wave Excitation Moment
UIO	Unkown Input Observer
WEC	Wave Energy Converter
WEC-Sim	Wave Energy Converter SIMulator
WECCCOMP	WEC control competition

Symbols

$exp(X)$	The natural exponential function of X
$\|X\|$	The Euclidean 2-norm of X
$\|X\|_\infty$	The Euclidean ∞-norm of X
$\|X\|$	The Modulo operation of X
$\mathfrak{Re}(X)$	The real operation of a complex signal X
I_p	An $p \times p$ identity matrix
Re^m	A vector with m-dimensional
$Re^{m \times n}$	A matrix of dimension $m \times n$
$\mathbb{R}$	Set of real numbers
$\mathbb{R}^m$	An m-dimensional real matrix
$\mathcal{L}_2[0, \infty)$	2-norm space
X^T	Transpose of matrix X
X^{-1}	Inverse of matrix X
$He(X)$	$He(X) = X + X^T$
$X^\dagger$	pseudo inverse of matrix X
$sign(X)$	Signum function of X.

List of Publications

1. **Li, D.**, Patton, R. J. Model Following Robust Control of a Wavestar-prototype Wave Energy Converter: Part 1 Control, *IFAC World Congress 2023*, 2023, 56(2): 10892-10897. (Chapter 5)

2. **Li, D.**, Patton, R. J. Model Following Robust Control of a Wavestar-prototype Wave Energy Converter: Part 2 Estimation and Optimal Reference Computation, *IFAC World Congress 2023*, 2023, 56(2): 11729-11734. (Chapter 4)

3. **Li, D.**, Patton, R. J. Model Predictive Energy-Maximising Tracking Control for a Wavestar-Prototype Wave Energy Converter, *Journal of Marine Science and Engineering*, 11(7): 1289, 2023. (Chapter 6)

Chapter 1

Introduction

1.1   Wave energy

Since the industry revolution, energy as a resoure has played a crucial role in the social and economic development of human society (Penalba, 2018) and the demand of carbon neutrality through reduction of fossil fuels and increase in use of renewable energy, keeps rising year by year. On the whole, the energy supply systems still mainly revolve around the fossil fuels (coal, oil, gas and their derivatives). Furthermore, the distribution of global energy resources (Prasad et al., 2022) used for electricity generation in 2019 as shown in Figure 1.1.
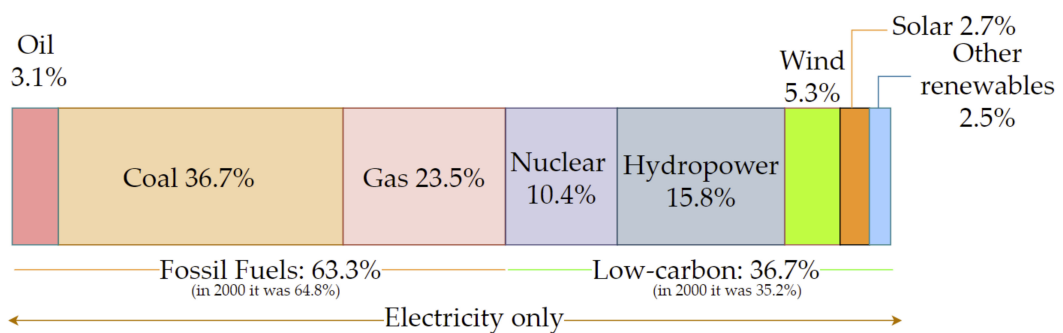
Figure 1.1: the percentage distribution of global energy resources used for electricity generation in 2019 (Prasad et al., 2022).

However, fossil energy sources have caused adverse problems manifested particularly as different aspects of climate change (Siegel, 2019). Examples are: global temperature increase, sea level rise, intensifying droughts and tropical storms, etc. Furthermore, for several decades governments and scientists realized that there is a crisis of fossil fuel

depletion (Abas et al., 2015) and the disadvantages of using traditional fossil fuels. Hence, the concept of exploring sustainable and renewable energy has been enhanced.

In the Global Energy Outlook report, renewable energy is considered to be the dominant source of main energy consumption by 2040 (Newell et al., 2019), particularly in electricity generation. At present, the main renewable energy sources (Ellabban et al., 2014) include bioenergy, geothermal energy, wind energy, solar energy, marine energy (tidal or wave energy), hydro energy, etc. One of the primary renewable sources is the unexploited wave energy, which shows great potential to fulfill the growing electricity demand worldwide.

Several studies have tried to estimate that the exploitable wave energy source is around $29500\,TWh/year$ (IRENA, 2020; Gunn and Stock-Williams, 2012; Reguero et al., 2015), which can cover global electricity consumption about $22300\,TWh$ (IEA, 2020) estimated in 2018. Compared with the wind and solar energy sources, wave energy has some prominent advantages, such as higher energy density ($2\,$-$\,3\,\dfrac{kW}{m^2}$) with respect to wind energy ($0.4\,$-$\,0.6\,\dfrac{kW}{m^2}$) and solar energy ($0.1\,$-$\,0.2\,\dfrac{kW}{m^2}$) (Pozzi et al., 2018), high availability for stable and continuous power production which is not limited by the daytime hours or no windy weather (López et al., 2013). Huge reserves and the availability of wave energy are distributed worldwide with higher energy densities at higher latitudes as illustrated in Figure 1.2.
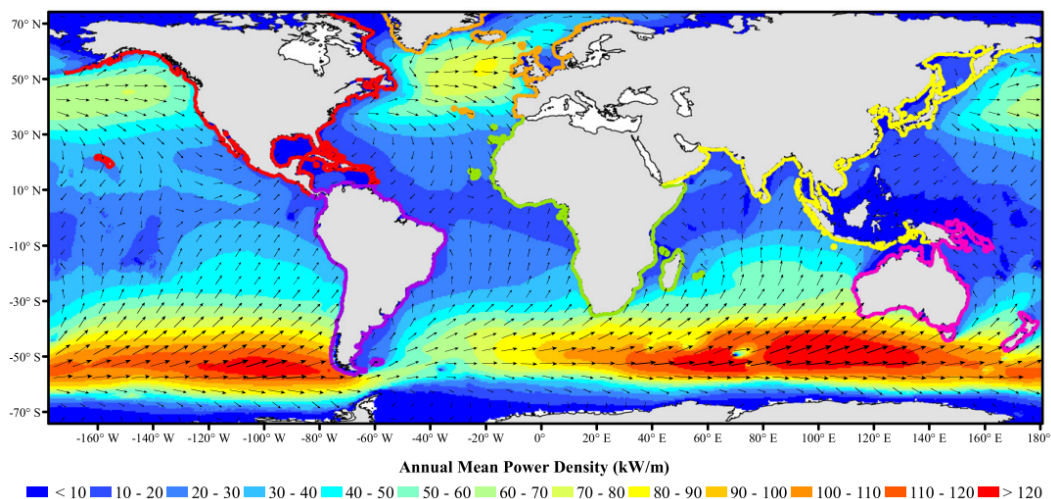
Figure 1.2: The global power density distribution of wave energy (Gunn and Stock-Williams, 2012).

Regarding the wave energy technology itself, the first idea of harvesting the energy

from the ocean waves dates back to a wave power patent (Ross, 1995) in 1799. But the initial utilization of the modern wave energy converter (WEC) was developed in Japan in 1940s. It is the first concept of floating oscillating water column (OWC) (Titah-Benbouzid and Benbouzid, 2015), which contains a navigation bouy equipped with an air turbine that can be powered by the ocean waves. From the very early work, a large number of WEC concepts have been proposed and frequently updated. WEC technology reached application developments during the 1990s (Babarit, 2017).
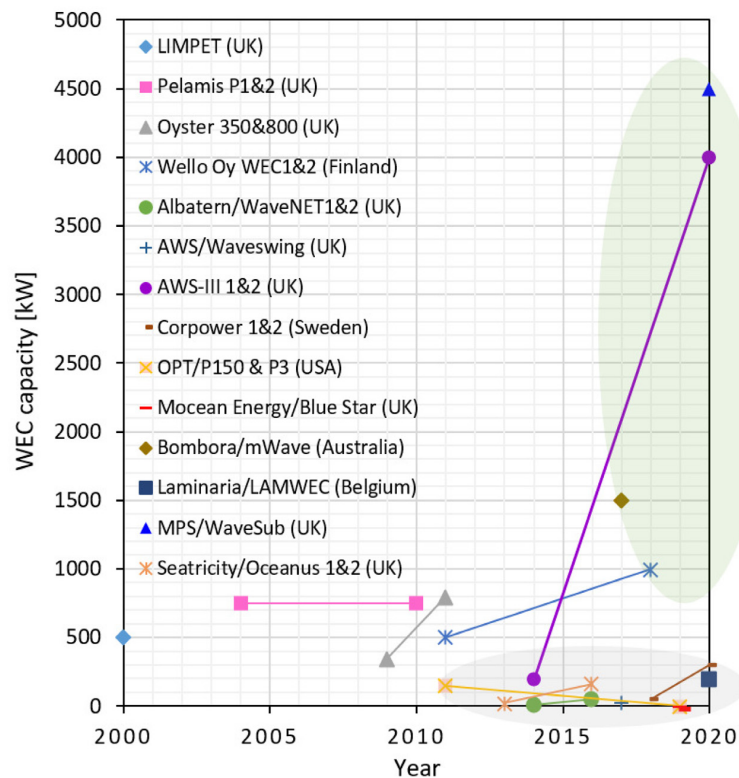
Figure 1.3: The capacity evolution of the WECs in the UK (Jin and Greaves, 2021).

In recent years various types of WEC devices have been evaluated, based on several subsystems and components. There is a substantial amount of development and testing by industry together with academic institutions (López et al., 2013; Prasad et al., 2022). Investigative wave tank tests follow design studies, including Power Take-Off (PTO) systems (Davidson et al., 2015; Martin et al., 2020; Bacelli et al., 2019) and tests in open sea were carried out by (Sheng et al., 2017; Kofoed et al., 2006; Li et al., 2022). There are also several WEC prize competitions (Scharmen, 2016; Dallman et al., 2018; Driscoll et al., 2018) in the literature. In view of summarising the WEC development in the UK, (Jin and Greaves, 2021) discussed the capacity of WECs that have been installed and developed in the UK, as shown in Figure 1.3.

1.2 WEC System Challenges

Despite the fact that many technically sound WEC applications have been developed, none of these has reached full economical and commercial development (Penalba, 2018). This is due to the fact that WEC devices have high Levelized Cost of Energy (LCoE) (Chang et al., 2018). It is estimated that the Cost of Energy from the offshore ocean wave is approximatly 5 times more than the other conventional energy resources (Guo, 2017). WEC technologies still lack development in terms of energy efficiency and significant improvements in driving down the LCoE. Furthermore, the development of full economic cost modelling has been slow. Some specific or salient challenges faced by WEC system developments are as follows:

- **Reduction of Construction, Deployment and Maintenance Cost:** It is inevitable that the construction expenditure of a full-scale prototype WEC or an array of such devices is usually high due to the fundamentally large mechanical, electrical components, mooring systems and long length scale cables to connect with the grid, etc. In addition, the investigation and analysis have to be done on how to deploy the WEC devices/array efficiently in a suitable place (Mwasilu and Jung, 2019). For a long time reliable working of WECs, the operation and maintenance (O&M) cost will naturally be higher as well. It is interesting to note that in most cases WEC systems continue to be designed and implemented without considering O&M issues at the design stage. There is clearly a need for "co-design" to consider these important issues.

- **Modelling of wave-WEC interaction:** Normally, Computational Fluid Dynamics (CFD) packages are used to build the fully non-linear modelling for the WEC applications in order to provide a suitable understanding of the precise hydrodynamics (Guo, 2017) for cases involving significant non-linear phenomerna in terms of wave and WEC interactions. For example dynamic issues involving viscosity and compressibility. However, it is pity that CFD modelling methods are computationally expensive and CFD results are not intuitive, which is not proper for a WEC control system design with the requirement of fast real-time response. On the other hand, linear modelling is based on linear wave theory which has strong assumptions, such as the ideal and small wave height by ignoring high oscillation motions of the WEC device, linearised hydrodynamic forces without the non-linear effects. Hence, the linear modelling is usually chosen by

many researchers as a control model to do control works for their selected WEC systems. But it is inevitable that the model errors between the plant dynamics and control model will cause the reduction of energy conversion efficiency.

- **Improvement of Energy Conversion Efficiency:** Real WEC systems involve considerable system modelling uncertainty and should account for external disturbance effects and faults. The modelling must also face the challenges arising from complex random wave characteristics, e.g. in terms of amplitude, phase, frequency and even wave direction. All these characteristics affect the efficiency of energy absorption from incident sea waves. Hence, to achieve power maximisation for a WEC system, a suitable control design method should be considered (Abdelrahman, 2019) to generate as much electricity as possible from incoming ocean waves. The control system should also be selected to minimise the effect of the WEC device and hydrodynamic parameters. This an important application of robust control to make sure that the best energy can be achieved over a defined range of parameter changes (Abdelrahman, 2019). Besides, the generated negative power should be diminished during the energy conversion procedure. Otherwise, the bi-directional power flow problem (Guo, 2017) will increase the burden of the PTO system and cause large energy loss. Therefore, the proper PTO system should be selected to provide a good electromechanical conversion efficiency and then reduce the cost of energy (CoE) (Penalba, 2018). If necessary, the novel PTO mechanisms should be developed for satisfying the requirement of the wave energy conversion.

- **Elevation of Survivability:** The WEC devices must be reliable and able to survive changing or extreme environmental conditions (Guo, 2017). For example, operating in rough sea surfaces, huge waves and stormy weather. The survivability strategy (Peña-Sanchez, 2020) has to be considered during the WEC design and installation procedures using co-design to minimise structural damage and for the purpose of life-time CoE reduction. Furthermore, the fault-tolerant strategy has potential to improve the reliability of the WEC system when the sensor or other component faults are arised in the WEC systems.

1.3   Research Aim and Objectives

Aalborg University built a 1:20 scaled point absorber wave energy converter (PAWEC) device in their wave tank (Zurkinden et al., 2014) (See Figure 1.4). This well-known prototype WEC device is taken from the Wavestar system concept of an array of such devices, sometimes referred to as a Wavestar-like device.

Figure 1.4: The 1:20 scaled Wavestar-like device (Zurkinden et al., 2014) built in Aalborg University.

Some researchers focus on this special PAWEC doing their research on modelling and control works (Zurkinden et al., 2014; Windt et al., 2020; Nguyen et al., 2016; Ringwood et al., 2023a; Guerrero-Fernandez et al., 2023). This thesis study also chooses the above 1:20 scaled Wavestar-like device as the research target and to do energy-maximising control design work.

1.3.1   Research Aim

The Aim of this PhD research work is to design advanced control robustness strategies for point absorber type WEC systems to achieve maximum energy generation. The study uses as a basis the Wavestar-prototype benchmark model contributed by National Renewable Energy Laboratory (NREL).

Note: a hierarchical tracking structure was first proposed by (Fusco and Ringwood, 2014a) and it is selected as the main scheme for this PhD study design as shown in Figure 1.5. The reference velocity signal is constructed based on a near-resonance

condition that can bring the WEC system into energy maximization operation when the tracking system is achieved. The near-resonance operation keeps the WEC float velocity share same phase with wave excitation force/moment. As for the numerical modelling, a 1:20 scaled Wavestar-prototype device is built in the famous open source WEC-Sim benchmark (Tom et al., 2018). The WEC-Sim software gives users some freedom to test their designed controllers.
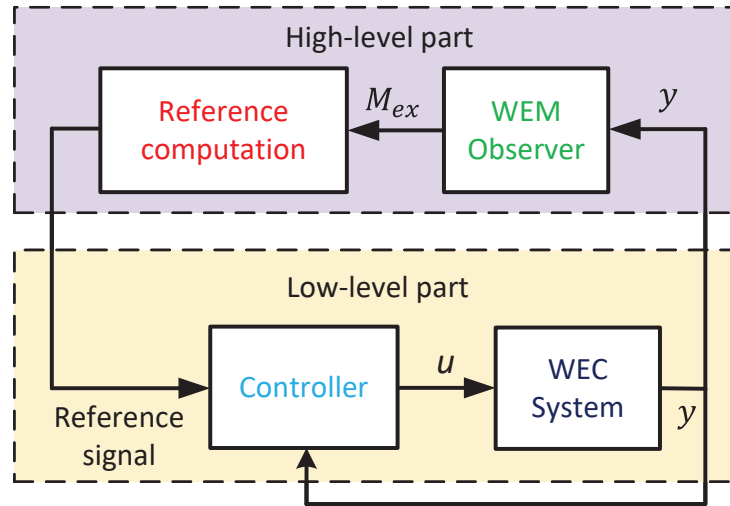
Figure 1.5: Selected hierarchical tracking structure for the whole WEC control system.

Where y is the WEC system output in Figure 1.5, which represents the position and velocity of the float, denoted θ and $\dot{\theta}$ in later chapters. u is the calculated power take-off (PTO) moment as the control input to the WEC system, denoted M_{PTO} in later Chapters. M_{ex} is the wave excitation moment (WEM).

- **High-level part:** To implement decision-making such as the reference generation, which includes wave excitation moment (WEM) estimation and optimal reference velocity computation.

- **Low-level part:** The controller directly drives the hardware of the WEC system.

The terms "high" and "low" are relative.

1.3.2 Research Objectives

1. Practical ways to design observers for wave excitation moment estimation.

2. Model-following robust strategy, based on a near-resonance condition for maximization of energy extraction.

3. Model-predictive velocity tracking control based on Gaussian Process model.

4. A comparison study between model predictive control (MPC) and robust control methods for energy maximization analysis.

1.4 Research Contributions and Thesis Structure

The main contributions in this thesis are listed below:

- **The practical ways for WEM estimators:** The WEM estimator should not only have low computation complexity for real-time requirement but should better be designed in a robust way for providing good estimation performance. The Unknown Input Observer (UIO) and Luenberger Observer (LO) based on Linear Matrix Inequality (LMI) methods (Zhu and Li, 2021b; Du et al., 2015) are restricted by the need for feasibility in the LMI design. This means that the estimation performance of both LMI methods is not that attractive but limited. Hence, in this study the LO is considered along with pole-placement, following (Laub and Wette, 1984) and also the Adaptive Sliding Mode Observer (AMSO) (Lan et al., 2017a). Both of these methods are chosen as they are considered to satisfy effcient and robust estimation performance. The LO with pole-placement is the simplest and most effective estimator (Li and Patton, 2023c). ASMO is a nonlinear estimation method that has a built in strategy for robustness. This approach has shown the best estimation performance. In this study the ASMO has provided a new vision for future nonlinear estimator design when considering a complex WEC system operating in a more uncertain, dynamical environment.

- **Model-following robust control methods:** Overall, the application of WEC control contains unmodeled uncertainties and nonlinear effects (Fusco and Ringwood, 2014a). Hence, a robust control method is important for minimizing or compensating the effects of uncertainty whilst, at the same time enhancing the energy capture from the ocean waves. Furthermore, a hierarchical tracking structure can provide design freedom to achieve the required WEC system energy

maximization. The model-following strategy (Spurgeon et al., 1996) is considered with the previous tracking structure, which forces the WEC system to follow a reference model to do tracking work that can reach a near-resonance operation (Li and Patton, 2023b). The near-resonance condition means that the WEC float velocity is in-phase with the WEM. The proposed both mixed LQR/H_∞ control and Sliding Mode Control (SMC) are able to show strong robustness against the so-called matched disturbance. The concept of the matched disturbance is explained in Chapter 5.

- **Model-predictive velocity tracking control:** Typically, MPC is a very popular method for the design of WEC systems, especially as an optimal energy maximizing solution can be considered, along with constraint-handling (Faedo et al., 2017). A new form of Model-predictive tracking control (Li and Patton, 2023a) is designed on the basis of the hierarchical tracking structure scheme and basic MPC idea. The energy maximization can be achieved when the WEC system can track the optimal reference velocity. In addition to tracking control this approach includes the important feature of constraint handling. This MPC reference velocity tracking strategy uses two Gaussian Processing (GP) Machine Learning models to provide the short-term forecasting work (Shi et al., 2018).

- **Comparisons study between robust control and MPC methods:** Usually, optimality and robustness are two important requirements of a WEC device to extract more energy from waves. However, the available WEC discussions appear to divide these issues into separate control methods of, on the one hand MPC (Li and Belmont, 2014; Faedo et al., 2017) and on the other hand robust control (Zou et al., 2023; Lao and Scruggs, 2020). Many researchers want to test the use of MPC even without constraint handling. Others, focus only robust WEC control design, without any consideration of the potential advantages of using MPC. This gap in understanding can mean that it is not straightforward to compare robust control and MPC methods for WEC, i.e. to determine suitable criteria for comparison. In order to overcome this, model-following WEC robust control strategy (Li and Patton, 2023b) is validated in Chapter 5. The MPC tracking strategy (Li and Patton, 2023a) is presented in Chapter 6. Thereby, a comparison study between MPC and robust control strategies is described in Chapter 7. This discussion sheds a new light on the use of these methods in WEC control.

Chapters 4, 5, 6 & 7 contain original work. The LO with pole-placement method and ASMO are investigated and tested for WEM estimation in Chapter 4. Next, the mixed LQR/H_∞ and sliding mode, model-following robust control strategies are proposed and compared in Chapter 5. Later, the model-predictive velocity tracking control based on GP model is designed in Chapter 6. Finally, to check robustness and optimility the proposed three control methods on the 1:20 scaled Wavestar-prototype WEC system, the comparison study between the MPC and robust control is given in Chapter 7.

The structure of the thesis is illustrated in Figure 1.6.
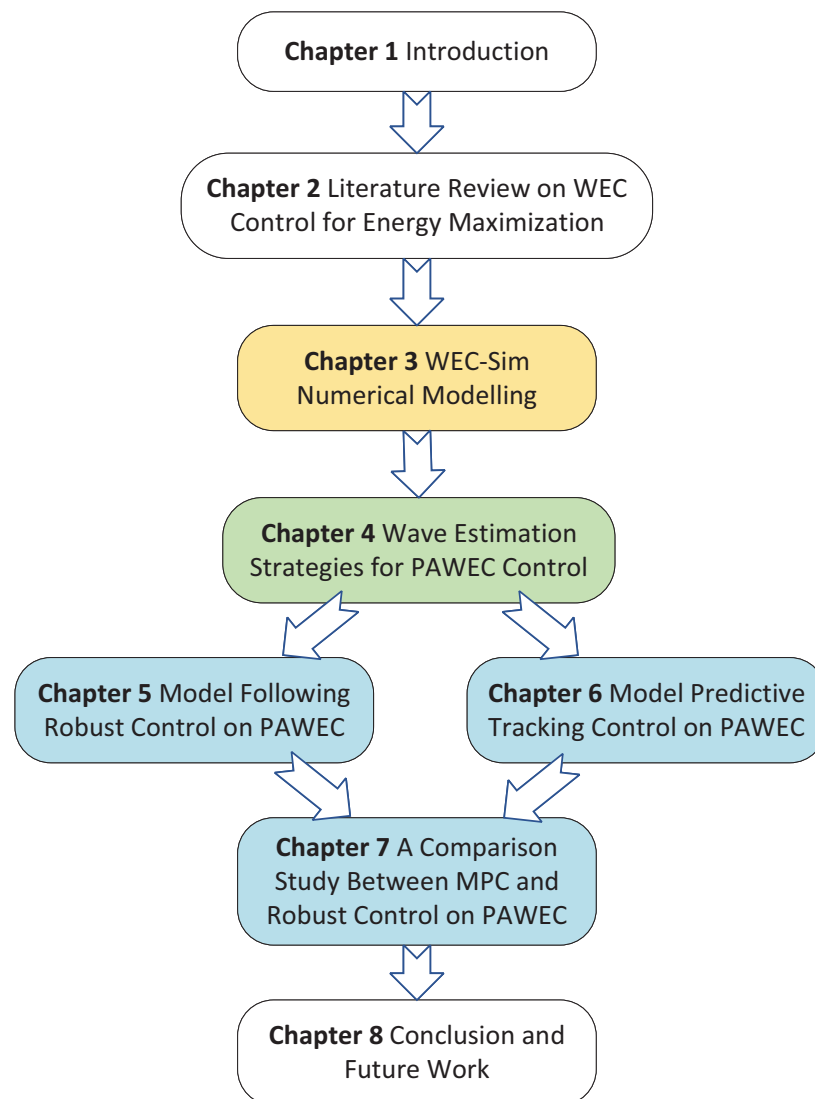
Figure 1.6: Thesis structure.

Chapter 1 concentrates on introducing the global trend of wave energy utilisation and some current related challenges, and then discusses the research Aim and Objectives

and outlines the Structural Arrangement of the thesis.

Chapter 2 is a brief literature review on WEC control is illustrated around four different parts as follows:

- Review of Wave Energy Converter Classification.

- Wave Excitation Force Estimation and Forecasting Methods.

- Classical Control Strategies.

- Modern Control Strategies.

Chapter 3 gives an overview of WEC-Sim software to introduce the WEC-Sim code structure, the building and running steps of a WEC-Sim simulation, the wave generation including regular and irregular waves, numerical modelling analysis through sinusoidal steady-state response or Convolution Integral formulation. And then a description of a numerical model is given for a 1:20 scaled Wavestar-prototype device in the WEC-Sim benckmark, which is used in a famous WEC control competition (WEC-CCOMP). Finally, some basic tests are conducted to check the numerical modelling.

Chapter 4 commences with the design of the first part of tracking structure for the focused Wavestar-like device, in view of the hierarchical tracking control structure for energy-maximising design is the main idea of the whole thesis. Based on continuous-time modelling, some practical ways are considered to do the WEM estimation work following a feasible scheme for real application requirement, such as the UIO with LMI, LO with LMI, LO with pole-placement and ASMO. On the other hand, the determination of the optimal reference signal is based on discrete-time modelling using an Extended Kalman Filter (EKF) that provides the instantaneous amplitude and frequency of WEM. The further designed low-level controllers in Chapter 5 and 6 will force the WEC system to perform suitable tracking to achieve energy maximising generation.

Chapter 5 turns attention to the design of the second part of the hierarchical tracking structure, and the low-level robust controller is based on the model-following strategy to force the WEC system to follow a reference model, which consists of reference position and velocity signals. A mixed LQR/H_∞ control and SMC robust methods are proposed based on continuous-time modelling in this Chapter, respectively, aiming to

enhance the WEC system robustness and the tracking way can bring the WEC system into a near-resonance operation to maximize energy absorption from irregular waves.

Chapter 6 continues to concentrate on designing of the energy-maximizing controller as the low-level part of the hierarchical tracking structure for the 1:20 scaled Wavestar-prototype device. On the basis of the hierarchical tracking structure scheme and basic MPC idea, a model-predictive velocity tracking control with GP model is designed based on discrete-time modelling in this Chapter. where two GP models are used to predict the future sequences of WEM and reference velocity which are needed in MPC objective function.

Chapter 7 performs a comparison study between the MPC and robust control approaches in order to give some discussions about the characterstic of these methods on energy maximization and do robustness analysis for the scaled Wavestar-like device modeled in WEC-Sim. Firstly, The frequently used MPC design is derived by choosing the average absorbed mechanical power as its objective function to solve an optimization problem for maximisation of energy capture, but it is not based on a tracking control way. Then, the popular MPC is selected to as a comparison with the model-following mixed LQR/H_∞ control, SMC presented in Chapter 5 and model-predictive velocity tracking control proposed in Chapter 6. The simulation results are based on absorbed energy, extracted energy, extracted power, PTO moment, and disturbance testing.

Chapter 8 gives a Concluding Discussion concerning the whole thesis work and comments about the PhD contributions. Suggestions are also made for pursuing future work at available opportunities. Future research is expected to investigate some more advanced control methods to further improve the robustness and optimality of the WEC system for extracting maximum energy.

Chapter 2

Literature Review on WEC Control for Energy Maximization

2.1 Introduction

In this Chapter, Section 2.2 starts to give a brief review of three different ways of the WEC classification including giving some examples of the main and well-known WEC applications, which can be found in the literature. Next, in view that the energy-maximising or optimal control needs the current and future knowledge of the wave excitation force (WEF). Section 2.3 describes the idea of WEF estimation and forecasting works, which should be done before the WEC systems control work design. Then, Section 2.4 lists some classical control approches that are used for the power maximisation purpose in the wave energy community. Furthermore, the mordern and advanced control methods are divided into model-based and model-free types and discussed separately in the Section 2.5. Finally, Section 2.6 is the Summary of this Chapter.

2.2 Review of Wave Energy Converter Classification

Several review papers discuss the classifications of WEC devices according to criteria defined in (Maria-Arenas et al., 2019). These include (a) location along the coast-line, (b) WEC orientation and dimension with respect to wave direction, and (c) working principles.

2.2.1 Deployment locations

WEC systems can be classified simply into three main types: onshore, nearshore and offshore (Farrok et al., 2020), based on relative distance between devices and their position in the sea (Figure 2.1).
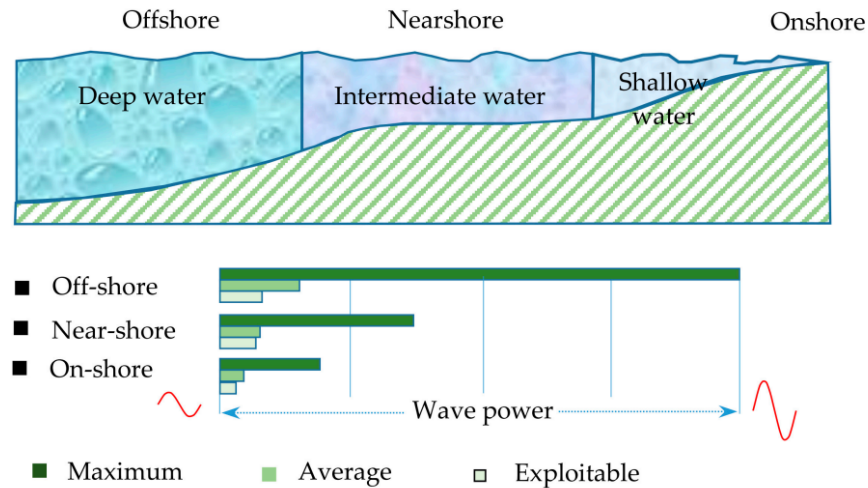
Figure 2.1: The classification by their deployment locations (Farrok et al., 2020).

- **Onshore devices:** The WECs are deployed onshore or installed above the sea in the shallow water regions with depth about 10-15m and the wave height can reach up to maximum 7.8m (Farrok et al., 2020). Onshore installation brings some advantages such as low maintenance cost and no requirement for mooring systems or long cable lengths (López et al., 2013) for transmitting the generated electricity to the grid. However, the shoreline waves contain less energy and there are limited sites (Czech and Bauer, 2012) that can install WEC devices.

- **Nearshore devices:** The WEC devices rest on the sea bed in the intermediate area for water depths of 15-25m (Farrok et al., 2020). In this case, the mooring systems are still not required. But the devices have to overcome the stress caused from the passing waves.

- **Offshore devices:** Floating or submerged structure WECs are set up in the deep water region and moored to the sea floor, for depths greater than 50m with a wave height reaching up to 30m (Farrok et al., 2020). The offshore open sea has vast wave power potential. However, WECs usually suffer from the large loads that will cause the reliability and survivability problems (López et al., 2013).

Moveover, the long length cables have to be considered and used to transmit the power to the grid (Czech and Bauer, 2012).

2.2.2   Dimension and orientation with respect to the waves

The second classification is based on the WECs dimension and orientation with respect to the incoming waves (Maria-Arenas et al., 2019). The WEC devices can be distinguished into three categories: point absorbers, attenuators, and terminators, as given in Figure 2.2.
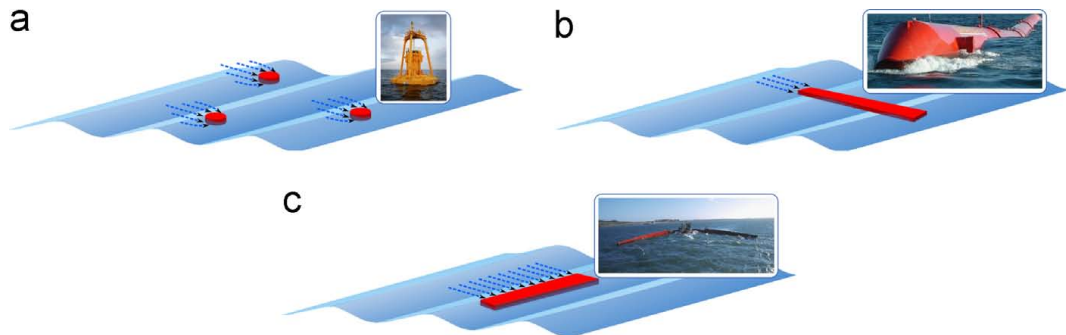
Figure 2.2: The classification by their dimension and orientation (López et al., 2013), including (a) point absorber (PowerBouy OPT), (B) attenuator (Pelamis), (c) terminator (Wave Dragon).

- **Point absorber:** It has small dimensions with respect to the wave length and the axisymmetric geometry is able to harvest energy from waves in any directions. The well known PowerBouy OPT (Artal-Sevil et al., 2018) is standard floating PAWEC, see Figure 2.3 (a), developed in the USA. The bouy can oscillate with the incident waves and the relative heave motion between the bouy and spar foundation will drive the generator to produce large amounts of energy.

  Another notable PAWEC is the Wavestar concept (Kramer et al., 2011) as a multiple structure device, as shown in Figure 2.3 (b), which is one of the leading WEC technologies, developed in Aalborg. The standard Wavestar was a commercial WEC array comprising two rows of PAWEC devices installed with a structural bridge. The floats of the system were connected with hydraulic PTO systems and were free to move up and down with the incoming ocean waves. The hydraulic fluid will be pumped into a common mainfold system to introduce high pressure flow into the hydraulic motor to drive the electric generator to produce power (Kramer et al., 2011).

(a) (b)
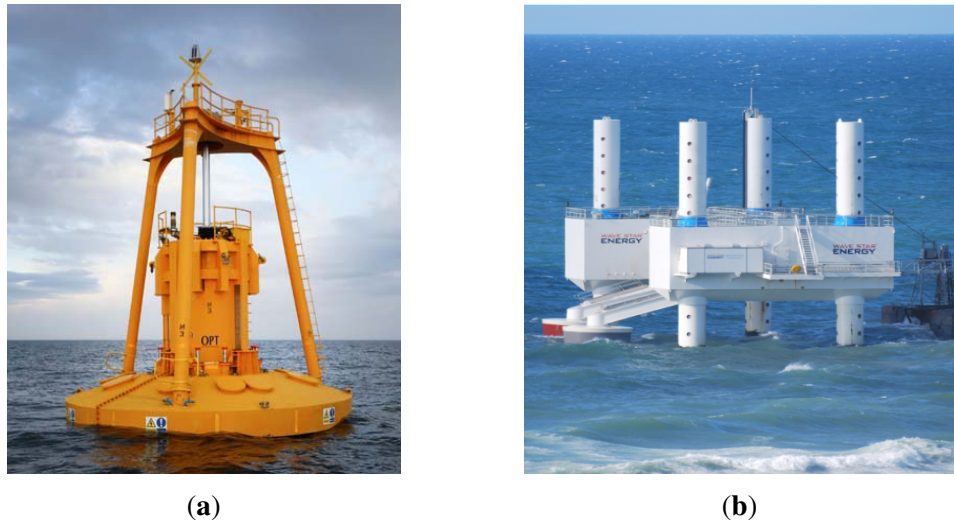
Figure 2.3: Single and array PAWEC schemes, (**a**) PowerBouy OPT WEC (Artal-Sevil et al., 2018), (**b**) Wavestar prototype WEC (Kramer et al., 2011).

(a) (b)
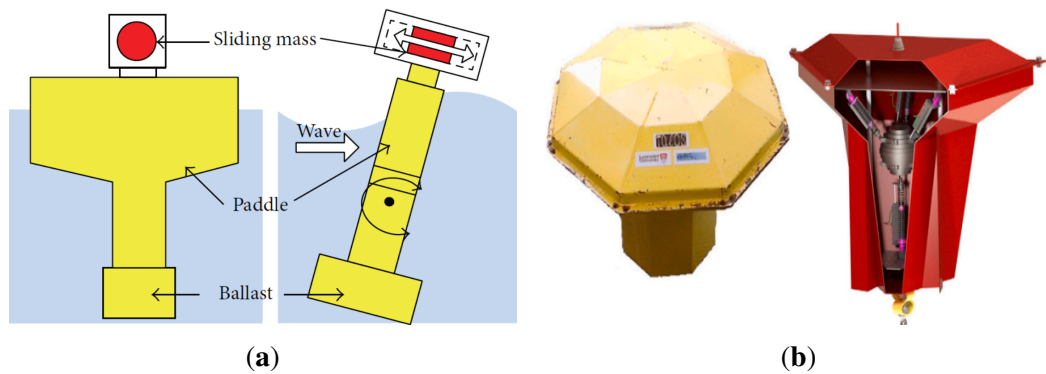
Figure 2.4: The other special designed PAWECs, (**a**) PS frog MK 5 WEC (Taylor et al., 2002; Faizal et al., 2014), (**b**) TALOS WEC (Aggidis and Taylor, 2017).

Apart from those two standard PAWECs, the Lancaster University Renewable Energy Group developed two specially designed PAWECs, such as the PS frog MK 5 and TALOS WECs, as given in the Figure 2.4. Regarding the PS frog MK 5 WEC, (see Figure 2.4 (a)), this is developed and described by (Taylor et al., 2002; McCabe et al., 2006). The device looks like a large buoyant paddle connected a handle with a sliding mass placed in. This PAWEC can react to the oncoming waves by pitching back and forth about its dynamic centroid (McCabe et al., 2006) but only the motion of internal sliding mass drives the hydraulic PTO system to generate power. The sliding mass can be controlled to do dynamic tuning for the WEC system to change its behaviour (Taylor et al., 2002), to maximise the generated power.

As for the TALOS PAWEC device, there is a moving mass (ball) connnected with hydraulic cylinders attached in the solid outer hull as shown in Figure 2.4 (b). The internal mass can move freely in multiple directions when the point abosrber oscillates with the wave motions (Aggidis and Taylor, 2017; Sheng et al., 2022b). The movement drives the hydraulic PTO systems to generate power. The multi-axis PTO structure provides a more efficient energy extraction from the three degrees of freedom motions of the heavy ball (Sheng et al., 2022a).

(**a**) The Pelamis WEC device (Heath et al., 2001).

(**b**) The new development Blue X Mocean WEC device (Mocean, 2023).

Figure 2.5: The standrad representative of attenuator WECs.

- **Attenuator:** A large device with two or more sections/tubes connected together and placed parallel to the expected wave direction. The earliest form of attenuator is the well-known Pelamis system (Westwood, 2004) first designed in the UK, as shown in Figure 2.5 (a). It is made up of several mechanical cylindrical segments that are connected by a few hinged points. The Pelamis floating system is held on a place moored to the seabed (Czech and Bauer, 2012), and it is activated to move vertically and laterally by the incoming waves to generate power and extract energy using hydraulic PTO. More recently, a development of Pelamis with 2 connected segments is being tested off the Aberdeen Coast called Blue X (Figure 2.5 (b)) through Mocean Energy Ltd.

- **Terminator:** Usually a large device with length the same or greater than wavelength and placed perpendicular to the direction of the incident waves. Wave Dragon (Kofoed et al., 2006) is a kind of terminator WEC that contains two reflectors linked with a reservoir, as shown in Figure 2.6, created in Denmark at Aalborg University. Two reflectors are used to focus sea waves towards a ramp and collect water in the reservoir (Kofoed et al., 2006) to drive several hydro turbines for generating electricity.

Figure 2.6: The terminator type Wave Dragon WEC (Kofoed et al., 2006).

2.2.3   WEC Working Principles

Thirdly, based on the working principle (Pozzi et al., 2018), WEC devices can be subdivided into 5 categories as follows:

- Oscillating Water Column (OWC): This type of device has an oscillating air chamber that can compress and decompress the sea water between the water line and a Wells air turbine that connected to a generator, using the changing airflow to produce electrical power. The basic structure of oscillating water column WEC is shown in Figure 2.7.
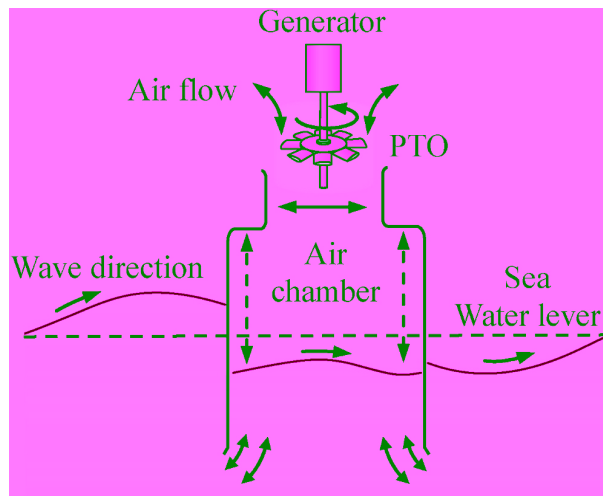
Figure 2.7: The basic structure of oscillating water column WEC (Zhang et al., 2021).

Examples of famous OWC WECs are: Limpet (Heath et al., 2001), Oceanlinx (Delmonte et al., 2014) as shown in Figure 2.8.

(**a**) The Limpet WEC device (Heath et al., 2001).

(**b**) The Oceanlix WEC device (Delmonte et al., 2014).

Figure 2.8: The standrad representative of OWC type WECs.

- Pressure Differential: The devices are fixed and submerged to the seabed and the wave motions can cause a pressure differential above the WEC device when

the sea level starts to rise and fall. The sketch of submerged pressure differential WECs is given in Figure 2.9.
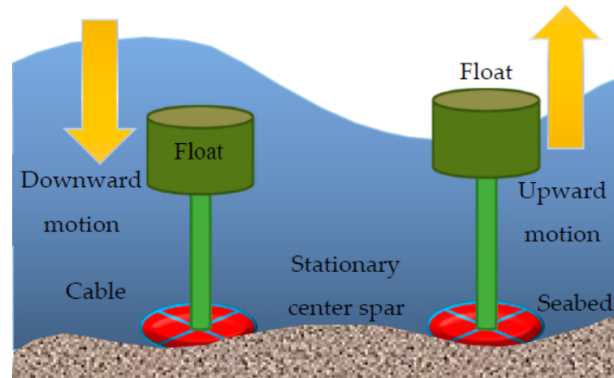
Figure 2.9: The sketch of submerged pressure differential WEC (Farrok et al., 2020).

Representative device examples are: CETO (De Chowdhury et al., 2015) and AWS (Nguyen et al., 2019) devices, see Figure 2.10.

(a)   (b)
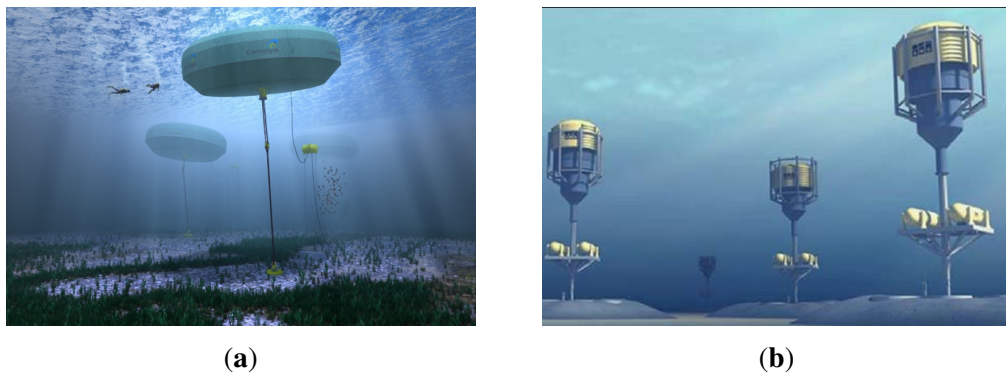
Figure 2.10: Pressure Differential structure WECs, (**a**) CETO WEC (De Chowdhury et al., 2015), (**b**) AWS WEC (Nguyen et al., 2019).
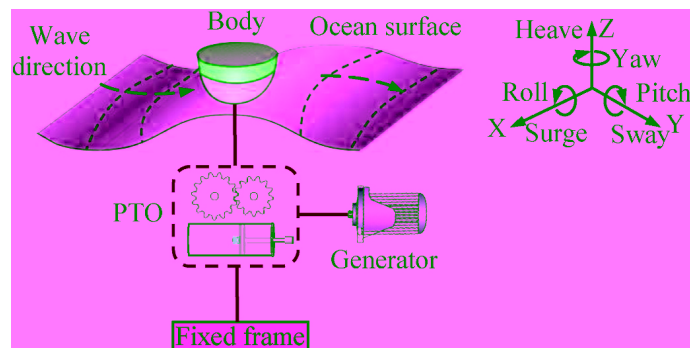
Figure 2.11: The basic idea of floating structure type WEC (Zhang et al., 2021).

- Floating structure: This can be further subdivided into single or multiple structures. The floating body/bodies can absorb wave energy and convert it into mechincal energy. Figure 2.11 illustrates the basic idea of floating structure type WEC.

  For example, PowerBouy OPT (Artal-Sevil et al., 2018) is single floating structure device, as shown in Figure 2.3 (a). Moreover, Wavestar (Kramer et al., 2011) and Pelamis (Westwood, 2004) are multiple floating structures, see Figure 2.3 (b) and Figure 2.5 (a), which have been introduced in Section 2.2.2.

- Overtopping: This device has a storage reservoir that can drop the water back to the ocean under gravity and several low-head turbines will be driven to generate electricity during the water falling process. Figure 2.12 shows the basic working principle of overtopping WEC.
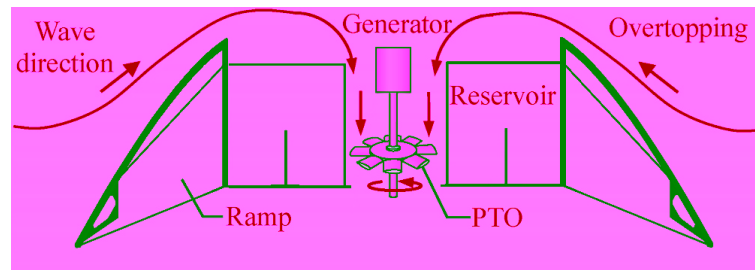
Figure 2.12: The basic working principle of overtopping WEC (Zhang et al., 2021).

The well known examples of overtopping devices SSG (Vicinanza et al., 2012), Waveplane (WavePlane, 2008) are shown in Figure 2.13, and Wave Dragon (Kofoed et al., 2006) can be seen in Figure 2.6.

| (a) | (b) |

Figure 2.13: The structure of overtopping WECs, (**a**) SSG WEC (Vicinanza et al., 2012), (**b**) Waveplane WEC (WavePlane, 2008).

- Oscillating Wave Surge (OWS): This device is fixed to the seabed through a pivoted joint, see Figure 2.14, and the device can oscillate like a pendulum when

the incoming waves drive a paddle and then harvest energy from wave surges and the horizontal movement of the wave particle.
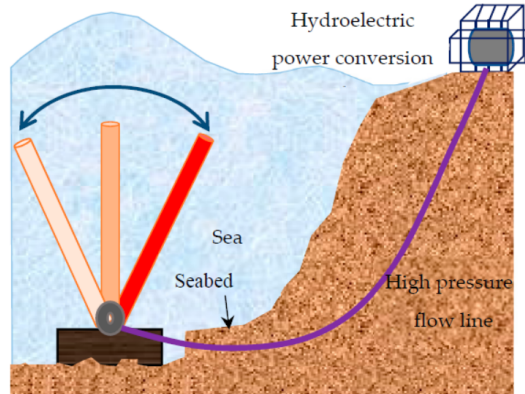
Figure 2.14: The basic illustration of oscillating wave surge WEC (Farrok et al., 2020).

OWS examples are: Oyster (Cameron et al., 2010) and Langlee (Pecher and Kofoed, 2017) belong to this type of WEC devices, see Figure 2.15.

| (a) | (b) |
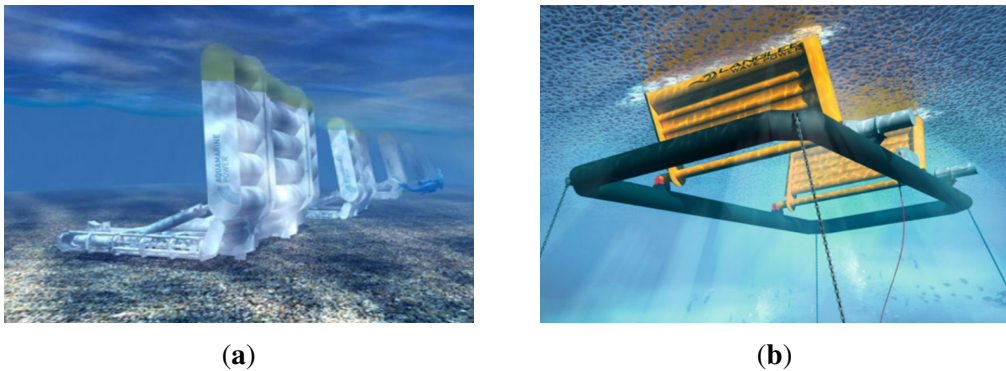
Figure 2.15: The structure of OWS WECs, (a) Oyster WEC (Oyster, 2012), (b) Langlee WEC (Pecher and Kofoed, 2017).

In addition to the WECs classified in 3 ways, according to Section 2.2, there are further WEC types with special characterstics. For example the rotating mass WEC (Wello Penguin) (Penguin, 2022), or Bulge Wave WEC, the Anaconda (Anaconda, 2023), etc, as shown in Figure 2.16. As for the Penguin WEC, it rotates with the movement of waves and spins the rotating mass around a shaft, which is connected with an electric generator to produce power. For Anaconda WEC, it is the different concept that a sealed rubber tube is filled with water, and anchored in the sea (Heller et al., 2000). The external waves can induce the bulge waves within the rubber tube and travel in it, which can be used to drive a PTO system to produce electricity at the tube stern.
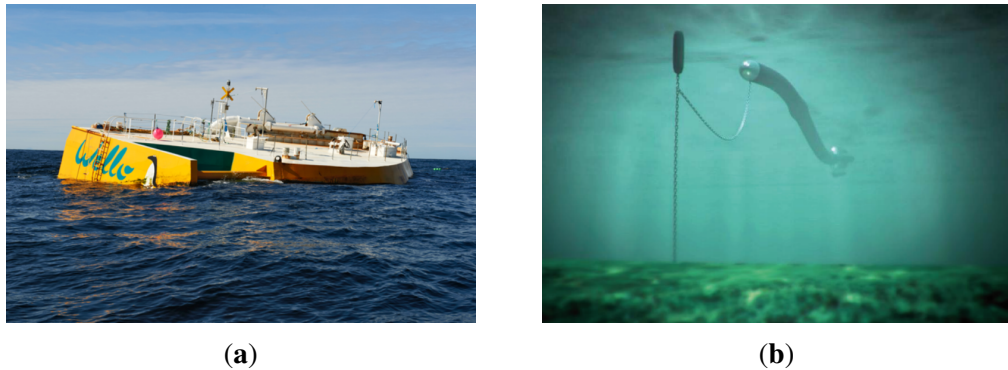
Figure 2.16: Further WEC examples of specially, (**a**) Wello Penguin WEC (Penguin, 2022), (**b**) Anaconda WEC (Anaconda, 2023).

Among the various WEC applications, PAWEC systems draw much more attention due to its following obvious merits. In general, the PAWEC has simple structure with small dimensions, as a relatively small device expected to be more economical. It can easily reach resonance between the bouy and the incident waves to capture much more wave energy compared with the other WEC types. The PAWEC is also well suited to research work to test new ideas (Guo et al., 2022). Typical research involves novel modelling methods, appropriate PTO mechanisms, advanced control approaches. This PhD study concentrates on the 1:20 scaled special Wavestar-prototype PAWEC device for energy maximising control system design, to improve the energy conversion efficiency. Furthermore, the PAWEC device can be arranged into an array (Stratigaki et al., 2014) and deployed in the offshore ocean area. In this case, the infrastructural costs can be reduced when the mooring and electrical connections be shared between all WEC devices in the array (Peña-Sanchez, 2020). The significance of this is that the LCoE from the WEC array can be decreased.

2.3 Wave Excitation Force Estimation and Forecasting Methods

In some cases the computation of the WEF (or WEM, in the case of a wave moment problem) plays an important part in wave energy maximum absorption for a PAWEC system (Guo et al., 2018). Several energy-maximising control strategies are available (Coe et al., 2017; García-Violini et al., 2020a; Guo and Ringwood, 2021; Li and Patton, 2023a; Ringwood et al., 2023b; Li and Patton, 2023b). Although, these have been used for the purpose of energy maximisation extraction, most require the information of the

WEF. Particularly, MPC requires the current and the future knowledge of the WEF to compute the optimal solution (Garcia-Abril et al., 2017).

In principle, for all fixed (or non-PAWEC) cases WEF signal could be computed after integrating the pressure over the submerged body surface (Peña-Sanchez et al., 2019). However, for the moving body (or PAWEC) device pressure sensing can still be used with sensor placed e.g. one typical wavelength away from the device itself. In general, the WEF is best determined by estimation based on the device displacement and velocity. This is a very convenient method for WEF computation, although to a small extent affected by viscous and friction force terms. This WEF computation fits well with the MPC requirement for forecasting (Fusco and Ringwood, 2010).

2.4 Classical control strategies

For the power maximization control work design of the WEC systems, the fundamental research can date back to the resonant concept for oscillating systems proposed by (Budar and Falnes, 1975) in 1975. The primary idea is based on linear hydrodynamics, the assumption of monochromatic waves and an ideal PTO system. According to linear potential flow theory, the physical meanings of the WEC hydrodynamic forces can be clearly described by a linear numerical modelling. At present, the Boundary Element Method (BEM) packages (time-domain or frequency domain) are widely used to provide the hydrodynamic coefficients (Penalba et al., 2017b; Pastor and Liu, 2014) for building a linear numerical modelling of a WEC device.

Usually, the Cummins' Equation of the dynamic motion of a PAWEC device (Rafiee and Fiévez, 2015; Lawson et al., 2014a) can be written as:

$$(M_b + M_\infty)\ddot{X}_b(t) + \int_{-\infty}^{\infty} K_r(t-\tau)\dot{X}_b(\tau)d\tau + K_{hs}X_b(t) = F_{ext}(t) \qquad (2.1)$$

where M_b is the Mass of bouy, X_b is heave position of the buoy, M_∞ is the added mass at the infinity frequency, K_r is the Impulse Response Function (IRF) of the radiation force and K_{hs} is the hydrostatic stiffness coefficient. F_{ext} means the external forces, which includes excitation force F_{exc}, PTO force F_{pto}, mooring force F_{mo}, etc. The F_{exc} is independent of the PAWEC system variables (position X_b, velocity $\dot{X}_b$, acceleration $\ddot{X}_b$) but restricted to the wave surface elevation $\eta(t)$. The F_{pto} is the desired controller term acting as the loading on the PTO system that can optimise the behavior of PAWEC

device, which means to maximise the absorbed energy over a wide range of ocean waves.

The Cummins' Equation (2.1) of a PAWEC device can be expressed into a frequency domain force-to-velocity form (Guo et al., 2022), given by

$$
\frac{V(\omega)}{F_{exc}(\omega) + F_{pto}(\omega)} = \frac{1}{Z_i(\omega)}
$$
$$
Z_i(\omega) = B(\omega) + j\omega \left[M_b + A(\omega) - \frac{K_{hs}}{\omega^2} \right]
$$

(2.2)

where $V(\omega)$ is the Fourier transform of the PAWEC body velocity $\dot{X}_b$ in frequency domain, and $Z_i(\omega)$ denotes the intrinsic impedance of the PAWEC system (Falnes and Kurniawan, 2020). $A(\omega)$ and $B(\omega)$ are the added mass and radiation damping coefficients.

From the maximum power transfer theorem (Svoboda and Dorf, 2013), the PTO system impedance for optimal power conversion (Guo and Ringwood, 2021) should satisfy the following form

$$
Z_{pto}(\omega) = Z_i^*(\omega)
$$

(2.3)

where $Z_i^*(\omega)$ is the complex conjugate of $Z_i(\omega)$. The PTO parameters can be easily determined by the Mass-Spring-Damper (MSD) coefficients of the PAWEC system.

This means that the power absorbed by the PAWEC device can be maximized if the PTO impedance Z_{pto} equals the complex conjugate of the system intrinsic impedance Z_i (Falnes and Kurniawan, 2020). This is the well known concept of "maximum power transfer" or complex-conjugate impedance matching, or alternatively "reactive control". In general, reactive control will bring bi-directional power flow in the PTO mechanism (Guo, 2017). However, some PTO systems might only allow uni-directional power flow. For these cases the passive control with a damping term can be considered as:

$$
B_{pto} = |Z_i(\omega)|
$$

(2.4)

This linear damping control is the simplest way that only requires to be tuned based on the frequency of the incoming waves (Abdelrahman, 2019), but it cannot generate the optimal and maximum power for a PAWEC device.

According to the requirement of resonance between the wave and PAWEC device, the optimal velocity of reactive control (Guo and Ringwood, 2021) can be defined as:

$$V_{opt}(\omega) = \frac{F_{exc}(\omega)}{2B(\omega)} \tag{2.5}$$

Thus, the optimal power conversion is achieved when the amplitude and phase conditions satisfy

$$|V_{opt}(\omega)| = \frac{|F_{exc}(\omega)|}{2|B(\omega)|}, \quad \angle V_{opt}(\omega) = \angle \frac{F_{exc}(\omega)}{2B(\omega)} \tag{2.6}$$

As for the optimal velocity phase condition, it can be used to implement the latching control (Babarit et al., 2004) or de-clutching control (Babarit et al., 2009) by using mechanical or hydraulic PTO systems. It is important to keep in mind that the wave prediction is necessary for setting the optimal duration of switching or releasing (Abdelrahman, 2019), in order to latch the WEC device after its velocity becomes minimum and unlatch the WEC device during the optimal time interval. Thereby, the PAWEC body velocity will keep in phase with the excitation force to maximise energy harvesting during the optimal latching duration. Several different latching approaches (Babarit et al., 2004; Sheng et al., 2015) have been compared and tested to increase the absorbed energy over a broad range of irregular wave conditions. On the other hand, the de-clutching control can be considered as an extension version of the latching control. It considers to disconnect the PTO system, so unloading the PAWEC device at specific moments during the power cycle (Garcia-Rosa and Ringwood, 2015), but to connect the PTO system when the device velocity keeps in phase with the WEF. The de-clutching control has strength to switch on and off the hydraulic PTO systems by using a simple by-pass valve. The optimal command theory can determine the control law of the valve (Babarit et al., 2009). A special combination of latching and de-clutching strategy has been tested in (Feng and Kerrigan, 2015). This new stratgey can increase the energy harvesting compared with the single use of latching or de-clutching approaches.

Overall, the classical control strategies are based on linear hydrodynamics and ideal PTO assumptions (Guo and Ringwood, 2021) that do not involve the physical operational constraints like PAWEC position, velocity limitations or PTO force maximum value. It is important to note that these approaches are limited to regular or monochromatic wave conditions. However, the optimal solutions are frequency-dependent, as described above, related to resonance concept. This implies that optimal settings are difficult to choose, especially when the PAWEC device is operated under irregular seas

(Faedo et al., 2017) that contains several frequencies. In addition, the power fluctuations are an inevitable problem that should be considered for choosing the PTO systems to reduce the energy losses during the conversion process.

2.5 Modern control strategies

2.5.1 Model-based type

To date, a number of advanced control strategies have been proposed and tested to obtain the maximized energy production for the WEC applications with system constraints and non-linearities over a wide range of sea states. Most of the published studies on WEC control focus on PAWEC type systems. A popular idea focuses on MPC (Li and Belmont, 2014; Tona et al., 2015; Zou et al., 2017; Ling et al., 2019; Hillis et al., 2020) is used by many researchers and engineers to provide an optimal solution of PTO force for the purpose of power or energy maximization and to deal with the PAWEC system physical and PTO input constraints. In other words, the energy maximization problem of a PAWEC system is converted into a quadratic programming problem with the properly defined objective function and the specific system constraints (Richter et al., 2014). The optimal control action will be calculated by solving the predetermined cost function in every discrete time step and the first term of control sequence will be chosen as the PTO force acting on the WEC system. Some related objective functions about the energy absorption have been discussed by (Faedo et al., 2017). The most representative form of the MPC objective fucntion is as follows:

$$min \ -E_J + E_J^*$$

$$subject \ to, \quad for \ t \in [t, t + T_h]:$$

$$\dot{x}(t) = f(x, \dot{x}, u, t) \quad dynamics \ equation \qquad (2.7)$$

$$\left. \begin{array}{l} |x(t)| \leq X_{max}, \\ |\dot{x}(t)| \leq \dot{X}_{max}, \\ |u(t)| \leq u_{max} \end{array} \right\} \quad state \ and \ input \ constraints$$

where the absorbed energy is $E_J = -\int_t^{t+T_h} u(\tau)\dot{x}(\tau)d\tau$ and E_J^* denotes the alternative penalty terms. But it should be notied that the additional penalty terms can modify the original optimal control objective and lead to a sub-optimal solution (Zhong and Yeung, 2019). T_h is the prediction horizon, X_{max} is the maximum of the displacement,

$\dot{X}_{max}$ is the maximum of the velocity, and u_{max} is the maximum of the PTO force. Generally, most of the references concentrate on both the PAWEC body displacement and control input constraints (Faedo et al., 2017), while some researchers attempt to consider the study of velocity or rate of change of the control input constraints.

The standard MPC methods for PAWEC are based on the linear modelling, without including the nonlinear viscous force, mooring term, etc (Penalba et al., 2017a). Actually, the performance of MPC relies on the accuracy of the modelling significantly. Otherwise, the MPC optimization of the WEC energy maximization may fail to find a proper solution or even give rise to the possibility of divergence, i.e. closed-loop instability. Hence, the MPC approaches may not be suitable for some complicated PAWEC applications with large uncertainties or modelling errors. On the other hand, the future knowledge of the excitation force is required in the MPC optimisation procedure (Ringwood et al., 2023b) and it should be obtained by doing short-term forecasting work as described in Section 2.3. The prediction errors (Hillis et al., 2020) will affect the MPC performance and lead to unsatisfactory reduction in absorbed energy. Some nonlinear model predictive control (NMPC) strategies are proposed that can deal well with the non-linear PAWEC devices. For example, in view of the possible nonlinear effects of mooring forces, (Richter et al., 2012) choose NMPC for a PAWEC device to optimize the absorbed energy whilst satisfying its system operational constraints. Considering the non-linear buoyancy force, (Li, 2017) chooses an efficient NMPC optimisation approach to exploit the differential flatness of the WEC model. (Karthikeyan et al., 2019) concentrates on the viscous drag force and non-ideal PTO loss model of the WEC system and applies a NMPC to maximize the generated power. However, the NMPC methods usually involve large online computation complexity due to the problem of non-convexity optimization. Thus, they may not satisfy the requirements of real-time control for the complex PAWEC applications.

Along with a consideration of MPC methods, some MPC-like spectral methods (Bacelli and Ringwood, 2011) and pseudo-spectral (Herber and Allison, 2013; Bacelli and Ringwood, 2014) approaches offer different choices to tackle the constrained optimization control problem and calculate its solution in a specific parameterization way. Those methods supply a flexible balance between the computational complexity and system performance index (absorbed energy) by altering the number of the approximating basis functions. Nevertheless, the main formulations of the spectral and pseudo-spectral methods have a drawback in a receding-horizon context when the trigonometric polynomials are considered to compute periodic solutions (Faedo et al., 2017).

Hence, some researchers pay attention to investigate and develop the receding horizon pseudo-spectral methods (Faedo et al., 2017) based on the Lagrangian polynomials or Half-Range Chebyshev Fourier (HRCF) polynomials as basis functions, to solve the real-time constrained optimization control problems for the different WEC systems. Not merely for the computation of control solution directly, another interesting application of the receding horizon pseudo-spectral (Genest and Ringwood, 2016; Auger et al., 2018) is based on using Fourier approaches to compute the optimal reference trajectory, meanwhile to take the system non-linearity and constraints into consideration.

Apart from the above, another choice for PAWEC optimization problem is proposed by (Zhan et al., 2016), in which the optimal feedback law can be obtained by solving the algebraic Riccati Equation. This scheme can also be combined with adaptive (Zhan et al., 2018) and robust (Zhang and Li, 2019) concepts, which demonstrate good practical prospects in the PAWEC applications. In addition, the linear quadratic Gaussian (LQG) control (Sun and Nielsen, 2018; Scruggs et al., 2013) is an alternative idea that has simple structure and can directly calculate the algebraic Riccati Equation whilst minimizing the objective function to give the optimal control solution for the PAWEC system. Gain-scheduling (Scruggs et al., 2013) is a fascinating concept that can be applied when the knowledge of the spectral content and the propagation direction of the sea conditions have been known. The remaining part of the optimized control can be based on a "bang-bang" type scheme or dynamic programming (DP). A few research studies describe the singular arcs control approach (Abraham and Kerrigan, 2012) or singular-bang control (Hendrikx et al., 2017) according to either Pontryagin's Minimum or Maximum Principle, to find the best solution for a dynamical WEC system with operational constraints. Referring to the non-convex problem of the control optimization during the programming procedure, (Li et al., 2012) introduces the bang-bang control concept and selects the DP algorithm to do the optimization work for giving an optimal solution to improve the efficiency of wave energy conversion. Besides, an adaptive DP strategy is formulated by (Na et al., 2018) to efficiently solve the constrained nonlinear optimal problem online, and reach the energy maximization absorption for the WEC system with non-linearity and constraints. Aiming at the non-linear effects of hydrostatic restoring force and viscous forces, a moment-based approach is demonstrated in (Faedo et al., 2021) on a CorPower-like device, mapping the original objective function of average absorbed mechanical energy into a new tractable nonlinear program, subject to both system physical and PTO input constraints.

Apart from the control optimization design, the literature describes other forms of control methods. For instance, a broadband solution LiTe-Con control is proposed by (García-Violini et al., 2020b), which is based on a approximated frequency domain optimality condition from the impedance matching. This energy maximising control strategy can efficiently help the PAWEC device to capture more energy from the sea. There is no need to consider prediction work in this controller design but only WEF estimation/calculation is required. On the other hand, a suboptimal mechanism is considered to do constraint handling, which results in a conservative performance in energy maximisation absorption. In view of that limitation, a new online adaptive mechanism (García-Violini et al., 2023) is replaced and being added into the LiTe-Con control method to provide a time-varying solution in order to improve the energy conversion efficiency for the scaled Wavestar-like device (described in Chapter 3). Regarding the adaptive control design of PAWEC, a gain-scheduling approach (Nguyen and Tona, 2017a) is investigated to continuously update the PI controller gain in an optimal way, based on the evaluation of the current irregular wave conditions. Where the proposed variable-gain PI strategy needs to do WEF estimation and calculate the dominant frequency of the WEF. Another interesting idea of adaptive control is based on a vectorial approach (Cantarellas et al., 2017) not only achieving the maximum power absorption but also reducing the Peak-to-Average Power Ratio (PAPR) under irregular wave conditions.

Except the requirement of the optimality, robustness is the another key point (Ringwood et al., 2018; Giorcelli et al., 2023) that should be considered for the PAWEC devices to overcome the non-linear phenomena viscous forces and Froude-Krylov forces (Penalba, 2018). In general, many researchers choose the linear modelling formulation to describe the WEC body motion according to the Cummins' Equation, which inevitably involves the unmodeled errors and system uncertainties. Additionally, the hydrodynamic parameters are time-varying and frequency-dependent with the changing of the incoming waves. Especially, the assumption of the linearity of the hydrodynamics might be violated when the PAWEC motion is amplified by some energy-maximising controllers (Fusco and Ringwood, 2014b). Therefore, the robust control work should be designed against the PAWEC system disturbances to maintain and ensure the energy maximization. However, generally, the main control objective of a PAWEC system is to optimize the generated power/energy from the incoming waves, which is different from the purpose of the traditional tracking control design. (Fusco and Ringwood, 2014a) first introduced a special hierarchical tracking structure that can

force the PAWEC system to track a reference velocity so as to reach a near-resonance condition to keep the WEC body velocity in phase with the excitation force for energy maximisation purpose. Even if the designed tracking structure only provides suboptimal solution onto the PAWEC system, but can show much more freedom on design control methods with other new features, such as the robustness (Fusco and Ringwood, 2014b) or adaptability (Davidson et al., 2018), etc. The similar tracking idea can also be found in (Wahyudie et al., 2015). In view of enhancing the PAWEC system to overcome the non-linearity and possible coupled dynamic terms, (Abdelrahman and Patton, 2017) tried to design a backstepping sliding mode control based on the hierarchical tracking structure for the PAWEC system to absorb energy from the irregular waves as much as possibly. But the designed robust controller just forces the PAWEC system to do a reference position tracking work, not the velocity tracking. That is why this PhD study foucses on the purpose of the energy maximising control to propose model-following LQR/H_∞ control and SMC methods to do position and velocity tracking in Chapter 5. On the other hand, a gap exists in the discussion of the robustness and optimality of the two aspects for PAWEC applications. This has motivated the design study of model-predictive velocity tracking control in Chapter 6. Following this, the Chapter 7 makes a comparison between robust control and MPC systems.

2.5.2 Model-free type

The second category of advanced control methods can be considered a "Model-Free". An example of this is a practical application of Fuzzy logic based PI control (Burgaç and Yavuz, 2019), which makes use of Fuzzy logic inference to tune the PTO system stiffness and damping coefficients according to the estimated dominant wave frequency, in order to obtain maximum energy extraction. With this, the PAWEC system can have the ability to reach the resonance condition for maximum power absorption. In another application the Hull Control Group developed a special data-driven method (Shi et al., 2019) using Bayesian optimization based on Gaussian Processing to achieve on-line PID coefficients tuning according to the WEC control performance. It was shown that the MSD coefficients of the PTO system can reach the optimum values after 25 iterations, i.e in a short time. This machine learning tuning strategy has been validated by the Hull team as one of three competing teams using an experimental wave tank implementation at Aalborg University during the second stage of the WECCCOMP (Ringwood et al., 2023a).

Another interesting application like extremum-seeking (Sun et al., 2018; Parrinello et al., 2020; Moens de Haste et al., 2021), has attracted significant attention in the literature. The extremum-seeking control has also given rise to the idea of optimizing the coefficients of the PAWEC PTO system (Parrinello et al., 2020) under realistic irregular wave conditions. This is used to maximise the average extracted power and conversion efficiency of the device as well as reducing the Peak-to-Average Power Ratio (PAPR), when a "Flower Pollination" algorithm is considered (Sun et al., 2018). However, some applications of extremum-seeking control have limitations when considering the panchromatic nature of wave excitation (Moens de Haste et al., 2021) due to the requirement for long performance evaluation times.

So far, Reinforcement Learning (RL) algorithms have been popular as model-free control design methods. These have been investigated by some researchers to achieve maximum energy absorption for different WEC applications (mainly PAWEC). For example, the classical Q-learning algorithm has been tested to provide the optimal PTO coefficients for resistive control (Anderlini et al., 2016; Bruzzone et al., 2020) or reactive control (Anderlini et al., 2018). The Q-learning algorithm can adapt well to the hydrodynamic variations and bias arising from the unmodeled errors. In addition, (Zou et al., 2022) used the Deep Q-Network (DQN) algorithm that as an improvement from the basic Q-learning to design deep reinforcement learning (DRL) controller for the PAWEC with PTO dynamics, to reach energy maximization absorption. The results show that the designed DRL control can provide better power quality in terms of Peak-to-Averate Ratio, the coefficient of variation compared with the MPC, PD control, etc. A study has been conducted by (Zadeh et al., 2022) to validate the proposed Bayesian Actor-Critic (BAC) scheme and compare it with reactive control and MPC when the PAWEC system contains large modelling errors. The RL control based on Bayesian optimization and Actor-Critic form has an advantage in robustness against the modelling errors, in which the control performance outperforms 20 % compared with reactive control and 27 % compared with MPC. Overall, RL control methods converge in a long time for training and typically achieve optimal policy in several hours (Anderlini et al., 2017; Zadeh et al., 2022) or even longer. Hence, in reality RL may not be suitable for real time WEC control. However, RL algorithms have demonstrated strengths in dealing with the system uncertainties (Anderlini et al., 2020; Zou et al., 2022), so this aspect should be explored in future research.

2.6 Summary

The purpose of this Chapter is to provide a literature review of WEC control for energy maximization. Section 2.2 starts by giving a brief review of the classification of WEC devices, including deployment locations, dimension and orientation with respect to the waves, as well as WEC Working Principles. On the whole, the current and future knowledge of WEF are needed in energy-maximising or optimal control design. Thus Section 2.3 discussed the requirements of WEF estimation and forecasting work as an important precursor for the control design studies. Next, the classical control methods are illustrated in Section 2.4 according to the complex conjugate concept or optimal phase condition, to achieve the optimal power conversion. Then the modern control strategies are classified into two different types, model-based and model-free. A literature review of WEC control system is elaborated based on some main advanced control methods used by many researchers in wave energy field.

Following the review of the state of the art of Control for PAWEC systems, the well-known 1:20 scaled Wavestar-like PAWEC device is chosen as a model for applying the thesis work. The WEC-Sim numerical simulation of this system is described in Chapter 3. Following the review of advanced control strategies for PAWEC systems robustness and optimality are considered two important aspects to explore in this work. Most research work related to PAWEC control system design is based on the MPC approach, which belongs to the subject of optimization control. However, there are not many studies focusing on robust control. Hence, in this study it is considered that there is significant scope for research work and discussion on this topic. Hence, in view of a requirement for robust control design and robustness enhancement of MPC for PAWEC devices, the model-following robust control and model-predictive tracking control methods are proposed in Chapter 5 and Chapter 6, respectively. In addition, to further assess the optimality and robustness of the proposed controllers on PAWEC system, a comparison study between model-following robust control and MPC is done in Chapter 7, based on some assessment metrics.

Chapter 3

WEC-Sim Numerical Modelling for Wavestar-prototype WEC

3.1 Introduction

In this Chapter, the numerical modelling of Wavestar-prototype device is described, based on a popular open-source Wave Energy Converter SIMulator (WEC-Sim) (Lawson et al., 2014b). This has been chosen as a benchmark in an open competition for the purpose of comparisons between different WEC energy-maximising control strategies (Ringwood et al., 2023a). It is thus appropriate that the thesis focuses on an energy-maximising controller together with a strategy for testing the control methods, based on WEC-Sim. The overview of the WEC-Sim software is discussed in Section 3.2, including some descriptions of a software flow chart and the numerical modelling of a PAWEC scheme based on Cummins' Equation. In Section 3.3, the rotational dynamics of Wavestar-like device system is given for building a state space model. Next, a basic form of SMC is designed as a test regulator for the PAWEC to force its float to remain it at the (original) equilibrium point. This is considered as the pre-test procedure before applying the tracking design discussed in Chapters 5 and 6. Section 3.4 provides a description of the basic tests on the numerical modelling, used to check and validate the WEC-Sim model. A SMC regulator is also described as a test procedure for checking the controllability and effectiveness of the PAWEC control system. Section 3.5 is the Summary of this Chapter.

3.2   Overview of WEC-Sim software

WEC-Sim software is an open-source tool (NREL and Sandia, 2014) developed jointly by National Renewable Energy Laboratory and Sandia National Laboratories, for the purpose of simulating and comparing the control performances of various PAWEC controllers (based on the Wavestar concept). The implementation is a combination of Matlab scripts and Simulink libraries, that can be visualised as an open-source GitHub repository (Yi-Hsiang Yu et al., 2014). The WEC-Sim code is based on Simscape Multibody to solve for a PAWEC's rigid body dynamics. Usually, the modular structure of WEC-Sim is implemented in Matlab code and Simulink blocks (SimMechanics) (Lawson et al., 2014b), as shown in Figure 3.1.
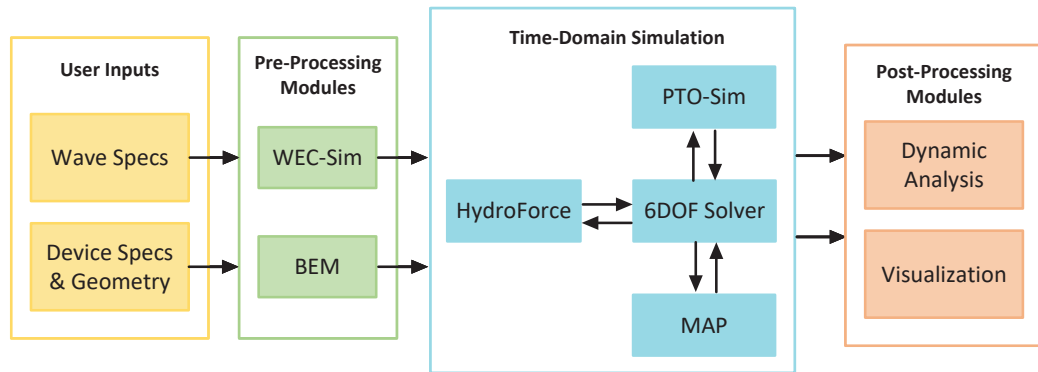
Figure 3.1: WEC-Sim code structure.

It can be seen that WEC-Sim has three main modules:

1. The first Pre-processing modules play a role in preparing user input of hydrodynamic data in frequency domain. The hydrodynamic data of a PAWEC device is obtained from the BEM software as external input of WEC-Sim.

2. The second modules calculate the time-domain hydrodynamic forces/torques, simulating specific components, and solve the Cummins' Equation to model the PAWEC system. WEC-Sim provides a 6 degrees of freedom (DOF) simulation of PAWEC device. The 6 DoF Coordinate System is shown in Figure 3.2 (NREL and Sandia, 2014), illustrating the motions of a 3-D floating body under incoming waves.
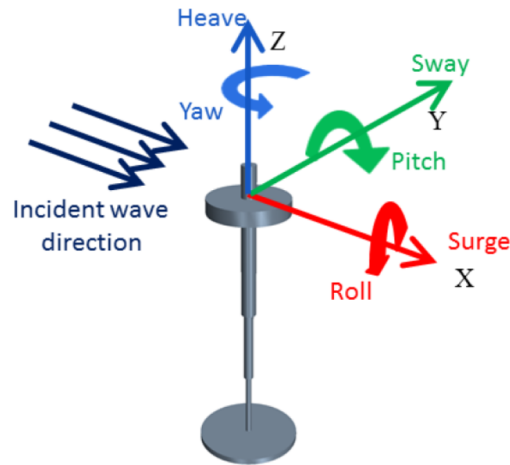
Figure 3.2: WEC-Sim Coordinate System (NREL and Sandia, 2014).

3. The third Post-processing modules are used to perform a visualization stage and result data (position, velocity, power, etc) analysis from the plotted figures.

Based on the above description, Figure 3.3 gives the four steps that have been followed in this study, to create a standard WEC-Sim simulation.
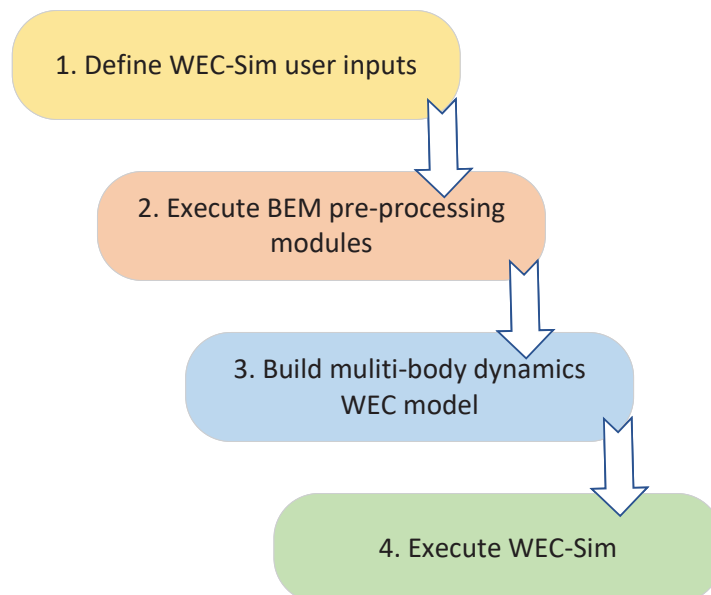
Figure 3.3: Primary steps to build and execute a WEC-Sim simulation (Lawson et al., 2014b).

Step 1: The user should choose wave properties, such as wave period and height for specifying a regular wave or wave spectrum type, peak wave period, significant

wave height for specifying an irregular wave. Besides, the user needs to define the WEC geometry properties such as mass, moments of inertia, centre of gravity (CoG) and centre of buoyancy (CoB).

Step 2: To execute the Pre-processing procedure, WEC-Sim modules can generate wave time series and BEM solver (WAMIT, AQWA, or NEMOH) can provide hydrodynamic coefficients for a designed PAWEC device.

Step 3: To choose the required components (hydrodynamic bodies, constraints, PTOs, etc) from WEC-Sim library blocks and connect them to build a multi-body dymamics model of the device.

Step 4: When the selected WEC model being constructed, the numerical simulation is performed by SimMechanics 6 DOF multi-body solver to sum hydrodynamic forces in time domain at every time step.

More information about WEC-Sim theory, code structure, implementation, advanced features and applications can be found in (NREL and Sandia, 2014).

3.2.1   Wave generation

Regular waves

Usually, planar sinusoidal waves are used to express regular or harmonic waves (Falnes and Kurniawan, 2020), and the incident wave elevation can be defined as:

$$\eta(x,y,t) = \frac{H}{2}cos(\omega t - k(xcos\bar{\theta} + ysin\bar{\theta}) + \phi), \quad \omega = \frac{2\pi}{T}, \quad k = \frac{2\pi}{\lambda} \qquad (3.1)$$

where ω is the wave angular frequency and H is the wave height. k is the wave number, λ is the wave length, $\bar{\theta}$ is the wave direction, and ϕ is initial wave phase.

Irregular waves

Generally, irregular waves are generated from linear superposition of a large number of harmonic waves with different frequencies and with random incidence angles (Falnes and Kurniawan, 2020). From this, the wave elevation can be defined as:

$$\eta(x,y,t) = \sum_i \frac{H_i}{2}cos(\omega_i t - k_i(xcos\bar{\theta}_i + ysin\bar{\theta}_i) + \phi_i) \qquad (3.2)$$

where i denotes the *i-th* harmonic wave component, and H_i is the *i-th* wave height.

For irregular waves, a particular wave energy spectrum, or wave spectral density function, is selected to represent the real sea waves in a statistical way. This description can be used to characterize the linear superposition of distinct harmonic waves in frequency domain. The general form of an irregular wave spectra can be expressed as:

$$S(f, \bar{\theta}) = S(f)D(\bar{\theta}) \tag{3.3}$$

where f is the incident wave frequency. $D(\bar{\theta})$ represents the wave directional distribution which should satisfy:

$$\int_0^\infty \int_{-\pi}^{\pi} S(f)D(\bar{\theta})d\bar{\theta}df = \int_0^\infty S(f)df \tag{3.4}$$

which means that the calculated energy in the directional spectrum equals the corresponding energy in a one-dimensional spectrum. The power spectrum $S(f)$ (Falnes, 2007) can be expressed as:

$$S(f) = A_{\omega s} f^{-5} exp[-B_{\omega s} f^{-4}] \tag{3.5}$$

where $A_{\omega s}$ and $B_{\omega s}$ are general forms for the coefficients of the spectrum, and *exp* is the natural exponential function. From this, the *j-th* related wave spectral moments m_j are defined as:

$$m_j = \int_0^\infty f^j S(f)df, \quad (j = 0, 1, 2, ...) \tag{3.6}$$

The signficant wave height H_{m_0} can be expressed by the zero-order spectral moment m_0 as:

$$H_{m_0} = 4\sqrt{m_0} \tag{3.7}$$

Note: the significant wave height is defined as the average wave peak-to-trough of the one third largest waves (Mérigaud, 2018).

Usually, the wave spectrum $S(f)$ can be modified into another form of the angular frequency ω. The corresponding term can be written as $S_\omega(\omega)$, given by

$$\int_0^\infty S_\omega(\omega)d\omega = \int_0^\infty S(f)df \tag{3.8}$$

The relationship between $S(f)$ and $S_\omega(\omega)$ (Falnes and Kurniawan, 2020) is

$$S(f) = 2\pi S_\omega(2\pi f) = 2\pi S_\omega(\omega) \tag{3.9}$$

The WEC-Sim software provides the user to choose one of the well-known wave spectra such as: Pierson-Moskowitz (PM) Spectrum, Bretschneider Sprectrum (BS) and JONSWAP Spectrum. The choice of spectrum is made according to typical characteristics of a particular sea or ocean. Additionally, the user is allowed to import their own special spectrum. The JONSWAP Spectrum (Hasselmann et al., 1973) has been selected as an irregular wave generator in later chapters of this thesis. According to the Equation (3.5), the general coefficients of the JONSWAP Spectrum are:

$$
\begin{aligned}
A_{\omega s} &= \frac{B_{\omega s}}{4} H_{m_0}^2 C_{\omega s}(\Upsilon) \Upsilon^{\alpha} \\
B_{\omega s} &= \frac{5}{4} f_p^4
\end{aligned}
\tag{3.10}
$$

$C_{\omega s}(\Upsilon)$ is a normalizing factor (NREL and Sandia, 2014) and can be defined as:

$$
C_{\omega s}(\Upsilon) = 1 - 0.287 \ln(\Upsilon)
\tag{3.11}
$$

The non-dimensional peak-shape parameter Υ is defined as:

$$
\Upsilon =
\begin{cases}
5 & for \quad \dfrac{T_p}{\sqrt{H_{m_0}}} \leq 3.6 \\[2ex]
exp(5.75 - 1.15 \dfrac{T_p}{\sqrt{H_{m_0}}}) & for \quad 3.6 \leq \dfrac{T_p}{\sqrt{H_{m_0}}} \leq 5 \\[2ex]
1 & for \quad \dfrac{T_p}{\sqrt{H_{m_0}}} > 5
\end{cases}
\tag{3.12}
$$

where T_p is the peak wave period.

The peak-shape exponent α is given as:

$$
\alpha = exp\left[-\left(\frac{\frac{f}{f_p} - 1}{\sqrt{2}\bar{\sigma}} \right)^2 \right], \quad \bar{\sigma} =
\begin{cases}
0.07 & f \leq f_p \\
0.09 & f > f_p
\end{cases}
\tag{3.13}
$$

where f_p is the peak wave frequency.

3.2.2 Numerical modelling analysis

The dynamic response of each rigid body in 6-DOF can be calculated by solving the Cummin's Equation (NREL and Sandia, 2014) about its centre of gravity in WEC-Sim. The dynamic motion of a PAWEC system can be expressed as:

$$
m\ddot{X} = F_{ra} + F_{hs} + F_{vis} + F_{exc} + F_{pto}
\tag{3.14}
$$

where m is the mass matrix, X is the (translational and rotational) displacement vector of the PAWEC device, F_{ra} is the radiation force and torque (6-element) vector, generated by the body motion in still water, F_{hs} is the total hydrostatic restoring force and torque vector, based on linear stiffness and bouyancy forces. F_{vis} is the viscous force and torque vector, due to linear damping and quadratic drag effects. F_{exc} is the wave excitation force and torque vector, acting on the PAWEC body from the incoming waves. F_{pto} is the PTO force and torque vector which is the system calculated control input from the control method. The wave-WEC interaction terms, F_{ra}, F_{hs} and F_{exc} are computed based on hydrodynamic coefficients generated by BEMIO functions for BEM solvers (NREL and Sandia, 2014). Where the calculation of F_{hs} depends on the hydrostatic stiffness K_{hs} coefficient, body displacement, and body mass.

WEC-Sim provides two numerical methods, sinusoidal steady-state response and convolution integral formulation, for calculating F_{ra} and F_{exc}.

Sinusoidal Steady-State Response

This approach can be used to do the regular wave simulations, if the system response is in the form of sinusoidal steady-state. The radiation term F_{ra} can be computed based on two terms the added mass and radiation damping (Falnes and Kurniawan, 2020) as follows:

$$F_{ra}(t) = -A(\omega)\ddot{X} - B(\omega)\dot{X} \qquad (3.15)$$

where $A(\omega)$ and $B(\omega)$ are the added mass and radiation damping coefficients.

Based on linear wave theory, the wave excitation term F_{exc} can be calculated as:

$$F_{exc}(t) = \mathfrak{Re}\left[R_{rf}(t)\frac{H}{2}F_{exc}(\omega,\bar{\theta})e^{i\omega t}\right] \qquad (3.16)$$

where $\mathfrak{Re}$ denotes the real part of (3.16). R_{rf} is the defined ramp function, H and ω is the pre-selected wave height and frequency, respectively. $F_{exc}(\omega,\bar{\theta})$ is the frequency-dependent complex wave-excitation amplitude vector and $\bar{\theta}$ is the wave direction.

As for the ramp function R_{rf}, it is included to avoid strong transient flow generation when the simulation is run during earlier time steps, given by

$$R_{rf}(t) = \begin{cases} \frac{1}{2}(1+cos(\pi + \frac{\pi t}{t_r})) & \frac{t}{t_r} < 1 \\ 1 & otherwise \end{cases} \qquad (3.17)$$

where t and t_r are simlulation time and ramp time, respectively.

Convolution Integral Formulation

For irregular wave simulations, or any simulations which involve the fluid memory effects, these effects can be expressed by the convolution integral approach based on Cummin's Equation (Cummins et al., 1962). Then the radiation term F_{ra} is calculated by

$$F_{ra}(t) = -A_\infty \ddot{X} - \int_0^t K_r(t-\tau)\dot{X}(\tau)d\tau \qquad (3.18)$$

where A_∞ is the added mass matrix at infinite frequency, and $K_r(t)$ is the Impulse Response Function (IRF) of the radiation term.

$$K_r(t) = \frac{2}{\pi}\int_0^\infty B(\omega)cos(\omega t)d\omega \qquad (3.19)$$

According to the Ogilvie relation (Ogilvie, 1964), the relationship between frequency-domain and time-domain coefficients of radiation term is given by

$$A(\omega) = A_\infty - \frac{1}{\omega}\int_0^\infty K_r(t)sin(\omega t)dt \qquad (3.20)$$

$$B(\omega) = \int_0^\infty K_r(t)cos(\omega t)dt \qquad (3.21)$$

The radiation convolution term can be approximated by a system of linear ordinary differential equations. A linear state space model can be obtained by doing time-domain system identification through Matlab functions such as imp2ss (Kung, 1978) or balmar (Safonov and Chiang, 1988). This approximation can help to reduce the computation burden of the convolution integral and this is convenient for PAWEC control system design since state space designs are usually made. The desired linear state space model is:

$$\begin{cases} \dot{X}_r(t) = A_r X_r(t) + B_r u(t); \quad X_r(0) = 0 \\ \int_0^t K_r(t-\tau)\dot{X}(\tau)d\tau \approx C_r X_r(t) + D_r u(t) \end{cases} \qquad (3.22)$$

where A_r, B_r, C_r, and D_r are the system matrix, input matrix, output matrix and feedthrough matrix of the identified state space model, respectively. u is the control input and X_r is the system state vector.

For irregular waves, the surface elevation is created from the linear superposition of several harmonic wave components. Each component is selected from a wave spectrum $S_\omega(\omega)$, which is characterized by a peak frequency f_p and significant wave height H_{m_0}, used to describe the wave distribution over a wide range of wave frequencies (NREL and Sandia, 2014).

Hence, the wave excitation term F_{exc} under irregular wave conditions (Babarit et al., 2012) can be computed from taking the real part of an intergal term that contains all wave frequencies, as shown below:

$$F_{exc}(t) = \mathfrak{Re}\left[R_{rf}(t) \sum_{j=1}^{N} F_{exc}(\omega_j, \bar{\theta}) e^{i(\omega_j t + \psi_j)} \sqrt{2 S_\omega(\omega_j) d\omega_j} \right] \tag{3.23}$$

where j means the j-th component, N is the number of wave frequency bands.

Apart from the hydrodynamics mentioned in (3.14), the WEC-Sim software also allows the user to consider a mooring load by choosing a mooring stiffness or MoorDyn block (Hall, 2015), and set the other weakly nonlinear hydrodynamics such as Nonlinear Buoyancy and Froude-Krylov Wave Excitation, Morison Elements, etc. More details can be found on the website (NREL and Sandia, 2014). Note: The wave slamming and breaking effects are not considered in WEC-Sim since the model of highly non-linear hydrodynamic effects are beyond the scope of the WEC-Sim code.

3.3 Wavestar Prototype PAWEC modelling and regulation work design

A large number of studies in the literature describe the determination of hydrodynamic parameters of specific devices operating under assumed wave conditions. Only a few of these studies compare a variety of control approaches on a standard platform considering consistent wave excitation. The well-known WECCCOMP (Ringwood et al., 2017) focused on a point absorber type WEC or PAWEC, named Wavestar-prototype device (Zurkinden et al., 2014). A numerical model of the Wavestar-prototype device was developed in WEC-Sim software in support of the competition (Tom et al., 2018). In the first stage of the competition competitors tested and compared their innovative control strategies through an objective of maximizing performance metrics over a range of sea states. The Hull Control Group took part in the second stage of the competition

(Ringwood et al., 2023a), in which there were 3 teams in total. This involved an experimental wave tank implementation based on the 1:20 scaled Wavestar-prototype device at Aalborg University (Denmark). The Hull Group came 3rd in the competition and was the only competing group not equipped at the University with the scaled prototype. The lack of this facility has meant that this current thesis could not be based on experimental work. The simulation work presented in Chapters 4-7 are based on the WEC-Sim numerical model used in WECCCOMP.

The scaled Wavestar-prototype device can be considered as a kind of wave-activated body PAWEC (Ringwood et al., 2019), as shown in Figure 3.4. A hemispherical float is mechanically connected to an arm that can rotate around a fixed hinge point A, which has three independent motions (surge, heave and pitch). At the other side of the arm, a linear motor (power take-off system) is attached on the rotating arm to provide the power take-off force, and it only has one degree of freedom. The linear position and force measurements can be converted corresponding to rotational angular position and control moment (Tom et al., 2018). Alternatively, several up-stream wave gauges can be used to provide wave elevation information. Two rods can be seen in Figure 3.4 (a) the sketch model such as Rod EC and Rod BC which will be appear in the numerical Simulink model.

(a) The sketch model. (b) The physical model in laboratory.
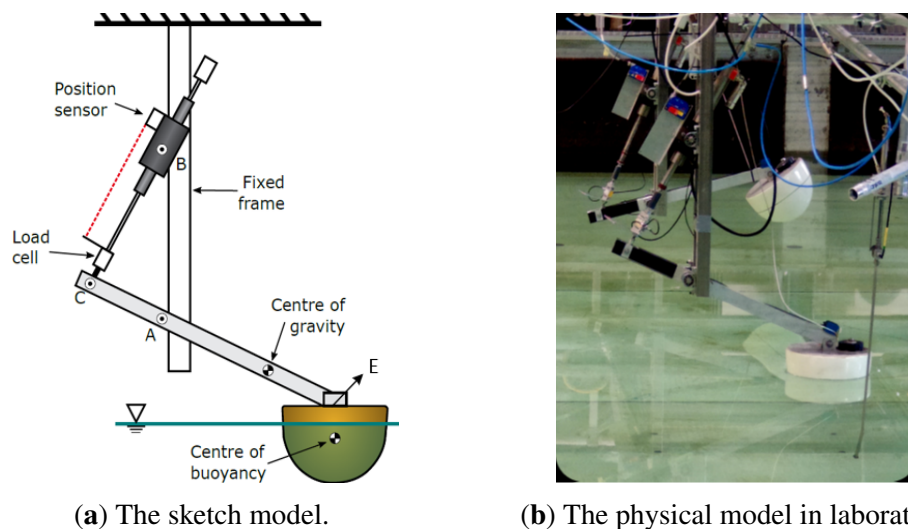
Figure 3.4: The scaled Wavestar-prototype PAWEC device (Peña-Sanchez, 2020).

The Wavestar-like device Simulink model in WEC-Sim not only includes the hydrodynamic response but also the physical inertia of linkages and joints, as shown in Figure 3.5, along with a CAD visualization see Figure 3.6.
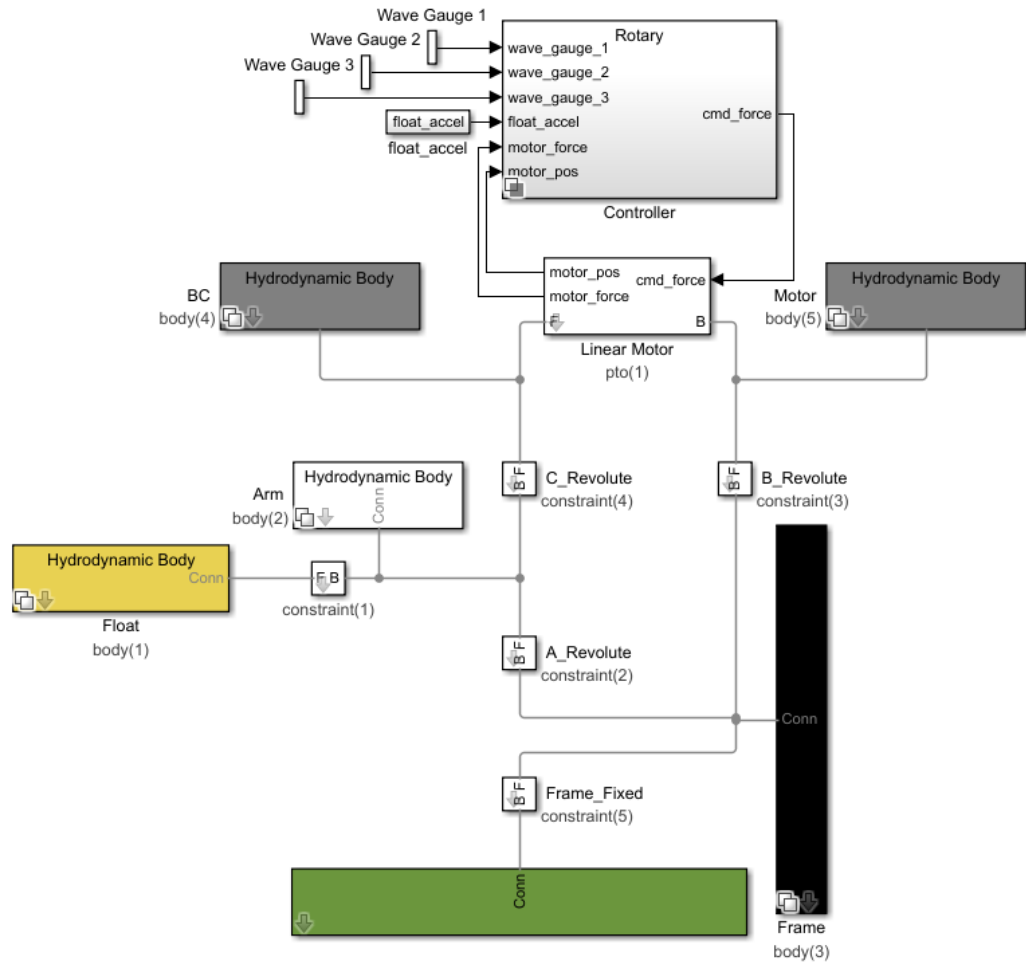
Figure 3.5: The scaled Wavestar Simulink model in WEC-Sim (Tom et al., 2018).
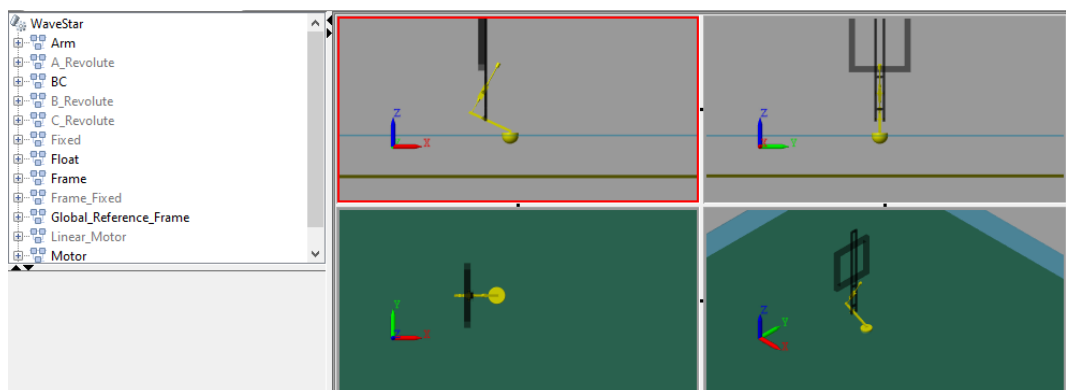
Figure 3.6: The WEC-Sim simulation visualization (Tom et al., 2018).

The Simulink model (Tom et al., 2018) contains body(1), a hydrodynamic body means the float, and body(2), body(3), body(4) and body(5), the other non-hydrodynamic

bodies which are the arm (Rod EC), frame, Rod BC and motor linear actuator mass. A linear motor (translational PTO) is labeled as pto(1), which represents the movement of Rod BC, and it is actuated by the control method designed in Controller block. The wave gauges, either linear motor position and force, or float angular displacement and motor rotary torque can be used as Controller inputs. There has a fixed connection block between the float and arm (point E), labeled as constraint(1). Additionally, the constraint(2), constraint(3) and constraint(4) denote the revolute joints A, B and C, respectively. The hydrodynamic solution from the BEM solver WAMIT is provided in advance. The hydrodynamic coefficients were computed at angular frequencies ∞ rad/s and between 0.2 rad/s and 40 rad/s. The Simulink model was validated by (Tom et al., 2018) through comparison to experimental data from Aalborg University. The model dimensions and mass properties relative to the still water line (SWL) are given in Table 3.1.

Table 3.1: Wavestar numerical mass properties and model dimensions at SWL (Tom et al., 2018).

Parameters	Values [Unit]
Float Mass	3.075 [kg]
Float Cg (x, z)	$(0.051, 0.053)$ [m]
Float MoI (at Cg)	0.001450 $[kg \cdot m^2]$
Float Draft	0.11 [m]
Float Diameter (at SWL)	0.256 [m]
Arm Mass	1.157 [kg]
Arm Cg (x, z)	$(-0.330, 0.255)$ [m]
Arm MoI (at Cg)	0.0606 $[kg \cdot m^2]$
Hinge A (x, z)	$(-0.438, 0.302)$ [m]
Hinge B (x, z)	$(-0.438, 0.714)$ [m]
Hinge C (x, z)	$(-0.621, 0.382)$ [m]

In order to reduce the design complexity for estimation and control, the hydrodynamic response of the float-arm can be equivalent to pitch moment only around the fixed hinge point. This means that the linear position and force measurements can be converted to the rotational displacement and moment. Then the following float rotational dynamics (Tona et al., 2019) at the hinge point A can be considered as the equivalent pitch moment:

$$
\begin{aligned}
(J_{fa} + J_\infty)\ddot{\theta}(t) &= -K_{hs}\theta(t) - K_v\dot{\theta}(t) + M_{ex}(t) - M_{ra}(t) - M_{PTO}(t) \\
\dot{r}_a(t) &= A_{ra}r_a(t) + B_{ra}\dot{\theta}(t) \\
M_{ra}(t) &= C_{ra}r_a(t) + D_{ra}\dot{\theta}(t)
\end{aligned}
\tag{3.24}
$$

where J_{fa} is the total (float and arm) mass moment of inertia, J_∞ is the added mass moment of inertia, $\ddot{\theta}$ is the rotational angular acceleration of the float, K_{hs} and K_v are the hydrostatic stiffness coefficient and linear damping coefficient, respectively, and M_{ra}, M_{ex} and M_{PTO} are the radiation damping moment, the equivalent wave excitation moment and PTO moment around the hinge point. The radiation damping moment $M_{ra} = \int_0^t h_r(t-l)\dot{\theta}(l)dl$ is a convolution integral term, which can dramatically increase computational burden and bring difficulties in estimation and control work design. To overcome these problems, the convolution term is converted into a second-order linear state space model by using system identification according to Prony's method (Tona et al., 2019) according to the realization theory. The internal variable $r_a(t)$ in the identified second-order state space model does not have physical meaning. $(A_{ra}; B_{ra}; C_{ra}; D_{ra})$ are the state space identified matrices of the convolution term of M_{ra}.

Theoretically, the equivalent wave excitation moment around the hinge point can be computed as:

$$M_{ex} = -F_{ex,x}sin(\theta_0 + \theta)l_{arm} - F_{ex,z}cos(\theta_0 + \theta)l_{arm} + M_{ex,\theta} \qquad (3.25)$$

where θ_0 is the initial angular displacement of the float when it is located at the equilibrium point, l_{arm} is the length of the arm, and $F_{ex,x}$, $F_{ex,z}$, $M_{ex,\theta}$ are the surge, heave and pitch direction components of the wave excitation force acting on the float.

The state space model of the PAWEC system can then be expressed as:

$$\begin{aligned} \dot{x} &= Ax + Bu + BM_{ex} \\ y &= Cx \end{aligned} \qquad (3.26)$$

where $A = \begin{bmatrix} 0 & 1 & \mathbf{0}_{1\times2} \\ -\dfrac{K_{hs}}{J_t} & -\dfrac{K_v + D_{ra}}{J_t} & -\dfrac{C_{ra}}{J_t} \\ \mathbf{0}_{2\times1} & B_{ra} & A_{ra} \end{bmatrix}, x = \begin{bmatrix} \theta \\ \dot{\theta} \\ r_a \end{bmatrix}, B = \begin{bmatrix} 0 \\ \dfrac{1}{J_t} \\ \mathbf{0}_{2\times1} \end{bmatrix}, u = -M_{PTO},$

$C = \begin{bmatrix} 1 & 0 & \mathbf{0}_{1\times2} \\ 0 & 1 & \mathbf{0}_{1\times2} \end{bmatrix}.$

The state variables θ and $\dot{\theta}$ are the angular displacement and velocity of the float. r_a is the internal variable of the identified state space model in Equation (3.24). Concerning the model parameters, $J_t = J_{fa} + J_\infty$ is the total inertia, where $\mathbf{0}_{p\times q}$ denotes a zero matrix with p rows and q columns.

The electrical energy E_e absorbed by the grid (Guerrero-Fernandez et al., 2023) can be defined as:

$$E_e(t) = \int_t^{t+T_l} P_{el}(r)dr = \int_t^{t+T_l} \Gamma(r)P_m(r)dr \tag{3.27}$$

where P_m is the absorbed mechanical power by the PTO system, Γ is the conversion efficiency, P_{el} is the extracted electrical power, T_l is a time horizon and r is the integration variable.

In general, the PTO systems will not be ideal and perfect in energy conversion in real-world applications. There are bound to have some energy loss. Additionally, there still have power flow between the PAWEC float and grid, which involves the bi-directional flow problem. When the energy is absorbed from the incident waves, the PTO system works as a generator. On the contrary, if the energy is poured from the PAWEC device into the waves, the PTO system plays like a motor.

The relationship between P_{el} and P_m is given below:

$$P_{el}(t) = \Gamma(t)P_m(t) = -\Gamma(t)M_{PTO}(t)\dot{\theta}(t), \begin{cases} \Gamma(t) = \mu_{gen} & if\, P_m(t) \geq 0 \\ \Gamma(t) = \mu_{mot} & if\, P_m(t) < 0 \end{cases} \tag{3.28}$$

where μ_{gen} is the efficiency when the PTO system is assumed to be working in generator mode and μ_{mot} is the motor mode efficiency.

Regulation work design based on SMC

As the research Aim and Objectives described in Section 1.3, the main idea of this PhD study is to design advanced control strategies (See Chapters 5 and 6) based on a hierarchical tracking structure for the 1:20 scaled Wavestar-like PAWEC to reach a near-resonance condtion in order to achieve the energy maximization generation. Before the tracking control work design, it is necessary to test the regulation work on the PAWEC device to check and see if the WEC-Sim numerical modelling is reasonable.

Here, the basic SMC method is selected to stabilize the PAWEC system and regulate it to stay at the equilibrium point, which means that the PAWEC float displacement and velocity will remain at the zero.

Based on the state space model (3.26), a switching function can be defined as:

$$s_r = S_r x \tag{3.29}$$

The hyperplane S_r (Edwards and Spurgeon, 1998) is defined by

$$S_r = \{x \in \mathfrak{R}^{1 \times 4} : s_r(x) = 0\} \tag{3.30}$$

The time derivative of s_r is

$$\dot{s}_r = S_r \dot{x} = S_r(Ax + Bu + BM_{ex}) \tag{3.31}$$

Considering the system states converge to and stay on the surface S_r, to define the SMC control law u as:

$$u = u_{lr} + u_{nr} \tag{3.32}$$

u_{lr} is the linear equivalent term and u_{nr} is the nonlinear switching term.

$$u_{lr} = -(S_r B)^{-1} S_r Ax - \hat{M}_{ex}, \; u_{nr} = -k_{nr}s_r - \varepsilon_r sign(s) \tag{3.33}$$

where k_{nr} and ε_r are positive constants. $\hat{M}_{ex}$ is the estimated WEM that can be obtained from the observers proposed in Chapter 4.

Next, define a Lyapunov function:

$$V_r = \frac{1}{2}s_r^2 \tag{3.34}$$

The time derivative of (3.34) has the form:

$$\dot{V}_r = s_r \dot{s}_r = s_r(S_r Ax + S_r Bu + S_r BM_{ex}) \tag{3.35}$$

Substituting (3.32) into (3.35) it follows that:

$$\begin{aligned} \dot{V}_r &= s_r[S_r B(M_{ex} - \hat{M}_{ex}) - k_{nr}s_r - \varepsilon_r sign(s_r)] \\ &\leq -k_{nr}||s_r||_2^2 - ||s_r||_2(\varepsilon_r - ||\Delta M||_2) \end{aligned} \tag{3.36}$$

where $\Delta M = S_r B(M_{ex} - \hat{M}_{ex})$, $sign(s_r)$ is the signum function of s_r.

According to (3.36), if $\varepsilon_r > ||\Delta M||_2$, then $\dot{V}_r \leq 0$ is satisfied. The stability of the control system is thus proved which means that the system states can reach and remain at the sliding surface with an ideal sliding motion in finite time.

3.4   Basic tests on numerical modelling

The parameters of the float rotational dynamics at hinge point A (Tona et al., 2019) are listed as shown in Table 3.2, used for doing numerical simulations in this thesis work. The JONSWAP wave Spectrum is adopted to generate six irregular waves (Ringwood et al., 2019) which can be seen in Table 3.3.

Table 3.2: The simulation parameters.

Parameters	Values
Total mass (float, arm and added) moment of inertia J_t	$1.4805 \ \text{kg} \cdot \text{m}^2$
Hydrostatic coefficient K_{hs}	$92.33 \ \text{Nm} \cdot \text{rad}^{-1}$
Linear damping coefficient K_v	$1.8 \ \text{Nm} \cdot \text{rad}^{-1}\text{s}^{-1}$
Length of the arm l_{arm}	$0.54875 \ \text{m}$
Efficiency of generator mode μ_{gen}	0.7
Efficiency of motor mode μ_{gen}	0.7^{-1}
System matrix A_{ra}	$A_{ra} = \begin{bmatrix} -13.59 & -13.35 \\ 8.0 & 0 \end{bmatrix}$
Input matrix B_{ra}	$B_{ra} = \begin{bmatrix} 8.0; 0 \end{bmatrix}^T$
Output matrix C_{ra}	$C_{ra} = [4.739 \quad 0.5]$
Feedthrough matrix D_{ra}	$D_{ra} = -0.1586$

The significant wave height H_{m0}, the peak wave period T_p and the wave peak enhancement factor $\varkappa$ are used to parametrize the various sea scenarios. The spectral energy distribution of the selected seastates are given in Figure 3.7. Combined with Table 3.3, it can be seen that the spectral energy will be increased when the significant wave height H_{m_0} and peak wave period T_p become larger from Seastate1 to Seastate3 and Seastate4 to Seastate6. On the other hand, if the H_{m_0} and T_p are held at constant values, the spectral energy gets larger when the wave peak enhancement factor $\varkappa$ is increased.

Table 3.3: JONSWAP Specturm sea states.

Sea State	H_{m_0}	T_p	$\varkappa$
Seastate1	0.0208	0.988	1
Seastate2	0.0625	1.412	1
Seastate3	0.1042	1.836	1
Seastate4	0.0208	0.988	3.3
Seastate5	0.0625	1.412	3.3
Seastate6	0.1042	1.836	3.3

(a) Sea State 1.

(b) Sea State 2.

(c) Sea State 3.

(d) Sea State 4.

(e) Sea State 5.
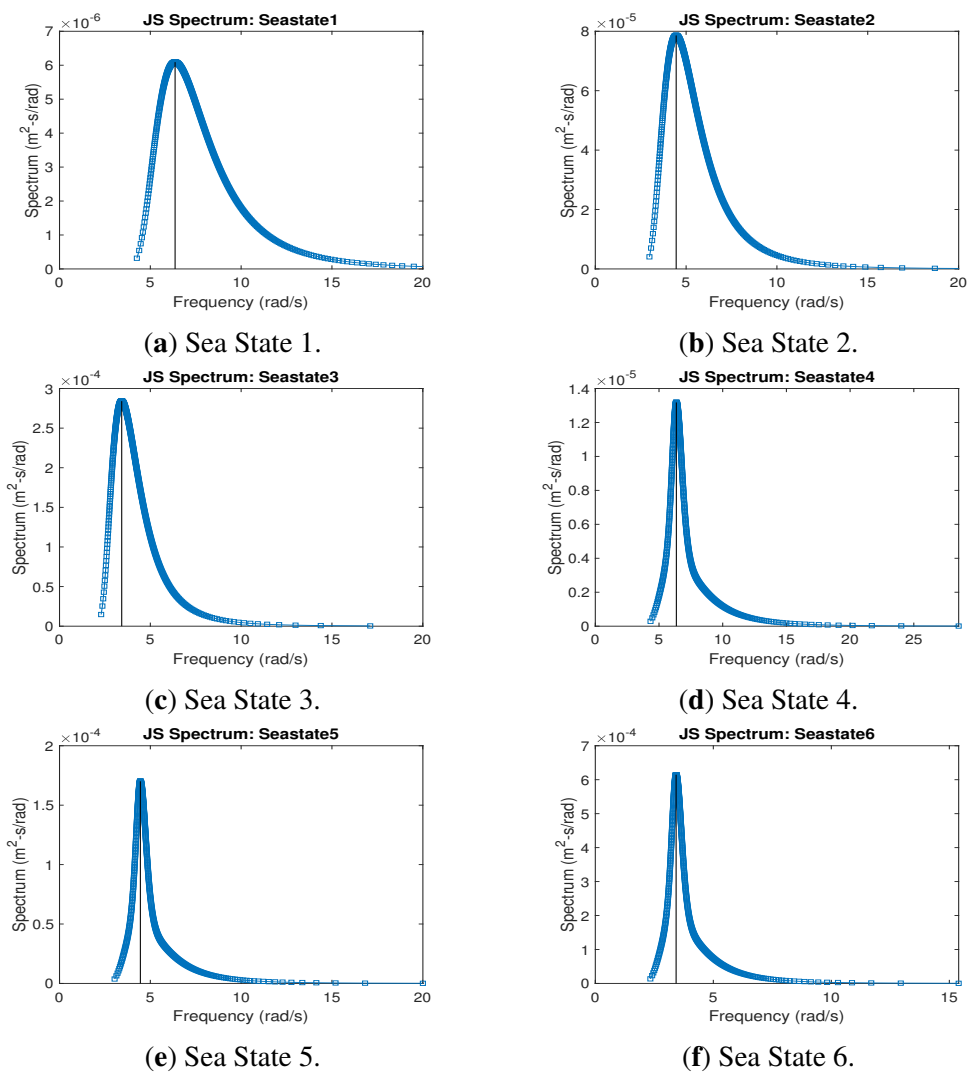
(f) Sea State 6.

Figure 3.7: The JONSWAP Spectrum for six sea states.

According to the Equation (3.25), the wave excitation moment M_{ex} can be calculated using the ideal formula. Apart from this, the default M_{ex} can also be obtained from

the WEC-Sim output measurement when the PAWEC device is fixed at Hinge point A. This means that the excitation test procedure can be carried out when the float is fixed and cannot oscillate, to measure and acquire the wave excitation moment. The results of two ways for computing M_{ex} under 6 irregular waves are given in Figure 3.8.

(**a**) Sea State 1.

(**b**) Sea State 2.

(**c**) Sea State 3.

(**d**) Sea State 4.

(**e**) Sea State 5.
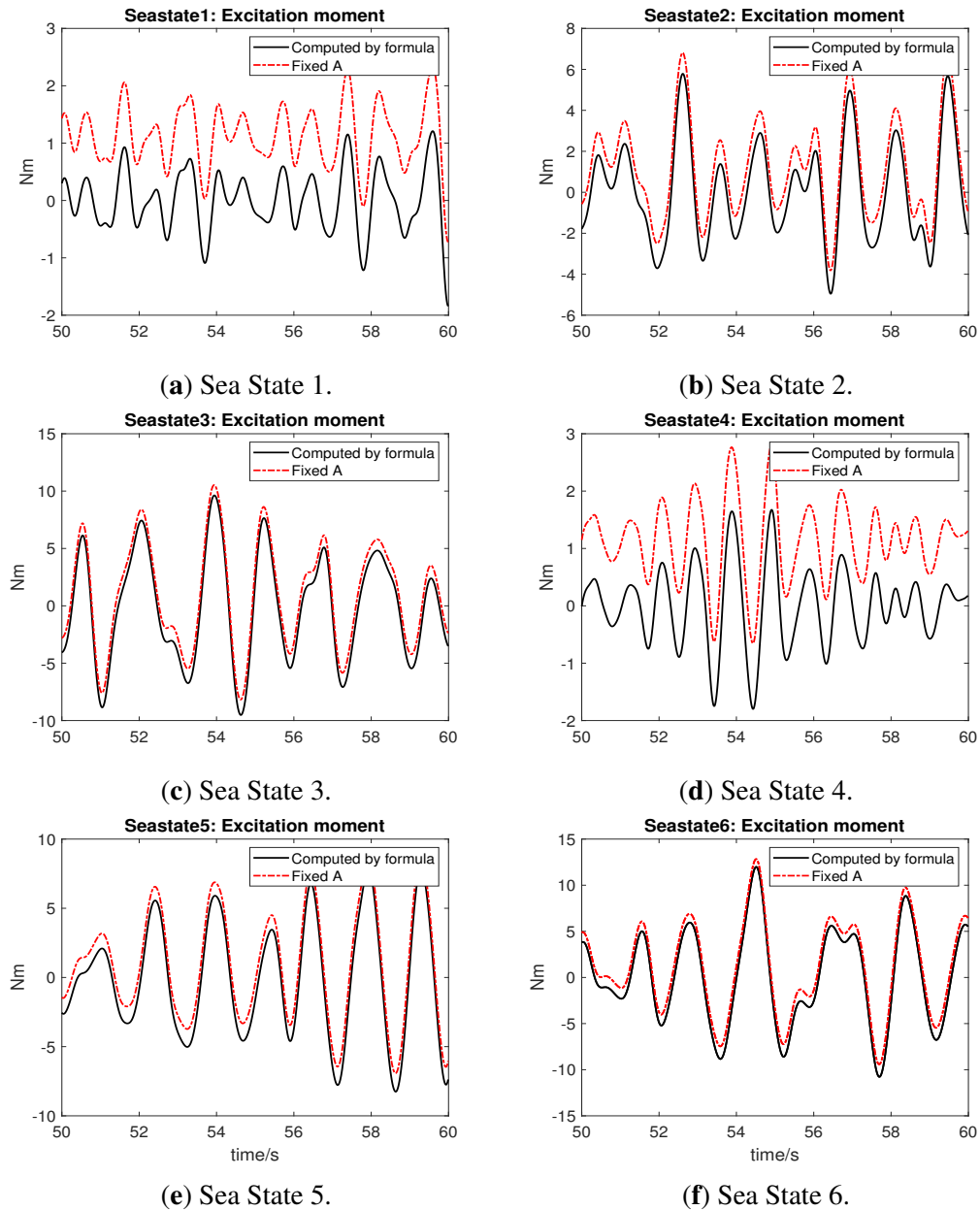
(**f**) Sea State 6.

Figure 3.8: Wave excitation moment measured at fixed point A vs computed moments for six sea states.

However, although the phase remains the same in both cases, there exists an amplitude offset between the computed M_{ex} and measured M_{ex} from a fixed A constraint. The

reason for this is that there is an additional moment due to the offset between CoG and CoB, and a static moment caused by the weight of the arm between the float and the point A. The bias of the excitation moment is ~ 1.25Nm. Figure 3.9 presents the computed M_{ex} from the formula and the compensated M_{ex}. It can be seen that the offset is almost removed from the value of the excitation moment.

(a) Sea State 1.

(b) Sea State 2.

(c) Sea State 3.

(d) Sea State 4.

(e) Sea State 5.
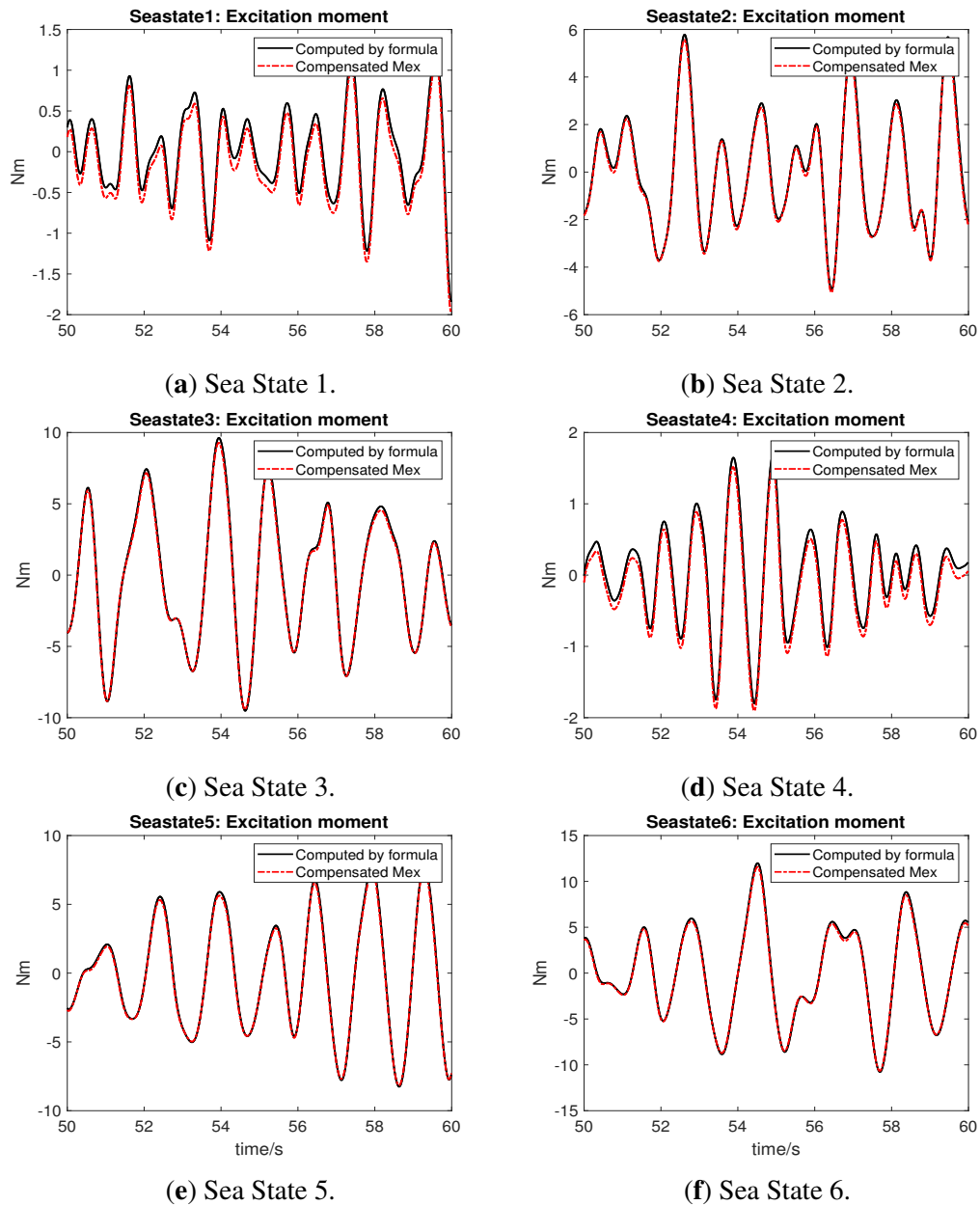
(f) Sea State 6.

Figure 3.9: Wave excitation moment being compensated vs computed by Equation (3.25) for six sea states.

In order to check and test the approximated state space model of the radiation damping moment M_{ra}, Figure 3.10 gives the results of the default radiation damping moment in

WEC-Sim and the calculated M_{ra} from state space model. This indicates that the state space model in Equation (3.24) is a feasible and proper representation of the radiation damping moment convolution integral term of the WEC-Sim under 6 Seastates, even if a small phase bias is evident between them.

(a) Sea State 1.

(b) Sea State 2.

(c) Sea State 3.

(d) Sea State 4.

(e) Sea State 5.

(f) Sea State 6.
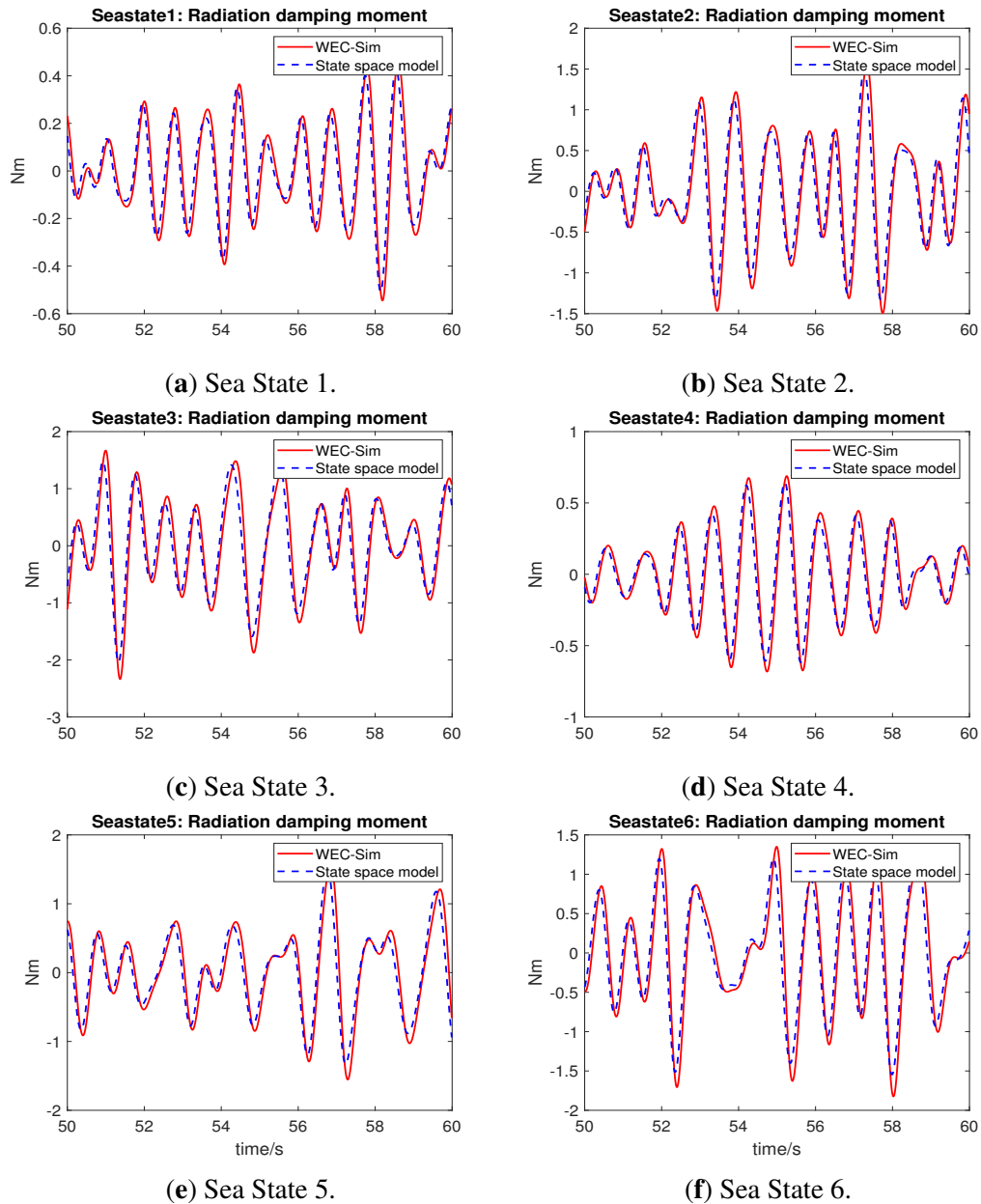
Figure 3.10: Radiation damping moment from WEC-Sim vs state space model approximation.

Figure 3.11 illustrates the surge, heave, pitch components of the wave excitation moment Equation (3.25) acting on the float. The equivalent excitation moment at the hinge

point A is also illustrated. This equivalent moment comprises the superposition of the three direction components based on the Equation (3.25).
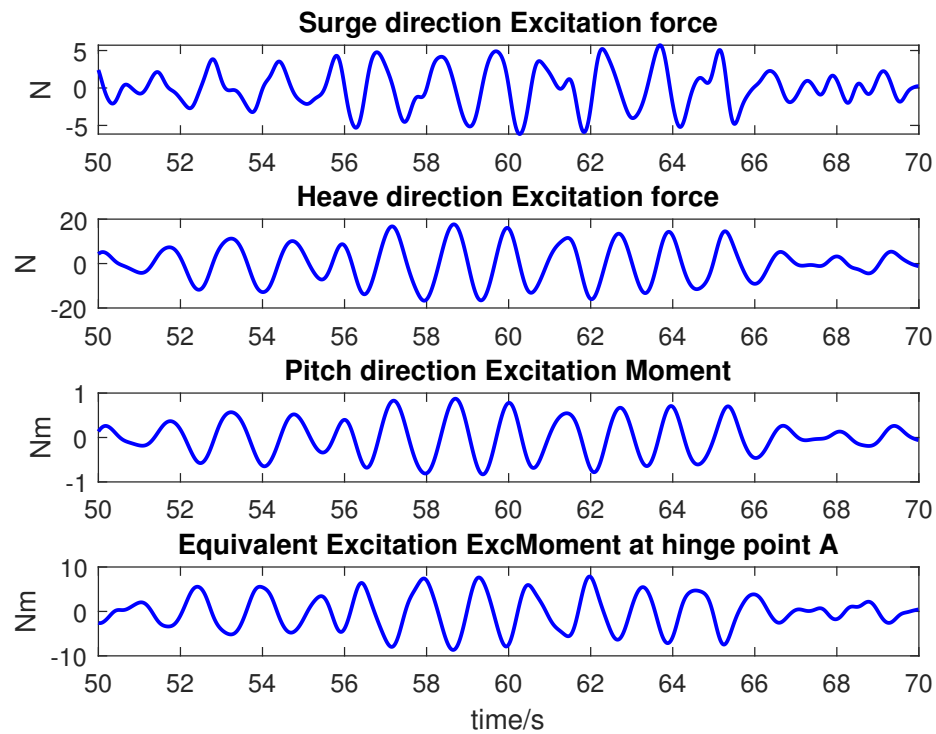
Figure 3.11: The components of wave excitation force in surge, heave, pitch directions and equivalent excitation moment at hinge point A (Seastate 5).

Additionally, the results of two different M_{PTO} forced motion tests are shown in Figures 3.12 and 3.13. The sinusoidal and mult-sine PTO moment signals are selected to do a simple checking on the scaled Wavestar-like numerical modelling. Figure 3.12 shows the sinusoidal signal test and Figure 3.13 shows the multi-sine signal test. The multi-sine signal consists of a linear combination of some simultaneously generated sinusoids. The float angular displacement and velocity results of both tests can be seen in both Figures 3.12 and 3.13.
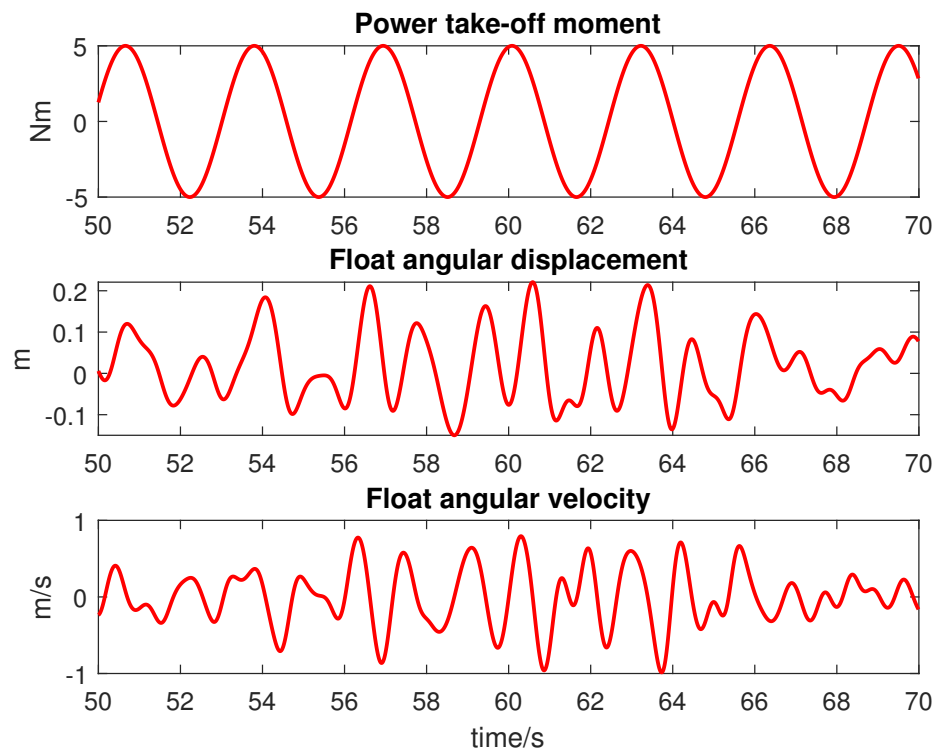
Figure 3.12: Sinusoidal signal of PTO moment test (Seastate 5).
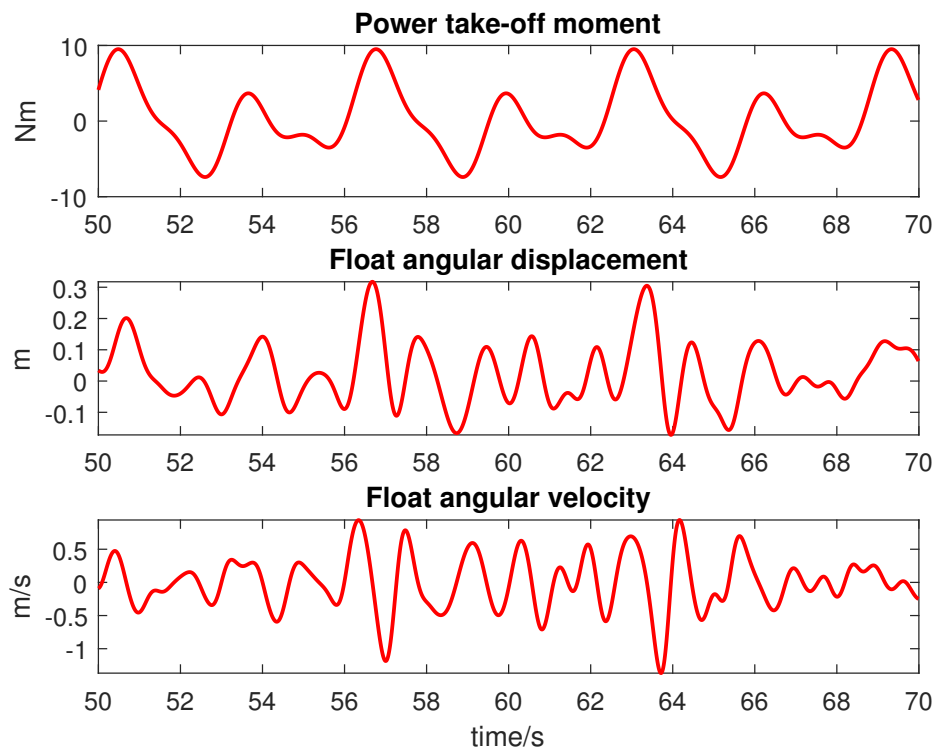
Figure 3.13: Multi-sine signal of PTO moment test (Seastate 5).

(a) Sea State 1.

(b) Sea State 2.

(c) Sea State 3.

(d) Sea State 4.

(e) Sea State 5.

(f) Sea State 6.
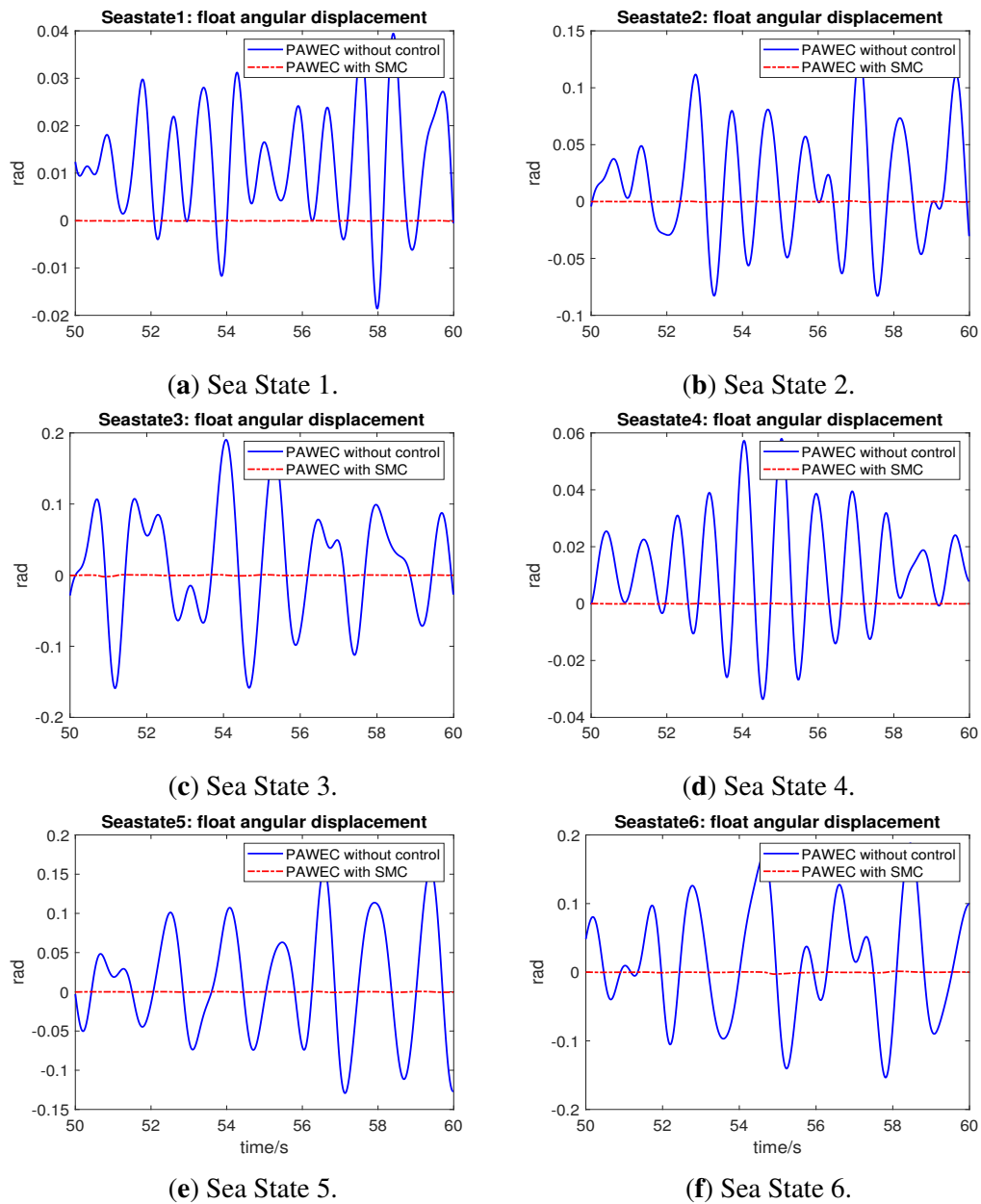
Figure 3.14: Regulation test: the float angular displacement of PAWEC without control or with SMC.

The SMC displacement and velocity regulation responses of the PAWEC device are shown in Figure 3.14 and Figure 3.15, respectively. The simulation results are also compared with the cases when the PAWEC system just oscillates by the incoming waves without any control force being acting on it. This is repeated for the six irregular Sea states. It is clear that the SMC scheme effectively provides sufficient effectiveness to maintain stability of the PAWEC Wavestar-prototype, at the equilibrium point. The results show that the PAWEC system states (float angular displacement and angular

velocity) remained close to zero.

(**a**) Sea State 1.

(**b**) Sea State 2.

(**c**) Sea State 3.

(**d**) Sea State 4.

(**e**) Sea State 5.

(**f**) Sea State 6.
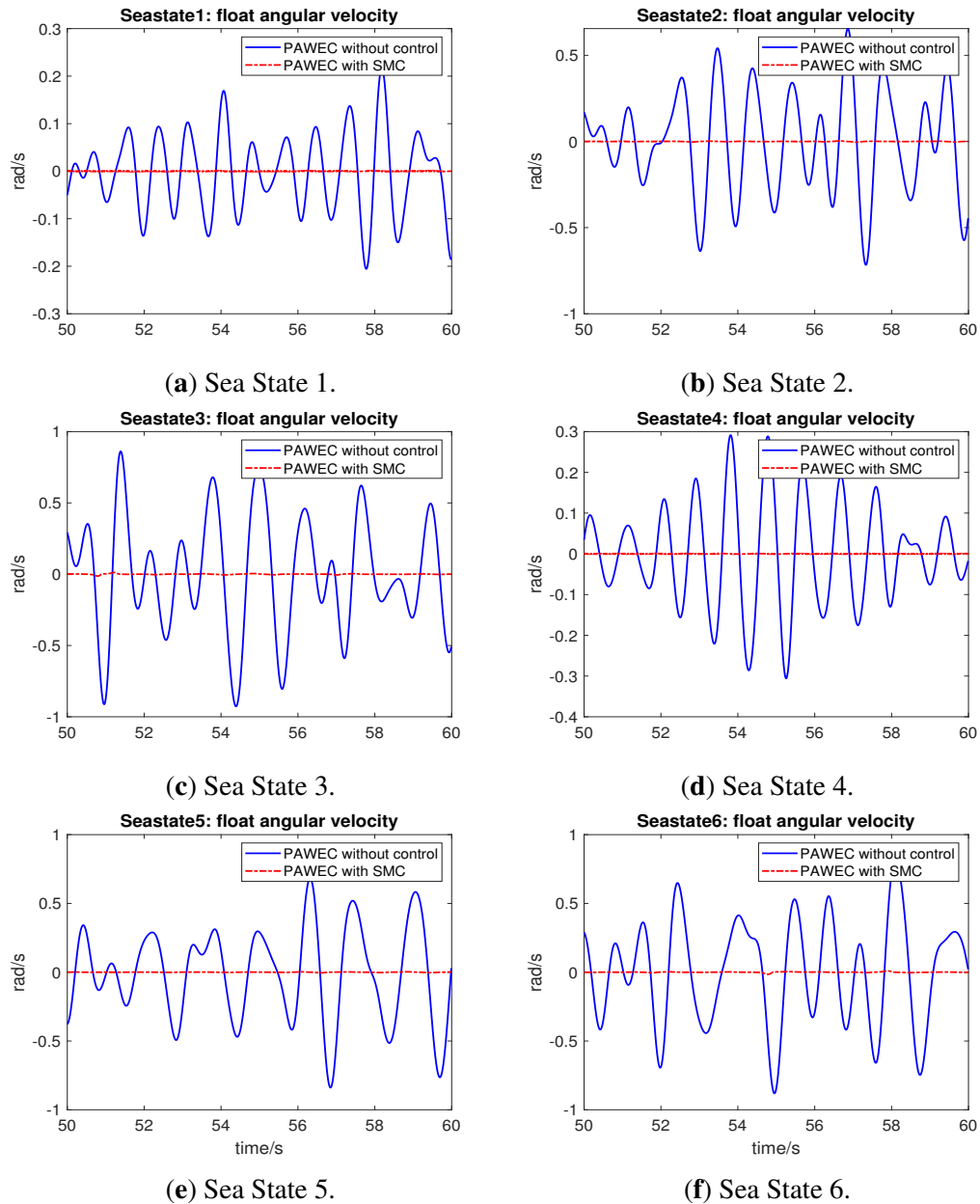
Figure 3.15: Regulation test: the float angular velocity of PAWEC without control or with SMC.

3.5 Summary

This Chapter introduces the flowchart of WEC-Sim software and described the steps of running a WEC-Sim numerical simulation. Following this the wave generation descrip-

tion and some background theory behind the numerical modelling analysis are given. Next, a numerical modelling for a Wavestar-like device (the 1:20 scaled benchmark) is illustrated including the WEC-Sim numerical model and its rotational dynamics based on the well-known Cummin's Equation at the hinge point A, in order to build a state space model for this thesis for the purpose of energy-maximizing control design. Finally, the numerical model in WEC-Sim is verified based on some basic tests. For example, the validation of ideal excitation moment formula (3.25) and the checking of radiation moment state space approximation (3.24), sinusoidal and mult-sine PTO moment signal tests, and the regulation test based on SMC.

Recall that the main focus of the thesis work is a study on the development of Energy-Maximizing Control Design for the 1:20 scaled Wavestar-prototype device, under irregular wave condtions. As a part of this work the WEM estimation and the determination of optimal reference have to be prepared before the tracking control work can be achieved. Hence, the purpose of Chapter 4 is to introduce some practical ways realising estimator designs for WEM estimation. Following this, the calculation of the optimal reference velocity, based on the WEC-Sim numerical model is described. The numerical model continues to be used in the WEC-Sim simulation studies described in Chapters 5, 6 and 7.

Chapter 4

Wave Estimation Strategies for PAWEC Control

4.1 Introduction

As described in Chapter 1 Figure 1.5, the hierarchical tracking control structure for PAWEC energy maximization is the main idea and contribution of this thesis, based on the use of the 1:20 scaled Wavestar-like device. The contribution contains two parts:

- The high-level part, including WEM estimation (Li and Patton, 2023c) and reference signal computation (Li and Patton, 2023a).

- The low-level work comprises the design of an energy-maximizing controller (Li and Patton, 2023b).

The low-level model-following mixed LQR/H_∞ tracking control and SMC work are discussed in Chapter 5 and the model-predictive velocity tracking control is proposed in Chapter 6. This Chapter focuses on the WEM estimation of the high-level part design. Some robust methods are proposed that can fit well in practice in simulation feasibility study. This also includes the determination of the optimal reference signal for the PAWEC tracking control. Theoretically, the WEM is assumed to be a narrow-band harmonic process and modelled as a single cyclical component based on Harvey's structural model (Li and Patton, 2023a). Following this, it is shown how an on-line estimation can be performed to obtain the instantaneous amplitude and frequency of WEM using an EKF to compute the reference velocity.

Some simple but effective robust methods are considered to design four different estimators (See Section 1.4):

(1) UIO with LMI,

(2) LO with LMI,

(3) LO with pole-placement, and

(4) ASMO.

The designs and derivations of each estimators are given in Section 4.2. The linear modelling including modelling errors and system uncertainty are inevitable in the PAWEC system. Hence, the estimator is better to be considered in a robust way, in order that its estimation performance satisfies the efficient and robust operation over a suitably wide enough range of irregular waves. The EKF is selected in Section 4.3 to obtain the instantaneous amplitude and frequency of the WEM in order to be able to calculate the optimal reference velocity. Recall that the reference velocity is required to achieve energy-maximising tracking control and this is essential for the study considered in Chapters 5 and 6. The simulation results of the WEM estimation work and the calculated reference velocity are shown in Section 4.4, where four estimators are analysed based on suitable performance indices. Section 4.5 summarises this estimation study, prior to applying it in the Control designs of Chapters 5 and 6.

4.2   Estimator designs

As mentioned in Chapter 2, the PAWEC oscillates with the incoming waves in a non-fixed body (Guo, 2017) structure. And the WEF is a physically unmeasurable quantity for the real application of PAWEC devices (Guo et al., 2018). However, for PAWEC systems the WEF itself is difficult to measure by some sensors and it usually needs to be calculated or estimated by one or more alternative approaches (Guo et al., 2018; Abdelrahman and Patton, 2019). Usually the estimation or calculation of WEF plays an important part of the PAWEC maximum energy absorption (Garcia-Abril et al., 2017). Moreover, the WEF is required to be as accurate as possible to further improve the control performance. There have abundant control strategies have been employed for the purpose of energy maximisation extraction (Guo and Ringwood, 2021) but most of them require the WEF information.

(Peña-Sanchez, 2020) illustrates a critical comparison of 11 different estimation methods in his thesis. According to the following classification, those methods can be divided into three groups: (i) The requirement of using wave elevation measurements: the WEF $F_{exc}(t)$ can be calculated by doing a convolution operation on wave elevation $\eta(t)$ and the time domain kernel function $k_e(t)$. $k_e(t)$ can be obtained from the inverse Fourier transform of the frequency domain response of excitation force (Guo et al., 2018). However, a frequently encountered challenge is that the kernel function $k_e(t)$ is non-casual feature which can render this approach as physically unimplementable. A time-shift technique (Guo, 2017) can be used to overcome this non-causality problem by choosing a wave predictor to provide the wave elevation prediction $\eta_p(t)$ to the causalised form $k_{e,c}(t)$ for computing the WEF, as shown in Figure 4.1. t_c is the selected causalisation time (Falnes, 1995). This type of approach is not affected by the viscous/friction forces, but it is not valid for calculating the WEF under irregular waves. Since this study is limited to irregular waves it is not considered in this work, beyond mention here.
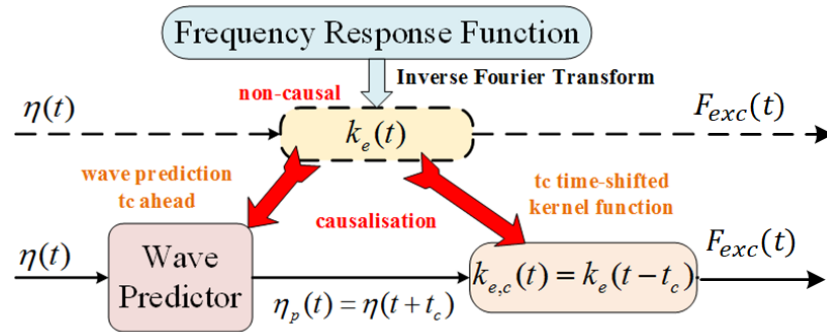
Figure 4.1: The wave elevation-based approach for WEF calculation (Guo, 2017).

(ii) The requirement of using both PAWEC motion and pressure measurements: the concept of this structure is to firstly obtain the total wave force $F_w(t)$ based on the pressure information form some pressure sensors installed on the wet surface of the WEC float. Then the radiation force $F_{ra}(t)$ and hydrostatic force $F_{hs}(t)$ can be calculated separately based on the linear variable displacement transducer and accelerometer (Guo et al., 2018). Thus the WEF $F_{exc}(t)$ can be computed by using $F_w(t)$ subtracting the Hydrostatic and Radiation forces $F_{hs}(t)$ and $F_{ra}(t)$, as can be seen in Figure 4.2. Where k_m is hydrostatic coefficient and $v(t)$ is the bouy velocity.
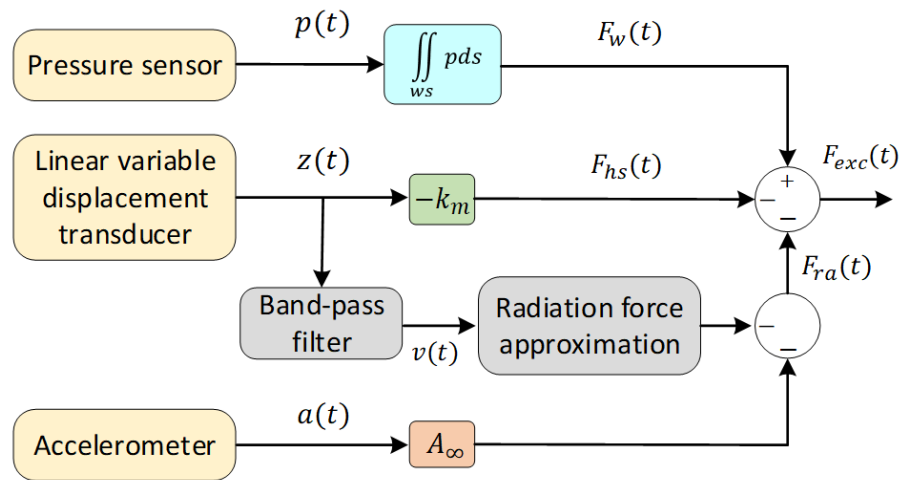
Figure 4.2: Both PAWEC motion and pressure meaurements based WEF computation (Guo, 2017).

This structure can be used to get $F_{exc}(t)$ under irregular wave conditions and is not affected by friction forces. But it relies on using lots of measurement sensors that will suffer significantly from the measurement noise, especially for real applications. Moreover, the WEC-Sim benchmark does not offer the pressure information of the WEC system, hence, this structure is also not involved to do research work in this PhD study.
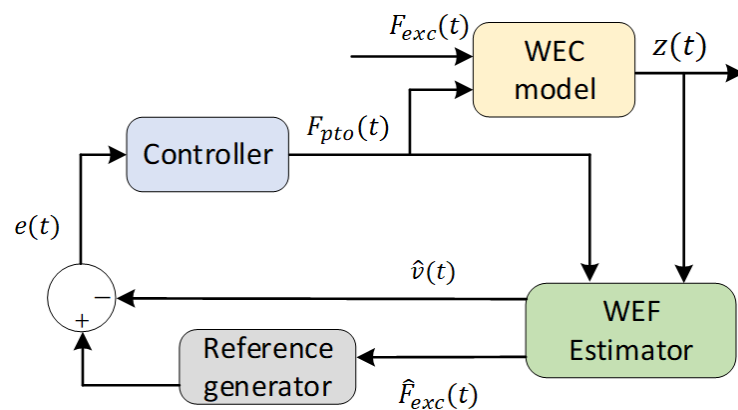
Figure 4.3: The PAWEC motion based way for WEF estimation (Guo, 2017).

(iii) The requirement of using PAWEC motion measurements: Figure 4.3 shows the idea of WEF estimation based on the WEF estimator that can be based on different estimation approaches (Peña-Sanchez et al., 2019), which can provide the more free-dom for the estimation computation according to the requirements on robust or optimal

mechanisms. This is a more general way that is followed by many researchers for estimating the WEF since only displacement meassurement is needed. Hence, it is easy to implement for PAWEC devices excited by irregular waves (Guo, 2017). This thesis follows the procedure of using the PAWEC motion measurement.

In the review paper (Peña-Sanchez et al., 2019), some of the approaches are based on Kalman filter (KF) (Nguyen and Tona, 2017b; Ling, 2015) or EKF (Crassidis and Junkins, 2004; Abdelkhalik et al., 2017), which requires *a priori* knowledge of the process and measurement covariance matrices. Otherwise, the KF and EKF methods lose their effectiveness and even suffer from a diverge problem due to lack of robustness resulting from parameter uncertainty. Both the Fast Adaptive Unknown Input Estimator (Abdelrahman et al., 2016) and Unknown Input Observer (Abdelrahman and Patton, 2017) are designed based on LMI and show the robustness to some extent. However, the LMI feasibility problem would bring a side effect in calculating the observer gain and limit the estimation performance. In addition, the other estimators are described and discussed, such as the receding horizon method (Nguyen and Tona, 2017b), convolution with predicted wave elevation (Guo et al., 2017), pressure acceleration displacement method (Guo et al., 2018), unified linear input and state approach (Yong et al., 2016) and so on. Basically, the majority of methods can show satisfactory estimation performance but with high computation burden or lack of robustness against system uncertainty. Moreover, most of the approaches are model-based and use linear WEC modelling which naturally involves unmodeled dynamics and system uncertainty from the real PAWEC applications. Therefore, the simple but effective robust WEF estimation design is required and should be developed.

As this study focuses on the use of the scaled Wavestar-prototype device, it can be seen (Figure 3.4 in Section 3.3) that the Cummin's Equation 3.24 for this problem concerns rotational dynamics, with the terms in the Equation representing moments rather than forces. Hence, the concept of Wave Excitation Moment (WEM) replaces the WEF as the modelling outline given in Chapter 3. However, the estimation can still be designed using the same procedure, but just with different dynamics. The assumption that equivalent M_{ex} is based on the hinge point A can reasonably be considered as an "unknown input" term for the special Wavestar-like device. This means that Unknown Input Observer designs which only use the PAWEC motion measurements can be used reliably.

Hence, for the M_{ex} estimation, an augmented form of the state-space system (3.26) will have to be used as follows:

$$\dot{x}_o = A_o x_o + B_o u + D_o d$$
$$y = C_o x_o$$

(4.1)

where $A_o = \begin{bmatrix} 0 & 1 & \mathbf{0}_{1\times 2} & 0 \\ -\dfrac{K_{hs}}{J_t} & -\dfrac{K_v + D_{ra}}{J_t} & -\dfrac{C_{ra}}{J_t} & \dfrac{1}{J_t} \\ \mathbf{0}_{2\times 1} & B_{ra} & A_{ra} & \mathbf{0}_{2\times 1} \\ 0 & 0 & \mathbf{0}_{1\times 2} & 0 \end{bmatrix}$, $x_o = \begin{bmatrix} \theta \\ \dot{\theta} \\ r_a \\ M_{ex} \end{bmatrix}$, $B_o = \begin{bmatrix} 0 \\ \dfrac{1}{J_t} \\ \mathbf{0}_{3\times 1} \end{bmatrix}$,

$u = -M_{PTO}$, $C_o = \begin{bmatrix} 1 & 0 & \mathbf{0}_{1\times 3} \\ 0 & 1 & \mathbf{0}_{1\times 3} \end{bmatrix}$, $D_o = \begin{bmatrix} 0 & 1 & \mathbf{0}_{1\times 2} & 0 \\ 0 & 0 & \mathbf{0}_{1\times 2} & 1 \end{bmatrix}$,

$d = \begin{bmatrix} d_1 \\ d_2 \end{bmatrix}$ denotes the lumped disturbances (unmodeled dynamics, uncertainties, etc).

The estimated WEM $\hat{M}_{ex}$ can be obtained after the estimation of the state vector x_o using the output measurements y.

4.2.1 UIO with LMI

The UIO (Zhu and Li, 2021b) can generally be defined as:

$$\dot{z} = M_u z + G_u u + L_u y$$
$$\hat{x}_o = z + H_u y$$

(4.2)

where $z \in \Re^5$ means the observer state vector, $M_u \in \Re^{5\times 5}$, $G_u \in \Re^{5\times 1}$, $L_u \in \Re^{5\times 2}$ and $H_u \in \Re^{5\times 2}$ are observer matrices desired to be designed. $\hat{x}_o \in \Re^5$ is the estimate of x_o. To give the estimation error of UIO as $e_u = x_o - \hat{x}_o$, and calculate its time derivative

$$\begin{aligned}
\dot{e}_u &= \dot{x}_o - (\dot{z} + H_u \dot{y}) \\
&= (I_5 - H_u C_o)\dot{x}_o - (M_u z + G_u u + L_u y) \\
&= \Xi(A_o x_o + B_o u + D_o d) - M_u z - G_u u - (L_{u1} + L_{u2})y \\
&= (\Xi A_o - L_{u1} C_o)e_u + (\Xi B_o - G_u)u + \Xi D_o d + (\Xi A_o - L_{u1} C_o)(z + H_u y) - M_u z - L_{u2} y \\
&= (\Xi A_o - L_{u1} C_o)e_u + (\Xi B_o - G_u)u + \Xi D_o d \\
&\quad + [(\Xi A_o - L_{u1} C_o)H_u - L_{u2}]y + (\Xi A_o - L_{u1} C_o - M_u)z
\end{aligned}$$

(4.3)

where, $\Xi = I_5 - H_u C_o$, $L_u = L_{u1} + L_{u2}$.

For convenient design, the matrices M_u, G_u and L_{u2} (Lan et al., 2017b) are defined as:

$$M_u = \Xi A_o - L_{u1}C_o, \quad G_u = \Xi B_o, \quad L_{u2} = (\Xi A_o - L_{u1}C_o)H_u \tag{4.4}$$

and further to reduce the error dynamics (4.3) into the form as:

$$\dot{e}_u = (\Xi A_o - L_{u1}C_o)e_u + \Xi D_o d \tag{4.5}$$

The estimated observer measurement is then defined as:

$$z_u = C_u e_u \tag{4.6}$$

where $C_u = I_6$. To check the asymptotic stability of the estimator system (4.5) a Lyapunov matrix must be selected, such that:

$$V_u = e_u^T P_u e_u \tag{4.7}$$

where P_u is a symmetric positive definite matrix.

The time derivative of the Lyapunov function V_u is:

$$\begin{aligned}
\dot{V}_u &= \dot{e}_u^T P_u e_u + e_u^T P_u \dot{e}_u \\
&= [(\Xi A_o - L_{u1}C_o)e_u + \Xi D_o d]^T P_u e_u + e_u^T P_u[(\Xi A_o - L_{u1}C_o)e_u + \Xi D_o d] \\
&= e_u^T [P_u(\Xi A_o - L_{u1}C_o) + (\Xi A_o - L_{u1}C_o)^T P_u]e_u + e_u^T P_u \Xi D_o d + d^T D_o^T \Xi^T P_u e_u
\end{aligned} \tag{4.8}$$

The H_∞ performance $||T_{z_u d}||_\infty < \gamma_u$ can be expressed as:

$$J_u = \int_0^\infty (z_u^T z_u - \gamma_u^2 d^T d)dt < 0 \tag{4.9}$$

Under zero initial conditions (Lan and Patton, 2017), it follows that

$$\begin{aligned}
J_u &= \int_0^\infty (z_u^T z_u - \gamma_u^2 d^T d + \dot{V}_u)\,dt - \int_0^\infty \dot{V}_u\,dt \\
&= \int_0^\infty (z_u^T z_u - \gamma_u^2 d^T d + \dot{V}_u)\,dt - (V_u(\infty) - V_u(0)) \\
&\leq \int_0^\infty (z_u^T z_u - \gamma_u^2 d^T d + \dot{V}_u)\,dt
\end{aligned}$$

Thus a sufficient condition of Equation (4.9) is

$$J_1 = z_u^T z_u - \gamma_u^2 d^T d + \dot{V}_u < 0 \tag{4.10}$$

By substituting Equation (4.8) into Equation (4.10) it follows that

$$J_1 = \begin{bmatrix} e_u \\ d \end{bmatrix}^T \begin{bmatrix} J_{11} & P_u \Xi D_o \\ * & -\gamma_u^2 I \end{bmatrix} \begin{bmatrix} e_u \\ d \end{bmatrix} < 0 \tag{4.11}$$

where $J_{11} = P_u(\Xi A_o - L_{u1}C_o) + (\Xi A_o - L_{u1}C_o)^T P_u + C_u^T C_u$

According to the Bounded Real Lemma (Boyd et al., 1994), if there exists a symmetric positive definite matrix P_u such that the following LMI is feasible,

$$\begin{bmatrix} P_u \bar{A}_o + \bar{A}_o^T P_u & P_u \Xi D_o & I \\ * & -\gamma_u^2 I & 0 \\ * & * & -I \end{bmatrix} < 0 \tag{4.12}$$

where $\bar{A}_o = \Xi A_o - L_{u1}C_o$.

Then the error system (4.5) is asymptotically stable with $\gamma_u > 0$. Next define $N_1 = P_u H_u$, $N_2 = P_u L_{u1}$, then the LMI (4.12) is equivalent to the next LMI:

$$\begin{bmatrix} He(P_u A_o - N_1 C_o A_o - N_2 C_o) & (P_u - N_1 C_o)D_o & I \\ * & -\gamma_u^2 I & 0 \\ * & * & -I \end{bmatrix} < 0 \tag{4.13}$$

The matrices P_u, N_1 and N_2 can be calculated by using Matlab LMI toolbox to solve the LMI (4.13). Furthermore, the matrices H_u and L_{u1} will be known from $H_u = P_u^{-1} N_1$, and $L_{u1} = P_u^{-1} N_2$. Finally, the matrices M_u, G_u and L_u can be obtained according to (4.4).

4.2.2   LO with LMI

The LO estimator (Du et al., 2015) usually has the form:

$$\dot{\xi} = A_o \xi + B_o u + L_{ol}(y - C_o \xi) \tag{4.14}$$

where $\xi \in \Re^5$ is the state vector of LO, $L_{ol} \in \Re^{5 \times 2}$ is the required observer gain matrix.

By defining its estimation error as $e_{ol} = x_o - \xi$, and taking the time derivative leads to:

$$\dot{e}_{ol} = \dot{x}_o - \dot{\xi} = (A_o - L_{ol}C_o)e_{ol} + D_o d \tag{4.15}$$

The design procedure of LO with LMI is similar to the UIO with LMI. Hence, considering the Bounded Real Lemma (Boyd et al., 1994), it is easy to show that if there exists a symmetric positive definite matrix P_{ol} ensuring the below LMI feasible:

$$\begin{bmatrix} He(P_{ol} A_o - Y_{ol} C_o) & P_{ol} D_o & I \\ * & -\gamma_{ol}^2 I & 0 \\ * & * & -I \end{bmatrix} < 0 \tag{4.16}$$

thereby the stability of the LO error system (4.15) is satisfied with $\gamma_{ol} > 0$ and a matrix $Y_{ol} = P_{ol}L_{ol}$. The observer gain is computed as $L_{ol} = P_{ol}^{-1}Y_{ol}$.

4.2.3   LO with Pole-Placement

The LO can be reconsidered in the form:

$$\dot{\xi} = A_o\xi + B_ou + L_{op}(y - C_o\xi) \tag{4.17}$$

Here to define $e_{op} = x_o - \xi$, $A_l = A_o^T$, $B_l = C_o^T$. The Matlab default function can help to place the desired poles (Laub and Wette, 1984), such as $L_{op} = place(A_l, B_l, p_o)$, to calculate the observer gain L_{op}. Where $p_o \in \Re^5$ are the user selected poles.

4.2.4   ASMO

To rearrange the float rotational dynamics described in Equation (3.24) into a new form as:

$$\begin{aligned}
\dot{x}_1 &= x_2 \\
\dot{x}_2 &= -\frac{1}{J_t}(K_{hs}x_1 + K_vx_2 + C_{ra}r_a + D_{ra}x_2) + \frac{u}{J_t} + \frac{M_{ex}}{J_t}
\end{aligned} \tag{4.18}$$

where $x_1 = \theta$ is the pitch angular position , and $x_2 = \dot{\theta}$ is the pitch angular velocity. The ASMO followed from (Lan et al., 2017a) can be defined as:

$$\begin{aligned}
\dot{\hat{x}}_1 &= \hat{x}_2 + \upsilon_1 \\
\dot{\hat{x}}_2 &= -\frac{1}{J_t}(K_{hs}y_1 + K_vy_2 + C_{ra}r_a + D_{ra}y_2) + \frac{u}{J_t} + \upsilon_2
\end{aligned} \tag{4.19}$$

where $\hat{x}_1$ and $\hat{x}_2$ are the observer states, and y_1 and y_2 are the system output measurements. Next to define the error signals as $e_{s1} = x_1 - \hat{x}_1$ and $e_{s2} = x_2 - \hat{x}_2$ and the switching functions υ_1 and υ_2 are given as:

$$\upsilon_1 = \eta_{\upsilon_1}sign(e_{s1}), \upsilon_2 = \eta_{\upsilon_2}sign(e_{s2}) \tag{4.20}$$

Thus, the estimation error system becomes

$$\begin{aligned}
\dot{e}_{s1} &= e_{s2} - \upsilon_1 \\
\dot{e}_{s2} &= \frac{M_{ex}}{J_t} - \upsilon_2
\end{aligned} \tag{4.21}$$

Choose the observer adaptive law as the following form

$$\dot{\hat{\rho}}_{v_1} = \sigma_{v_1}||e_{s1}||_2, \ \dot{\hat{\rho}}_{v_2} = \sigma_{v_2}||e_{s2}||_2 \qquad (4.22)$$

Then, define the switching function parameters in (4.20) as $\eta_{v_1} = \hat{\rho}_{v_1} + \varepsilon_{v_1}$ and $\eta_{v_2} = \hat{\rho}_{v_2} + \varepsilon_{v_2}$, where σ_{v_1}, σ_{v_2}, ε_{v_1} and ε_{v_2} are all positive constants. Hence, the estimated M_{ex} can be obtained from $\hat{M}_{ex} = J_t v_{eq,2}$. $v_{eq,2}$ is the equivalent switching function of v_2, and $v_{eq,2} \cong v_2/(1+\tau s)$. Where τ is a time constant.

4.3   Optimal reference computation

Following on from the high-level part of the hierarchical tracking structure shown in Figure 1.5, the instantaneous amplitude and frequency of WEM are required before computing the reference velocity $\dot{\theta}_{ref}$. Therefore, an efficient EKF method is selected to do the recursive estimation for those two coefficients. Here, assume that the WEM signal is a narrow-band process (Fusco and Ringwood, 2014a), and to express its harmonic model as

$$M_{ex}(t) = A_{ex}(t)cos(\omega(t) \cdot t + \beta(t)) \qquad (4.23)$$

where $A_{ex}(t), \omega(t)$ and $\beta(t)$ are the time-varying amplitude, angular frequency and phase of the M_{ex} signal, respectively. Considering the Harvey's structural model given in (Harvey, 1990), the M_{ex} can be converted into a single cyclical component (Fusco, 2012):

$$\begin{bmatrix} \psi(k+1) \\ \psi^*(k+1) \\ \omega(k+1) \end{bmatrix} = \begin{bmatrix} cos(\omega(k)T_s) & sin(\omega(k)T_s) & 0 \\ -sin(\omega(k)T_s) & cos(\omega(k)T_s) & 0 \\ 0 & 0 & 1 \end{bmatrix} \begin{bmatrix} \psi(k) \\ \psi^*(k) \\ \omega(k) \end{bmatrix} + \begin{bmatrix} \varsigma(k) \\ \varsigma^*(k) \\ \kappa(k) \end{bmatrix}$$

$$M_{ex}(k) = \psi(k) + \zeta(k)$$

$$(4.24)$$

where $d_e(k) = [\varsigma(k) \quad \varsigma^*(k) \quad \kappa(k)]^T$ and $\zeta(k)$ are random process and measurement noise, and $\psi(k)$ and $\psi^*(k)$ are state components related to the amplitude and phase. The state vector $x_e(k) = \begin{bmatrix} x_{e,1}(k) & x_{e,2}(k) & x_{e,3}(k) \end{bmatrix}^T = \begin{bmatrix} \psi(k) & \psi^*(k) & \omega(k) \end{bmatrix}^T$ and $x_e(k) \in \Re^{3 \times 1}$, corresponding to the sampling time T_s.

Then the non-linear time-varying model of (4.24) (Welch et al., 1995) is formulated as:

$$\begin{aligned} x_e(k) &= f(x_e(k-1), d_e(k-1)) \\ z_e(k) &= h(x_e(k), \zeta(k)) \end{aligned} \qquad (4.25)$$

where the estimated $\hat{M}_{ex}$ is considered as the actual measurement $z_e(k)$. According to the above descriptions and without knowing the noise information arised in the PAWEC system, the *a priori* state and measurement from time $k-1$ are

$$
\begin{aligned}
\hat{x}_e(k|k-1) &= f(\hat{x}_e(k-1|k-1),0) \\
\hat{z}_e(k|k-1) &= h(\hat{x}_e(k|k-1),0)
\end{aligned}
\tag{4.26}
$$

where $\hat{x}_e(k|k-1)$ is the estimate of $x_e(k)$ and $\hat{z}_e(k|k-1)$ is the estimate of $z_e(k)$ based on measurements from time $k-1$. On application of a first-order Taylor series expansion of the Equation (4.26), the linearized system time-varying Jacobian matrix $F(k)$ (ASSEL, 2014) is obtained as

$$
\begin{aligned}
F(k) &= \left.\frac{\partial f}{\partial x_e}\right|_{\hat{x}_e(k-1|k-1)} \\
&= \begin{pmatrix}
cos(\omega(k)T_s) & sin(\omega(k)T_s) & T_s(-sin(\omega(k)T_s)\psi(k)+cos(\omega(k)T_s)\psi'(k)) \\
-sin(\omega(k)T_s) & cos(\omega(k)T_s) & T_s(-cos(\omega(k)T_s)\psi(k)-sin(\omega(k)T_s)\psi'(k)) \\
0 & 0 & 1
\end{pmatrix}
\end{aligned}
$$

The observed Jacobian matrix is

$$
H(k) = \left.\frac{\partial h}{\partial x_e}\right|_{\hat{x}_e(k|k-1)} \triangleq \begin{bmatrix} 1 & 0 & 0 \end{bmatrix}
$$

Thus, the time-update equations of EKF are

$$
\begin{aligned}
\hat{x}_e(k|k-1) &= f(\hat{x}_e(k-1|k-1),0) \\
P_e(k|k-1) &= F(k)P_e(k-1|k-1)F^T(k)+Q_e
\end{aligned}
$$

The utilize of Jacobian matrices $F(k)$ and $H(k)$ to achieve both the model and measurement updates lead to

$$
\begin{aligned}
K_e(k) &= P_e(k|k-1)H^T(k)(H(k)P_e(k|k-1)H^T(k)+R_e)^{-1} \\
\hat{x}_e(k|k) &= \hat{x}_e(k|k-1)+K_e(k)(z_e(k)-h(\hat{x}_e(k|k-1),0)) \\
P_e(k|k) &= (I-K_e(k)H(k))P_e(k|k-1)
\end{aligned}
$$

where Q_e and R_e are the covariance process and measurement noise matrices, which should be properly chosen. After the on-line estimation procedure, the estimated amplitude $\hat{A}_{ex}$ and frequency $\hat{\omega}$ (Fusco, 2012) are

$$
\begin{aligned}
\hat{A}_{ex}(k|k) &= \sqrt{\hat{x}_{e,1}(k|k)^2+\hat{x}_{e,2}(k|k)^2} \\
\hat{\omega}(k|k) &= \hat{x}_{e,3}(k|k)
\end{aligned}
\tag{4.27}
$$

Next, consider the float can reach a near-resonance condition for the purpose of energy maximising. The near-resonance condition means that the float angular velocity is in-phase with the WEM. The reference angular velocity (Fusco and Ringwood, 2014a) is presented as:

$$\dot{\theta}_{ref}(t) = \frac{1}{T(t)} \hat{M}_{ex}(t) \tag{4.28}$$

$$where \quad \frac{1}{T(t)} = \begin{cases} \dfrac{1}{2B(\hat{\omega}) + 2K_v^{(0)}}, & if \quad \dfrac{\hat{\omega}\theta_{lim}}{\hat{A}_{ex}} > \dfrac{1}{2B(\hat{\omega}) + 2K_v^{(0)}} \\ \dfrac{\hat{\omega}\theta_{lim}}{\hat{A}_{ex}}, & otherwise \end{cases} \tag{4.29}$$

$B(\hat{\omega})$ is the radiation damping coefficient, and $K_v^{(0)}$ is the extra viscous damping coefficient. θ_{lim} denotes the maximum angular displacement of the Wavestar float. Finally, the optimal reference velocity $\dot{\theta}_{ref}$ can be computed when the instantaneous amplitude $\hat{A}_{ex}$ and frequency $\hat{\omega}$ of the $\hat{M}_{ex}$ signals are obtained from the EKF.

4.4   Simulation results

In this Section WEM estimation results are derived, based on WEC-Sim, for the four different estimators (1) UIO with LMI, (2) LO with LMI, (3) LO with pole-placement, and (4) ASMO. EKF estimation results are also obtained, for instantaneous amplitude $\hat{A}_{ex}$ and frequency $\hat{\omega}(t)$ of the WEM, These are also required in the reference generation step, prior to implanting the PAWEC tracking control.

The parameters of four estimators: $\gamma_u = 1.5$, $\gamma_{ol} = 1.5$, $\sigma_{v_1} = 3$, $\varepsilon_{v_1} = 2.5$, $\sigma_{v_2} = 10$, $\varepsilon_{v_2} = 6$, $\tau = 0.01$, $p_o = [-26, -24, -18, -16, -40]^T$.

The estimated M_{ex} from four methods at six different sea states are shown in Figure 4.4. On account of convenience and to avoid redundancy, the following discussion and analysis focus on the estimation result corresponding to Seastate 2. The ideal in Figure 4.4 means the theoretically calculated equivalent wave excitation moment around the hinge point A, see Equation (3.25).

(a) Estimated $\hat{M}_{ex}$ at Seastate 1.

(b) Estimated $\hat{M}_{ex}$ at Seastate 2.

(c) Estimated $\hat{M}_{ex}$ at Seastate 3.

(d) Estimated $\hat{M}_{ex}$ at Seastate 4.

(e) Estimated $\hat{M}_{ex}$ at Seastate 5.

(e) Estimated $\hat{M}_{ex}$ at Seastate 6.
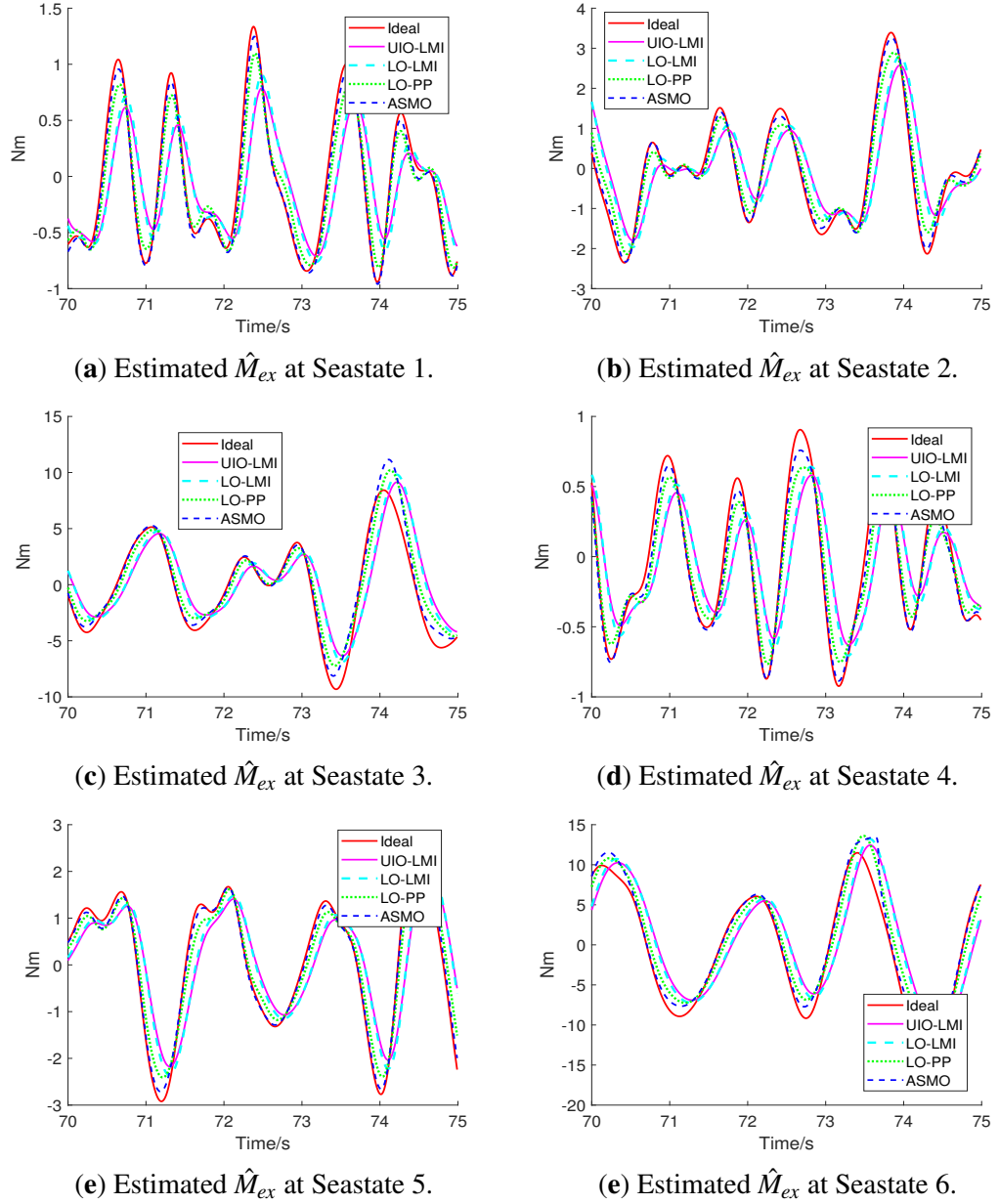
Figure 4.4: Estimated $\hat{M}_{ex}$ from four methods at six sea states.

In order to compare and analyse the estimation performances of all estimators presented in Section 4.2, some indices are considered here, such as the average error (AE) (Zhang et al., 2019), normalized root-mean-square accuracy (NRMSA) (Peña-Sanchez et al., 2019) and delay.

The AE is chosen as:

$$AE = \frac{1}{L_s - N_s} \sum_{k=N_s}^{L_s} |M_{ex}(k) - \hat{M}_{ex}(k)| \tag{4.30}$$

and the NRMSA is selected as:

$$NRMSA = \left(1 - \sqrt{\frac{\sum_{k=N_s}^{L_s}(M_{ex}(k) - \hat{M}_{ex}(k))^2}{\sum_{k=N_s}^{L_s} M_{ex}(k)^2}} \right) \tag{4.31}$$

where L_s is the total number of samples and N_s is the selected first data sample. It is appropriate to set N_s as 0.6 L_s to remove the effects of the transient response. The maximum value of NRMSA is 1 which means the best estimation. Here, to set $L_s = 141200$, and the calculated performance indices for analysis are given in Table 4.1.

Table 4.1: Performance indices of estimators in Seastate 2.

Performance index	AE	NRMSA	Delay
UIO-LMI	1.0824	0.6790	0.113
LO-LMI	1.0436	0.7014	0.109
LO-PP	0.3577	0.9635	0.026
ASMO	0.0818	0.9938	0.002

It can be seen that both UIO and LO based on LMI show large AE and delays, which means that the estimation performance is restricted, to some extent by these indices. Furthermore, the computed NRMSA from both LMI methods are less than the other two approaches (LO-PP and ASMO). Theoretically, the robustness of an observer based on H_∞ performance can be improved, but the LMI feasibility problem brings a limitation into the computation of the observer gain. Considering the enhancement of the estimation performance, a small H_∞ performace index γ is required here, but to attempt to achieve this LMI infeasibility was a challenging issue which was difficult to overcome. This is the main reason why the estimation performance based on LMI method is limited.

On the other hand, the LO-PP method performs well with a small AE and delay, and its NRMSA is larger than the UIO-LMI and LO-LMI estimators. The estimation result of ASMO presents very little AE and delay as the sliding mode has the fast response property. Besides, ASMO has strong robustness and provides the high value of NRMSA. However, ASMO may introduce some high frequency components that could potentially increase the burden of a PTO system operating with the PAWEC system. This can be aggravated especially when ASMO is used with sliding mode control, although there are methods to ensure that the sliding occurs close to but not on the sliding boundary, and so removing the effect of switching discontinuities (Utkin, 2013).

On balance, the LO-PP method has the simplest structure and is very attractive in real applications. ASMO is a nonlinear approach and can provide better performance if a more complex form of PAWEC model is considered.

(a) Amplitude of $\hat{M}_{ex}$ at Seastate 1.

(b) Amplitude of $\hat{M}_{ex}$ at Seastate 2.

(c) Amplitude of $\hat{M}_{ex}$ at Seastate 3.

(d) Amplitude of $\hat{M}_{ex}$ at Seastate 4.

(e) Amplitude of $\hat{M}_{ex}$ at Seastate 5.

(e) Amplitude of $\hat{M}_{ex}$ at Seastate 6.
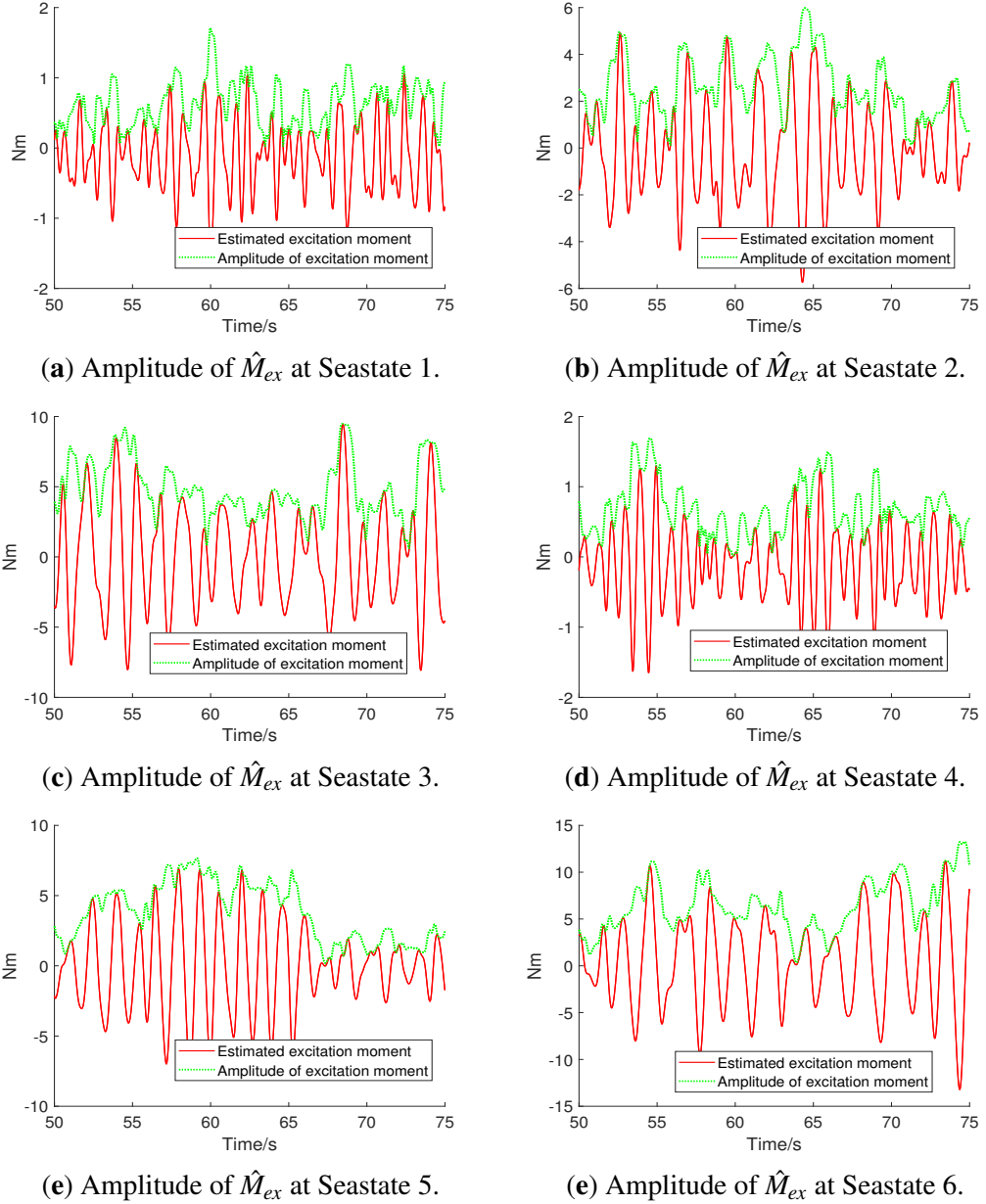
Figure 4.5: Instantaneous amplitude of $\hat{M}_{ex}$ at six sea states.

The instantaneous amplitude $\hat{A}_{ex}$ of $\hat{M}_{ex}$ is given in Figure 4.5 along with estimated $\hat{M}_{ex}$. The estimated instantaneous frequency $\hat{\omega}$ of $\hat{M}_{ex}$ is shown in Figure 4.6. The estimated frequency $\hat{\omega}$ fluctuates with a range around the peak frequency of the Sea states spectrum in Figure 3.7. Generally, the EKF needs long time to converge, and its

initial values should be properly selected, which close to the expected values in order
to avoid there has a long time for the result convergence.

(**a**) Frequency of $\hat{M}_{ex}$ at Seastate 1.

(**b**) Frequency of $\hat{M}_{ex}$ at Seastate 2.

(**c**) Frequency of $\hat{M}_{ex}$ at Seastate 3.

(**d**) Frequency of $\hat{M}_{ex}$ at Seastate 4.

(**e**) Frequency of $\hat{M}_{ex}$ at Seastate 5.

(**e**) Frequency of $\hat{M}_{ex}$ at Seastate 6.
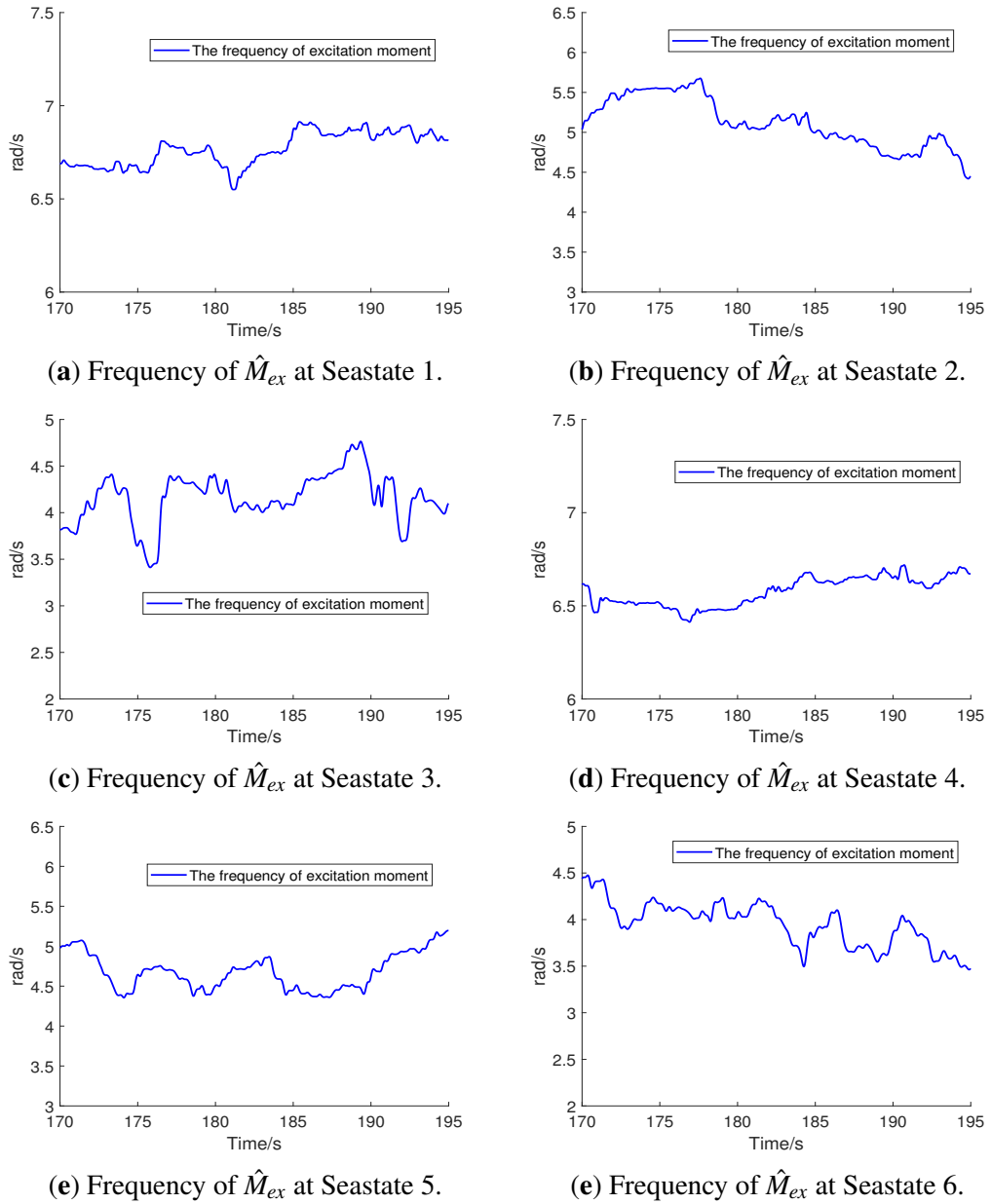
Figure 4.6: Instantaneous frequency of $\hat{M}_{ex}$ at six sea states.

(**a**) Seastate 1.

(**b**) Seastate 2.

(**c**) Seastate 3.

(**d**) Seastate 4.

(**e**) Seastate 5.
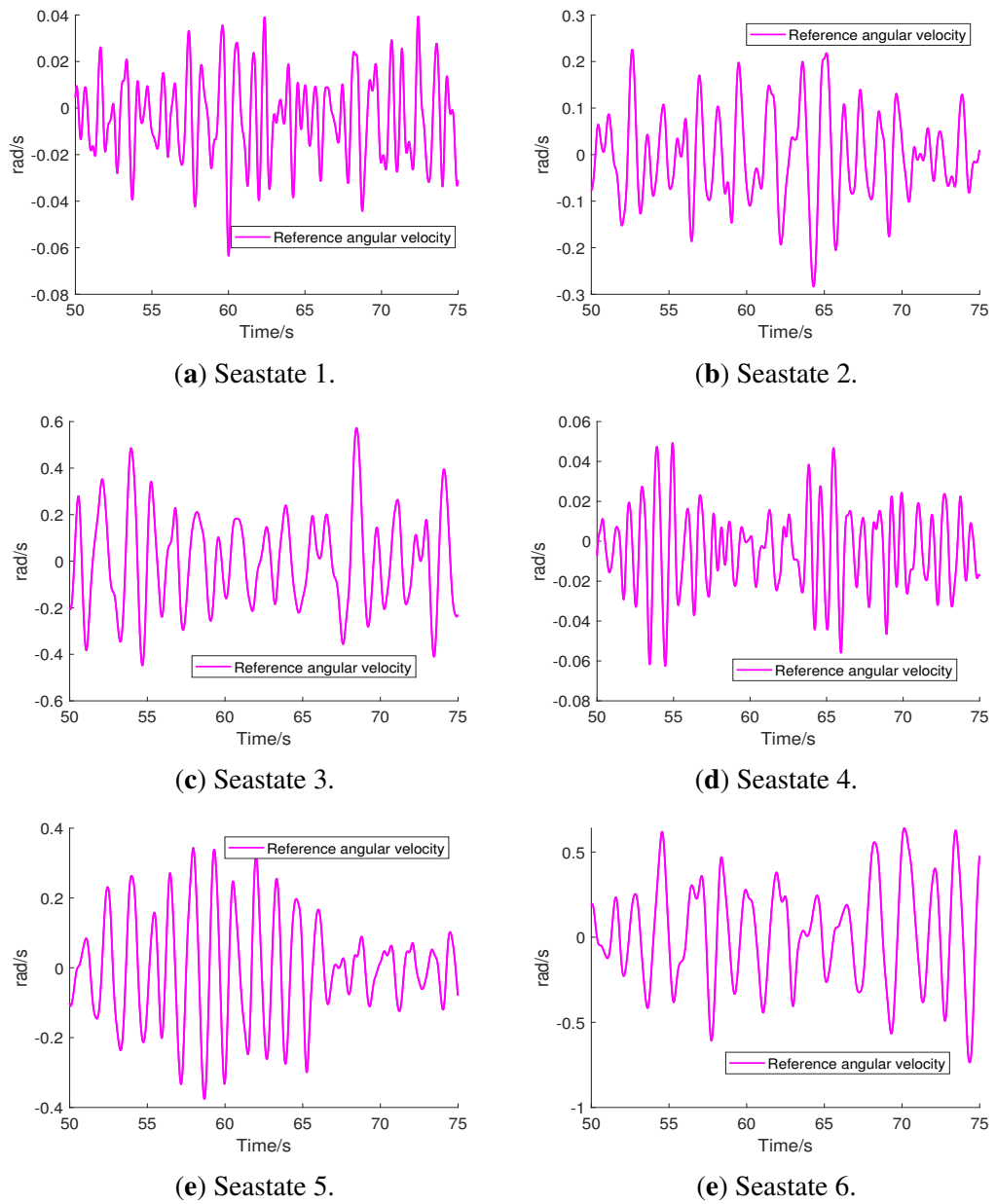
(**e**) Seastate 6.

Figure 4.7: Optimal reference angular velocity at six sea states.

Figure 4.7 gives the calculated optimal reference velocity based on the Equation (4.28). It serves a function in guiding the scaled Wavestar-prototype device into a near resonance condition for the purpose of energy-maximising control design. For example, it is adopted to derive the angular displacement reference and build a reference model for model-following tracking work illustrated in Chapter 5. The optimal velocity reference is also used for the MPC veloctity tracking control work designed in Chapter 6.

4.5   Summary

This Chapter provides a comparison study between four estimators for WEM estimation work and it contributes to give some insight of a scaled Wavestar-prototype WEC developed in WEC-Sim. From the analysis of the simulation results, UIO and LO methods designed with LMI have restrictions but still give feasible solutions. AMSO provides the best estimation performance as a nonlinear and robust approach. LO pole-placement actually is the simplest and most effective method in estimating the WEM, which might be very valuable when used in future real applications. On the other hand, the EKF can perform well in estimating the instantaneous WEM amplitude and frequency, and then these two signals are sufficient to build the reference velocity.

Overall, The WEM estimation and the calculation of the optimal reference velocity in this Chapter 4 are the preliminary work for Chapter 5 in model-following robust control design and for the MPC velocity tracking method in Chapter 6. A near-resonance condition can be reached for the energy maximisation generation when the tracking work is done by the PAWEC system.

Chapter 5

Robust Tracking Control Methods based on Model-Following

5.1   Introduction

In general, the WEC device aims to capture energy from the ocean waves and convert the absorbed mechanical power into some electrical power to the grid by a selected PTO system (Sheng, 2019). The primary task in wave energy is to lower the Levelized Cost of Energy (LCOE). There are two attractive aspects of this. One aspect is to reduce the device maintenance cost (Mérigaud and Ringwood, 2016), and the second is to maximize the energy conversion by a designed energy-maximising control system (Ringwood et al., 2014), considered to operate over a range of sea states. At present, the control for the purpose of energy maximisation is one of the most popular topics (Ringwood et al., 2023b) for which lots of research focuses on PAWEC devices due to some advantageous features, as outlined in Section 2.2.

In early work, some researchers preferred to consider the use of the complex-conjugate control (CCC) (see Section 2.4) method to achieve energy maximization generation, based on the linear resonance theory (Falnes and Kurniawan, 2020). The interest is to achieve significant amplification of the WEC motion, in order to harvest as much energy as possible from waves. However, this requirement usually violates the assumption of linear modelling, by considering the action of large motion in non-linear dynamics. Furthermore, CCC tends to give rise to significant power fluctuations (Faedo et al., 2017) that make it difficult to choose a suitable PTO system for a PAWEC device. The most significant argument against the use of reactive control is that it has

an inherent non-causal characteristic. An additional negative feature is that reactive control is frequency-dependent for monochromatic or regular wave conditions, for giving an optimal solution (Faedo et al., 2017). Clearly, regular wave conditions do not exist in practice as sea waves contain several random frequency components. These deficiencies prompted researchers to move away from CCC designs towards MPC.

As introduced in Section 2.5.1, the key point of using MPC is to choose the average absorbed mechanical power as an objective function to maximize the absorbed mechanical energy (Soltani et al., 2014). MPC not only provides the optimal solution for energy maximization but also solves the physical constaints during its optimization procedure. There are several MPC studies (Faedo et al., 2017) which have been shown in the literature with attractive results in energy generation. However, the frequently used MPC is based on linear theory that is susceptible to system uncertainties. Some nonlinear MPC approaches (Li, 2017; Richter et al., 2012; Tom and Yeung, 2014) are tested on the PAWEC system but the computational complexity are relatively large involved result from the non-convexity optimization. Additionally, the future knowledge of WEF is needed in optimal control calculation due to the non-casual nature (Fusco and Ringwood, 2010), and the prediction work will cause prediction errors, which is not desirable in control design. In contrast, the more obvious deficiency lies in the robustness of MPC (Zhang and Li, 2022) and it is possible to diverge in some real PAWEC devices. Overall, a real PAWEC application contains unmodeled uncertainties and nonlinear effects, making the robust control design becomes a crucial work.

In addition to the above widely used methods, there is a new alternative way to design energy-maximising control. It is a kind of hierarchical tracking structure that contains two-level parts first proposed by (Fusco and Ringwood, 2014a). The high-level part relates to WEF/WEM estimation and optimal reference profile building (Li and Patton, 2023c). As for the low-level part, a controller can be designed to track the optimal reference signal and reach a near-resonance condition for energy-maximizing generation (Li and Patton, 2023b). The near-resonance operation keeps the PAWEC float velocity share same phase with the WEF/WEM. The hierarchical approach can accommodate lots of different strategies, which will has great potential in the exploration of the PAWEC control systems, such as robust control, adaptive control, etc.

Following from the hierarchical structure of tracking control, a model-following strategy is described in Section 5.2 this Chapter. The main idea of the model-following concept is to force the PAWEC system to follow a reference model, which consists of

reference position and velocity signals, in order to enhance the system robustness and maximize energy absorption from irregular waves. The basic LQR and two different robust methods are proposed separately in Section 5.3. A mixed LQR/H_∞ controller is based on a combination of linear quadratic regulator (LQR) index and H_∞ performance. The other one is sliding mode controller that has strong robustness but simple structure. A comparison study is conducted and analysed in Section 5.4 between the basic LQR, mixed LQR/H_∞ and SMC approaches. Finally, Section 5.5 provides the Summary.

5.2 The Model-Following Tracking Structure

From the early description of (Erzberger, 1967), a feedback control law is designed to ensure that the output of a physical system (the plant) can effectively follow the desired output of a given reference model, which contributes to a "model-following control system". In other words, it is called "asymptotic model matching" (Isurugi, 1990). The error-dynamics between the plant output and the conceptual reference model should be asymptotically stable. An intuitive example for understanding of model-following control is discussed in (Durham, 1989). If a conventional airplane (the plant) aims to simulate the Dutch roll characteristics or correct some flying qualities deficiency in the airplane, the model-following control is a good idea since the desired dynamics contained in the description of a model, and the airplane roll and yaw responses can keep in the same manner as that of the reference model when the control law drives the plant's control surfaces. Apart from the application utilized in field of in-flight, some other applications of model-following control adjust the plant to have the desired behaviors (Isurugi, 1990), such as handling qualities or transient responses, etc.

In general, there are two categories, so-called implicit or explicit model-following (Isurugi, 1990). In terms of implicit model-following, it is normally a matching decision that can modify the plant dynamics by using the feedback to approximate the dynamics of the reference model (Erzberger, 1967). But there is no attempt to guide the plant to track the model's state trajectory. However, the explicit model-following considers doing both the dynamics and state trajectories matching between the plant and the model (Isurugi, 1990). In this case, the error vector between the model and plant states will be eliminated, even if the external disturbances involved to the plant. The

properly designed model-following (robust) controller will drive the plant states approaching to the undistubed states of the model. Here, the explicit model-following technique is considered to force the PAWEC system to follow the states (Calculated reference trajectories) of the reference model robustly by designed mixed LQR/H_∞ and sliding mode controllers. When the PAWEC device can track the position and velocity reference signals, the near-resonance condition will be achieved for the energy maximization purpose (Li and Patton, 2023b).

As described in Chapter 1 Figure 1.5, the hierarchical tracking structure is the main idea of this thesis work for a Wavestar-like device (the 1:20 scaled benchmark). The overall tracking structure of model-following control is shown in Figure 5.1. The high-level part: WEM estimation work and optimal reference velocity generation are described in Chapter 4. This Chapter is based on low-level part model-following robust control design.
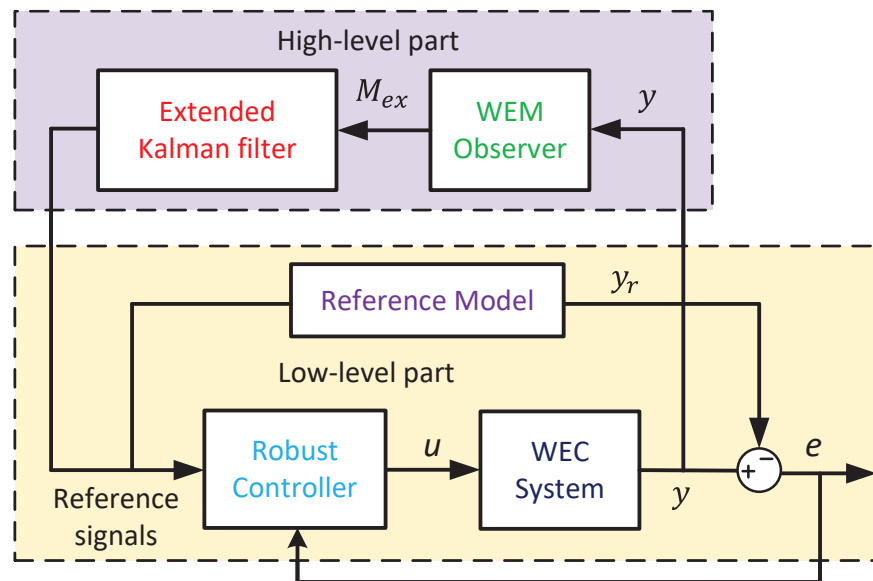
Figure 5.1: Overall tracking structure of model-following control.

Different from the conventional tracking work, here the optimal reference postion and velocity signals are considered to build a reference model. And the designed robust controller will drive the PAWEC system output to follow the reference model output effectively, yield so as to reach position and velocity tracking together. In other words, the controller role is to eliminate the state errors between the PAWEC system and a reference model, and to achieve the control system asymptotically stable. When

the tracking work is accomplished, the PAWEC system can reach a near-resonance condition for the energy maximization.

Note: the discussed WEM observer, reference model building and robust controller in this Chapter are all based on continuous system design. But the Extended Kalman Filter (EKF) is designed in discrete system, which follows the details described in Section 4.3 Chapter 4.

If the PAWEC float is treated as an oscillating mass point, the reference velocity $\dot{\theta}_{ref}$ can be assumed (Falnes and Kurniawan, 2020) as below:

$$\dot{\theta}_{ref}(t) = \theta_a \cos(\hat{\omega}t + \varphi_\theta) = \frac{1}{2}\hat{\theta}_{ref}e^{i\hat{\omega}t} + \frac{1}{2}\hat{\theta}_{ref}^* e^{i\hat{\omega}t} = \Re\{\hat{\theta}_{ref}e^{i\hat{\omega}t}\} \qquad (5.1)$$

where θ_a is the amplitude of $\dot{\theta}_{ref}$, $\hat{\omega}$ is the instantaneous frequency of WEM, to see more details in Chapter 4. φ_θ is the phase information, $\hat{\theta}_{ref}$ is the complex amplitude of the position reference θ_{ref}, and $\hat{\theta}_{ref}^*$ represents the complex conjugate of θ_{ref}.

Then, the reference position θ_{ref} of the oscillating mass will have the form of

$$\theta_{ref}(t) = \frac{\theta_a}{\hat{\omega}}\sin(\hat{\omega}t + \varphi_\theta) = \frac{\theta_a}{\hat{\omega}}\cos(\hat{\omega}t + \varphi_\theta - \frac{\pi}{2})$$
$$= \frac{1}{2i\hat{\omega}}\hat{\theta}_{ref}e^{i\hat{\omega}t} - \frac{1}{2i\hat{\omega}}\hat{\theta}_{ref}^* e^{-i\hat{\omega}t} = \Re\{\frac{\hat{\theta}_{ref}}{\hat{\omega}}e^{i\hat{\omega}t}e^{-i\frac{\pi}{2}}\} \qquad (5.2)$$

The maximum energy generation can be realized if the PAWEC system be able to track a resonant system with the optimal displacement and velocity references. Considering the utilization of the model-following strategy, a proper linear model can be defined as:

$$\dot{x}_m = A_m x_m + B_m u + B_m (M_{ex} - M_{ra})$$
$$y = C_m x_m \qquad (5.3)$$

where $A_m = \begin{bmatrix} 0 & 1 \\ -\dfrac{K_{hs}}{J_t} & -\dfrac{K_v}{J_t} \end{bmatrix}, x_m = \begin{bmatrix} \theta \\ \dot{\theta} \end{bmatrix}, B_m = \begin{bmatrix} 0 \\ \dfrac{1}{J_t} \end{bmatrix}, C_m = \begin{bmatrix} 1 & 0 \\ 0 & 1 \end{bmatrix}.$

The parameters K_{hs}, K_v and J_t can be seen in Table 3.2.

Next, the reference model can be represents as:

$$\dot{x}_r = A_m x_r + B_m r$$
$$y_r = C_r x_r \qquad (5.4)$$

where $x_r = \begin{bmatrix} \theta_{ref} \\ \dot{\theta}_{ref} \end{bmatrix}$ is the state vector of the reference model, $r = K_{hs}\theta_{ref} + K_v\dot{\theta}_{ref} + J_t\ddot{\theta}_{ref}$. $\ddot{\theta}_{ref}$ is the time derivative of $\dot{\theta}_{ref}$.

Then, define the tracking error states between PAWEC system and reference model as:

$$e = x_m - x_r \tag{5.5}$$

and based on Equations (5.3) and (5.4), the model-following error system can be obtained as:

$$\dot{e} = A_e e + B_e u + B_e (M_{ex} - M_{ra} - r) \tag{5.6}$$

where $e = \begin{bmatrix} \theta - \theta_{ref} \\ \dot{\theta} - \dot{\theta}_{ref} \end{bmatrix}$, $A_e = A_m$ and $B_e = B_m$.

The tracking error e will be minimised by the designed robust controller in Section 5.3.

5.3 Model-Following Tracking Controller Designs

5.3.1 Basic LQR control design

The general idea of LQR is to design a controller to minimise the given performance index J_{LQR} and this can be referred to as the optimal design for quadratic control problems.

Considering the error system (5.6), define a control law:

$$u = u_{lb} + u_{lf} \tag{5.7}$$

where $u_{lf} = -(\hat{M}_{ex} - \hat{M}_{ra}) + r$ is the feedforward control term and $u_{lb} = -K_{LQR}e$ is the LQR feedback term. $\hat{M}_{ex}$ is the estimated WEM using a pole-placement Luenberger observer and $\hat{M}_{ra}$ is the calculated radiation damping moment, according to the identified state space model in Equation (3.24).

To substitute control law (5.7) into error system (5.6) and assume the uncertainty term $(M_{ex} - M_{ra}) - (\hat{M}_{ex} - \hat{M}_{ra})$ is zero, then a new error system corresponding to the LQR control input will be

$$\dot{e} = A_e e + B_e u_{LQR} \tag{5.8}$$

Define a quadratic performance index of the error system as

$$J_{LQR} = \int_0^\infty [e^T Q_l e + u_{LQR}^T R_l u_{LQR}] dt \tag{5.9}$$

where Q_l is a positive definite matrix and R_l is a positive constant. The feedback gain matrix can be computed from $K_{LQR} = R_l^{-1} B_e^T P_l$ after a positive definite matrix P_l can be obtained by solving the following Riccati Equation:

$$A_e^T P_l + P_l A_e - R_l^{-1} P_l B_e B_e^T P_l + Q_l = 0 \tag{5.10}$$

5.3.2 Mixed LQR/H_∞ control design

The mixed robust controller (Zhu and Li, 2021a) combines LQR index and H_∞ performance to force the PAWEC sysetm track the reference position and velocity trajectories robustly. The H_∞ performance can guarantee the robustness of control system and LQR index is able to constrain the control input by tuning the weight matrices (Li and Patton, 2023b).

To define its control law as:

$$u = u_m + u_f \tag{5.11}$$

the feedforward term is $u_f = -(\hat{M}_{ex} - \hat{M}_{ra}) + r$, and the feedback term is $u_m = -K_m e$.

Next, substituting Equation (5.11) into Equation (5.6), the rearranged error system then takes the form:

$$\dot{e} = A_e e + B_e u_m + B_e w \tag{5.12}$$

where $w = (M_{ex} - M_{ra}) - (\hat{M}_{ex} - \hat{M}_{ra})$.

Following the LQR Principle, a quadratic cost function is defined as:

$$J_M = \int_0^\infty [e^T Q_m e + u_m^T R_m u_m] dt \tag{5.13}$$

The square-root of the quadratic objective J_M can be expressed as the 2-norm form of a controlled output (Liu et al., 2018):

$$z_M = E e + F u_m \tag{5.14}$$

where $E = \begin{bmatrix} Q_m^{1/2} \\ 0 \end{bmatrix}$, $F = \begin{bmatrix} 0 \\ R_m^{1/2} \end{bmatrix}$, $Q_m = \begin{bmatrix} c_1 & 0 \\ 0 & c_2 \end{bmatrix}$, $R_m = r_1$.

A trade-off exists to minimise the effect from external input to tracking error by tuning the elements of the positive-definite weighting matrices Q_m and R_m. The tuning weight coefficients c_1 and c_2 can reduce the system steady-state error and the weight coefficient r_1 can adjust the control input.

It is assumed that the disturbance term w of (5.12) is bounded in l_2 space. Hence, an H_∞ performance index to perform robustness optimization on the system, such that

$$J_M < \gamma_m^2 ||w||_2^2 \tag{5.15}$$

From this original optimal control problem is converted to calculate a controller gain K_m, such that the closed-loop system is asymptotically stable and can satisfy corresponding to the H_∞ performance index:

$$||z_M||_2 < \gamma_m ||w||_2 \tag{5.16}$$

where $||z_M||_2$ is the 2-norm of the control objective, and $||w||_2$ is the 2-norm of disturbance w.

By using the H_∞ performance index the transfer from the external input to objective siganl z_M can be minimized. In this way an optimal and robust control design can be obtained.

The performance measure can be defined as (Du et al., 2015):

$$||T_{z_M w}||_\infty = sup_{||w||_2 \neq 0} \frac{||z_M||_2}{||w||_2} \tag{5.17}$$

where $||z_M||_2^2 = \int_0^\infty z_M^T(t) z_M(t) dt$, and $||w||_2^2 = \int_0^\infty w^T(t) w(t) dt$.

From the Bounded Real Lemma (Boyd et al., 1994), it is easy to determine that the system (5.12) is asymptotically stable with $||T_{z_M w}||_\infty$ minimized, if there exists a symmetric positive definite matrix $P > 0$ such that the following LMI is feasible,

$$\begin{bmatrix} (A_e - B_e K_m)^T P + P(A_e - B_e K_m) & PB_e & (E - FK_m)^T \\ * & -\gamma_m^2 I & 0 \\ * & * & -I \end{bmatrix} < 0 \tag{5.18}$$

Next, define $P^{-1} = Z$, $M = K_m Z$, and multiply the left and right of LMI (5.18) by $diag(Z, I, I)$ and its transpose leading to a new LMI:

$$
\begin{bmatrix}
(A_e Z - B_e M)^T + (A_e Z - B_e M) & B_e & (EZ - FM)^T \\
* & -\gamma_m^2 I & 0 \\
* & * & -I
\end{bmatrix} < 0 \qquad (5.19)
$$

The controller gain K_m can be obtained as $K_m = MP$ after solving the LMI (5.19) using the Matlab LMI toolbox.

5.3.3   Sliding mode control design

The SMC plays a role in forcing the PAWEC system to do tracking work with strong robustness and providing insensitivity to the matched disturbance arised in the PAWEC system. The first design step of SMC is to choose a switching function (Edwards and Spurgeon, 1998) in order that the motion of the error system is stable when it is restricted to the hyperplane N_s. The second step is to design a variable structure control law to force the error system states reach and subsequently remain at the silding mainfold, with an ideal sliding motion in finite time.

Considering the error system (5.6), the switching function can be defined (Lan et al., 2017b) as:

$$
s = N_s e \qquad (5.20)
$$

where $N_s = B_e^\dagger - Y(I - B_e B_e^\dagger)$ with a design matrix $Y \in \mathfrak{R}^{1 \times 2}$ and a pseudo-inverse matrix $B_e^\dagger = (B_e^T B_e)^{-1} B_e^T$.

then, considering the reachability of e down to the sliding mainfold (5.20), to get the time derivative of s

$$
\dot{s} = N_s \dot{e} = N_s(A_e e + B_e u + B_e(M_{ex} - M_{ra} - r)) \qquad (5.21)
$$

To define the sliding mode control law in the form of

$$
u = u_{eq} + u_{nl} \qquad (5.22)
$$

u_{eq} is the linear equivalent control term and u_{nl} is the nonlinear switching control term.

$$
u_{eq} = -N_s A_e e - (\hat{M}_{ex} - \hat{M}_{ra}) + r, \; u_{nl} = -k_n s - \varepsilon_n \overline{sign}(s, \delta) \qquad (5.23)
$$

where k_n and ε_n are positive constants, the smooth function $\overline{sign}(s, \delta) = \dfrac{s}{||s||_2 + \delta}$ is a differentiable approximation of $sign(s)$, which can handle the chattering phenomenon, during sliding mode (Edwards and Spurgeon, 1998). The approximated error is $\Delta sign = sign(s) - \overline{sign}(s, \delta)$. It can be proved that $||\Delta sign||_2 \leq \left(\dfrac{1}{||s||_2/\delta + 1}\right) \leq 1$ with $||s||_2 \neq 0$, and $||\Delta sign||_2$ becomes small if δ is sufficiently small.

Certainly, the chattering rejection will lead to a loss of robustness to some extent. The value of δ is set to 0.003 in the SMC smooth function, considering trade-off between chattering and tracking performance.

Next, define a Lyapunov function:

$$V_s = \frac{1}{2}s^2 \tag{5.24}$$

The time derivative of V_s is

$$\dot{V}_s = s\dot{s} = s(N_s A_e e + u + M_{ex} - M_{ra} - r) \tag{5.25}$$

On substituting (5.22) into (5.25):

$$\begin{aligned}
\dot{V}_s &= s[(M_{ex} - M_{ra}) - (\hat{M}_{ex} - \hat{M}_{ra}) - k_n s - \varepsilon_n \overline{sign}(s, \delta)] \\
&= s[w - k_n s - \varepsilon_n sign(s) + \varepsilon_n \Delta sign] \\
&\leq -k_n ||s||_2^2 - ||s||_2 (\varepsilon_n - ||w||_2 - ||\varepsilon_n \Delta sign||_2)
\end{aligned} \tag{5.26}$$

According to (5.26), if the condition $\varepsilon_n > ||w||_2 + ||\varepsilon_n \Delta sign||_2$ is satisfied, then it follows that $\dot{V}_s \leq 0$. It is then easy to see that $\dot{V}_s = 0$ holds only when $s = 0$ and $V_s \geq 0$, and if $\dot{V}_s < 0$, $\lim_{t \to \infty} V_s(t) = 0$. Therefore, the SMC law ensures stability of the error system (5.6) with tracking guaranteed along the sliding mainfold.

5.4 Simulation results

In this Section, the comparative results of LQR, mixed LQR/H_∞ control and SMC are illustrated for a Wavestar numerical modelling (1:20 scaled benchmark), described in Chapter 3. The proposed PAWEC control system is designed in doing continuous version simulation with sampling rate (simulation step) 0.001s. Two cases are discussed in the simulation results with/without the added matched disturbance $B_e \cdot d_m =$

$\frac{1}{J_t}(4sin(3t + \frac{\pi}{4}) - sin(2t + \frac{\pi}{3}))$. The matched disturbance $B_e \cdot d_m$ accounts for uncertainty in control channel, which is an important consideration in PAWEC control system design.

Note: to specify a uncertain linear system as follows:

$$\dot{x}_{md}(t) = A_{md}x_{md}(t) + B_{md}[u_{md}(t) + \xi_{md}] \tag{5.27}$$

where uncertainty ξ_{md} means the so-called matched disturbance, which appears in the system same control channel.

The LQR parameters: $Q_l = diag(1, 1)$, $R_l = 0.01$;
The mixed LQR/H_∞ control parameters: $\gamma_m = 0.03$, $c_1 = 0.7$, $c_2 = 0.5$, $r_1 = 0.01$;
The SMC parameters: $k_n = 2$, $\varepsilon = 5$, $\delta = 0.003$, $Y = [-0.1, 0.1]$.

More discussion and analysis will be given Chapter 7, in a comparison study between frequently used MPC (Chapter 7), MPC velocity tracking (Chapter 6), Mixed LQR/H_∞ and SMC (Chapter 5) for the purpose of PAWEC energy maximisation.
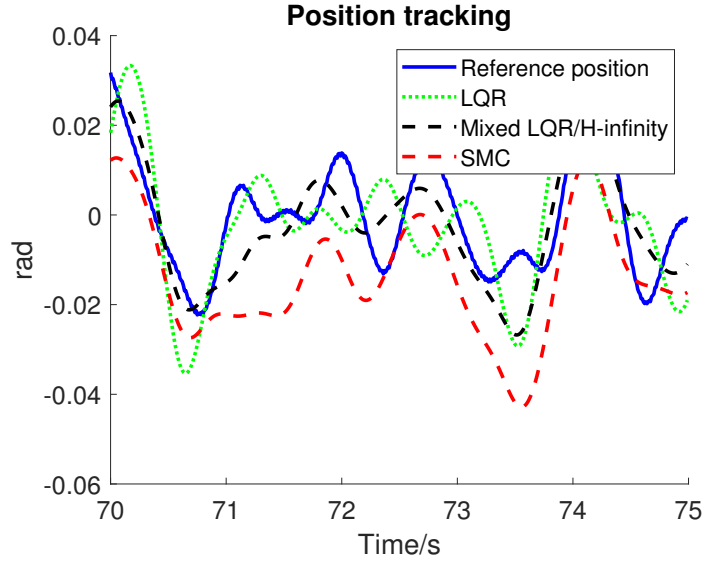
Figure 5.2: Position tracking of three methods (Seastate 2).

Figure 5.2 shows the postion tracking results of LQR, mixed LQR/H_∞ control and SMC methods corresponding to Seastate 2. It is clear that no methods are able to provide accurate position tracking as there is an additional moment from the offset between the CoG and CoB, and a static moment caused by the weight of the arm between the float and the hinge point A.
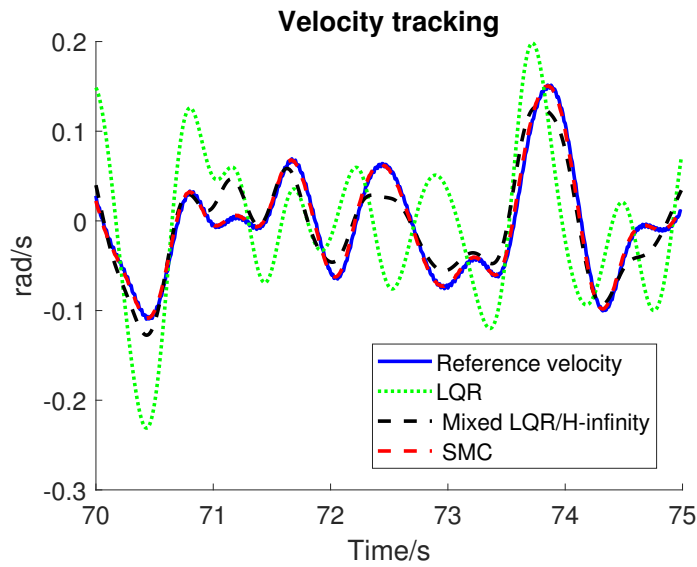
Figure 5.3: Velocity tracking of three methods (Seastate 2).

The velocity tracking results of all methods under Seastate 2 are given in Figure 5.3. It can be seen that the basic LQR approach fails to enable the PAWEC system to track the reference velocity, due to lack of robustness. However, both the mixed LQR/H_∞ control and SMC possess strong robustness that present low velocity tracking errors.
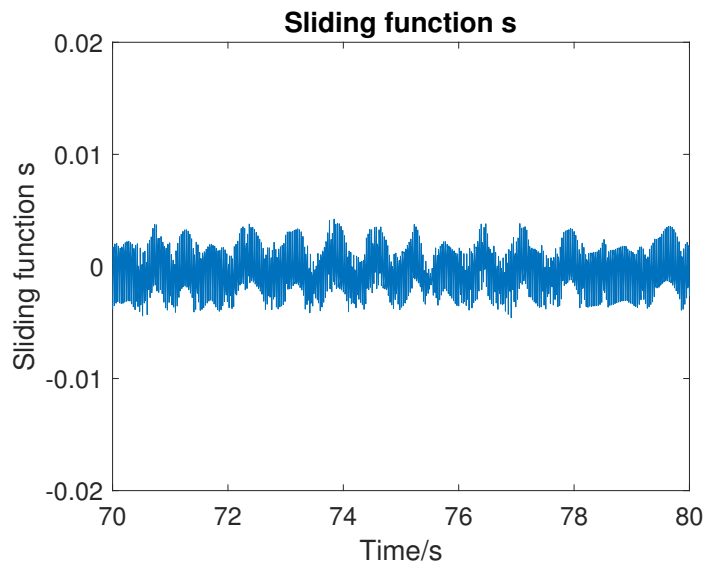
Figure 5.4: Velocity tracking of three methods (Seastate 2).

The switching procedure of the switching function s is shown in Figure 5.4, which demonstrates the states of error system can reach a state close to the sliding mainfold.
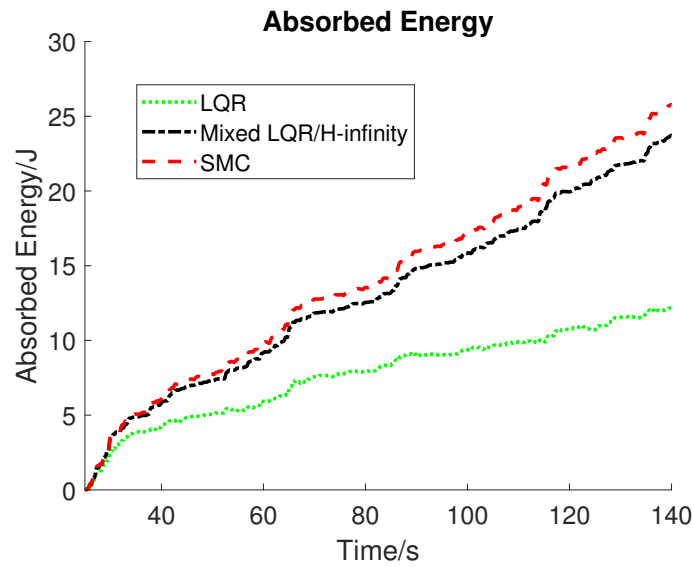
Figure 5.5: Absorbed energy from three methods (Seastate 2).

Figure 5.5 gives the absorbed energy E_{abs} from all methods corresponding to Seastate 2. The total simulation time is 100 times the peak period and the first 25s is omitted in the energy computation, since its role of wave ramp. Obviously, the mixed LQR/H_∞ control and SMC methods can absorb more energy from the waves than the basic LQR approach. But the SMC can generate slightly more energy than the mixed LQR/H_∞ control strategy, owing to its stronger robustness property.
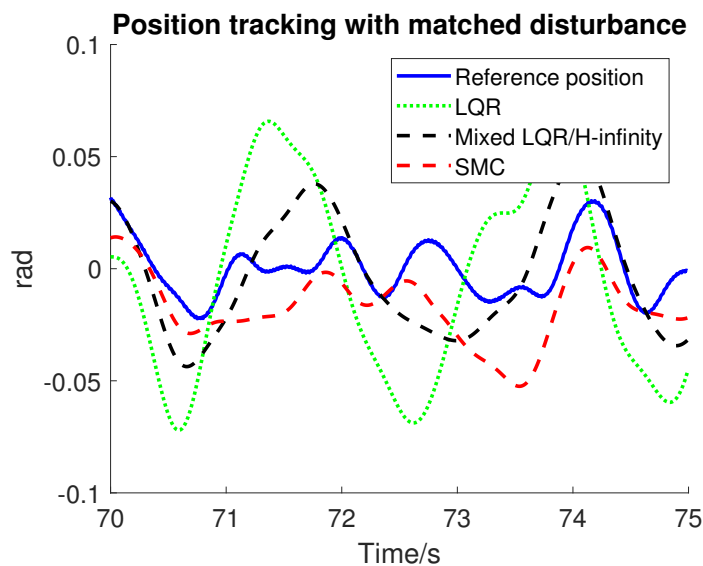
Figure 5.6: Position tracking of three methods with added matched disturbance (Seastate 2).

Figure 5.6 shows the position tracking of three methods with added matched distur-

bance corresponding to Seastate 2. It is still the same that all three methods are unable to accurately do position tracking, due to the additional static moments.

Additionally, the velocity tracking results of three methods with matched disturbance are given in Figure 5.7. It may not be surprising that the LQR design presents a large velocity tracking error, once again. The SMC design demonstrates a good PAWEC system disturbance suppression capability in the velocity tracking result. However, the velocity tracking result from the mixed LQR/H_∞ control strategy shows a larger magnitude than the corresponding result in Figure 5.3, when the matched disturbance affects the PAWEC system.
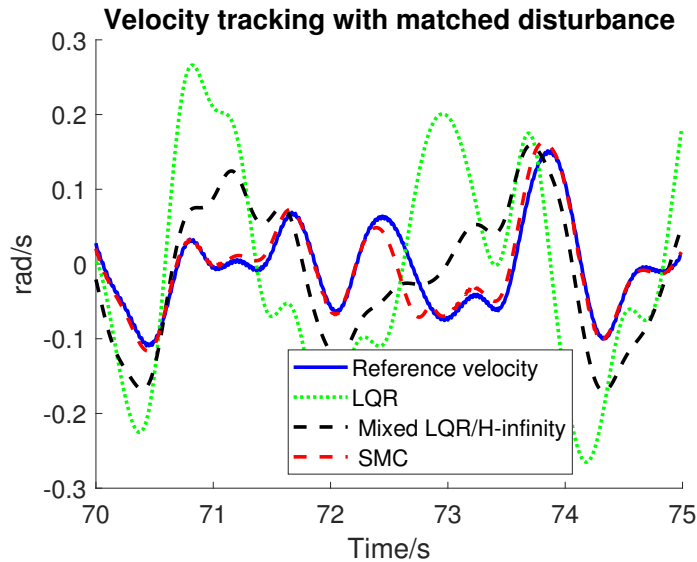
Figure 5.7: Velocity tracking of three methods with added matched disturbance (Seastate 2).

Figure 5.8 gives the absorbed energy E_{abs} from all three methods with added matched disturbance, corresponding to Seastate 2. It is clear that the energy production of the LQR design degrades significantly with the additional disturbance. There is a slight reduction in E_{abs} of the mixed LQR/H_∞ strategy. However, the SMC provides the best robustness in wave energy conversion, when the matched disturbance is presented in the control channel as system uncertainty. The disturbance is eliminated during sliding mode, as expected for a matched uncertainty.
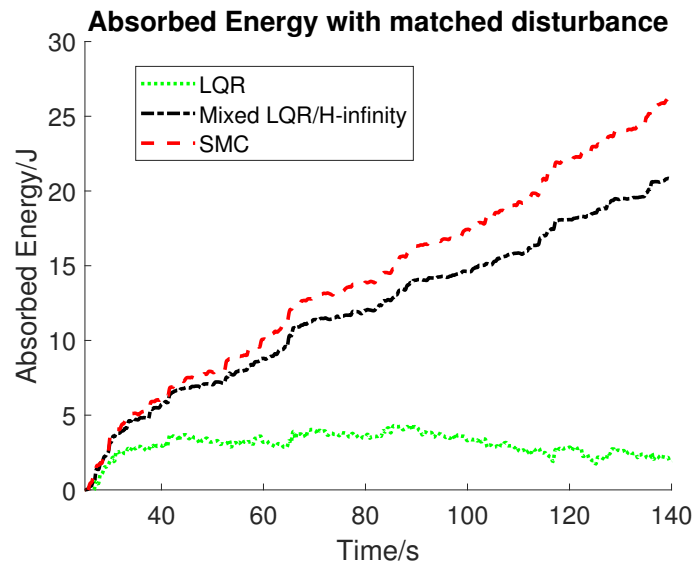
Figure 5.8: Absorbed energy from three methods with added matched disturbance (Seastate 2).

5.5 Summary

This Chapter focuses on the model-following tracking concept and the designed two robust control methods, mixed LQR/H_∞ control and SMC. A comparison study is conducted between the basic LQR, mixed LQR/H_∞ control and SMC approaches in numerical simulation, based on the WEC-Sim modelling. The comparative simulations demonstrate that the proposed model-following mixed LQR/H_∞ control and SMC can perform well with good PAWEC system tracking. Each of two robust methods have strong robustness and the designs have achieved fast response in control performance. In summary, the robustness analysis is a very important topic for energy production in the wave energy field. Separate studies must be made for the robustness of control methods applied to a wider class of non-PAWEC systems.

In preparation for a comparison study between the robust control and MPC methods in Chapter 7, the model-predictive velocity tracking control is proposed in Chapter 6 using the same hierarchical tracking structure as described in Chapter 1. More discussions of the comparison between model-following robust control and MPC are shown in Chapter 7.

Chapter 6

Model-Predictive Tracking Control Approach based on Gaussian Process Model

6.1   Introduction

Apart from the CCC and MPC, there are several PAWEC control design methods in the literature, to achieve energy maximization. For example, adaptive Dynamic Programming (Na et al., 2018), moment-matching based control (Faedo et al., 2018), Reinforcement Learning control (Anderlini et al., 2020), as well as several forms of basic LTI control (García-Violini et al., 2020b), etc. Usually adaptive Dynamic Programming can provide optimal solution in each time step but it has very large complexity in both time and space, which is difficult to be applied to the real PAWEC applications. As for Reinforcement Learning control, it needs very long time for training an agent to provide optimal policy. In general, it is a black box and not always to be wised enough to make the good decision to obtain optimal PTO coefficients. Sometimes misjudgments occur in the Reinforcement Learning control system. Regarding moment-matching based control and basic LTI control depend on strong assumptions to approximate the optimal objective condition or PAWEC dynamics, which are not always feasible or can only give suboptimal solution in PAWEC control design.

Different from these methods, MPC is the most frequently used method for wave energy application studies. MPC is used to set the average absorbed mechanical power as its objective function to achieve energy maximization on a PAWEC device. MPC

not only provides an optimal solution for energy production but deal with system constraints simultaneously. However, MPC is often combined with WEF/WEM prediction, which usually involves prediction errors that possibly limit its value in practice.

This Chapter continues to concentrate on energy-maximizing control of a Wavestar-like device described in Chapter 3, by placing the MPC system at the low-level part of the hierarchical tracking structure of Figure 1.5. The MPC objective function then consists of the velocity error signal and control input term. Its objective can be transformed into a quadratic index to reach optimality with a control input constraint (Li and Patton, 2023a). It is shown that the PAWEC system can get into a near-resonance operation with promising results for energy maximization, by achieving optimal reference velocity tracking (Li and Patton, 2023a). The near-resonance operation means that the WEC float velocity is in-phase with the WEF/WEM.

On the other hand, for the design of high-level part of the hierarchical structure, following (Nguyen and Tona, 2017b), a Kalman filter is chosen to estimate the WEM signal. When used correctly the Kalman filter shows a potential for following the high frequency components as this makes the estimation better matched with MPC design than other estimators, when the system sampling time is increased. Following the work of (Fusco, 2012) the reference velocity is computed using an Extended Kalman Filter (EKF). The EKF computes the instantaneous amplitude $\hat{A}_{ex}$ and frequency $\hat{\omega}$ of the WEM (see its design details in Chapter 4).

The short-term predictions of the WEM sequence and the reference velocity sequence are required in the MPC objective function. Considering the short-term prediction of the WEM sequence, an Auto-Regressive (AR) model is often used to perform this function (Guo et al., 2018). However, the AR model should be updated frequently in the real-time forecasting function. This has the effect of a considerable increase in computation and real-time prediction capability. As an alternative to the use of AR a Gaussian Processing (GP) approach (Williams and Rasmussen, 2006) has been used with two GP models to perform more realistic forecasting. Typically, the hyperparameters of the GP models are preselected before the training process with no requirement on updating the parameters during real-time forecasting, thereby reducing the prediction time. The GP is a kernel-based and nonparametric learning method (Williams and Rasmussen, 2006) having the advantages of modelling flexibility, prediction with learning smoothness and the use of noise parameters, based on a training set.

This approach was used by the Hull team in the real-time application of the competition completed at Aalborg University (Ringwood et al., 2023a) and has been adopted here to make the study consistent with potential real application. For the competition the Hull team used GP modelling with Bayesian learning control (Shi et al., 2018), i.e. without the use of MPC. However, the different work in this Chapter describes the combination of GP for prediction along with MPC.

This Chapter Section 6.2 presents the whole concept of the model-predictive tracking control structure. The Kalman filter for implementing WEM estimation is described in Section 6.3. Section 6.4 describes the design of the model-predictive velocity tracking control with GP model for short-term forecasting. Section 6.5 gives the simulation results and discussions. Section 6.6 provides the Chapter Summary.

6.2 The tracking structure of model predictive control

After referring to the hierarchical tracking structure described in Chapter 1 and Figure 1.5 again, the velocity tracking idea of MPC design is presented in Figure 6.1.
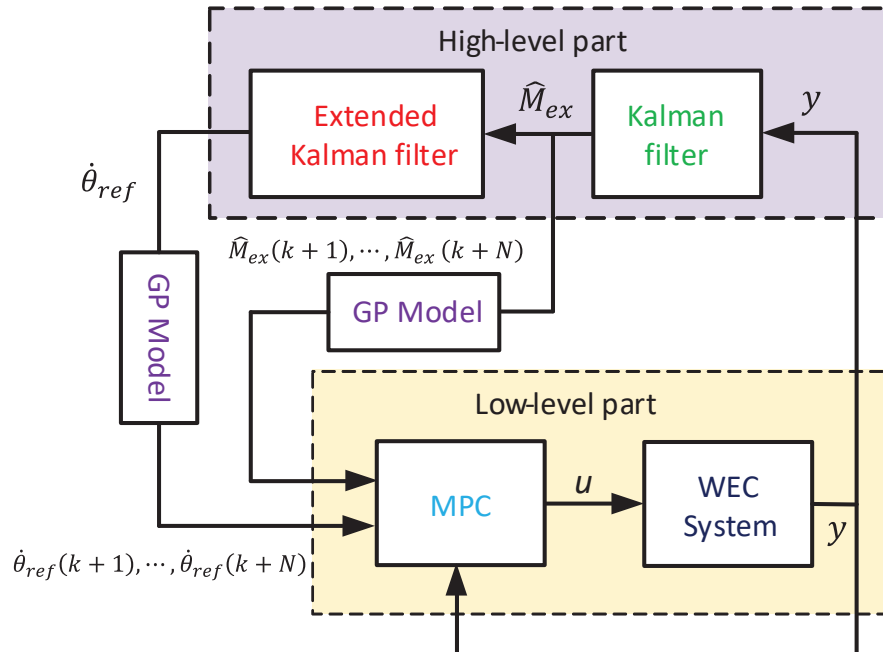
Figure 6.1: Tracking structure of model predictive control.

The high-level part still includes the WEM estimation and reference velocity generation

in which the Kalman filter is used to achieve the WEM estimation, with a focus on following the high frequency wave components which is more matched with MPC design than other estimators when the system sampling time is increased. The reference velocity $\dot{\theta}_{ref}$ computation is still based on the EKF for providing the instantaneous amplitude and frequency of the estimated $\hat{M}_{ex}$.

Furthermore, for the low-level controller design, MPC is selected to force the scaled Wavestar-like device to perform velocity tracking in order to reach the energy maximization generation. Two GP models are chosen to do predictiton works with multiple steps ahead of the future WEM $\hat{M}_{ex}(k+1), \cdots, \hat{M}_{ex}(k+N)$ and future reference velocity $\dot{\theta}_{ref}(k+1), \cdots, \dot{\theta}_{ref}(k+N)$, which both are required in MPC velocity tracking design.

Note: Different from Chapter 5 Figure 5.1 model-following tracking design, all of Kalman filter, EKF, two GP models and MPC velocity tracking in this Chapter is based on discrete system design.

6.3   Kalman filter with random walk

For this Wavestar-prototype device WEM is a physical unmeasurable quantity, since the required device total pressure measurements are not available in the benchmark. However, a suitably accurate WEM signal is crucial for designing the optimal energy-maximising controller. As mentioned in Section 3.3, the equivalent WEM around the hinge point A can be regarded as an external term. Hence, the WEM can be generated by a Kalman filter (or other estimator). All of this work can be based on discrete-time state space model (6.1) of the PAWEC system:

$$
\begin{aligned}
x(k+1) &= A_d x(k) + B_d u(k) + B_d M_{ex}(k) + \varepsilon_x(k) \\
y(k) &= C_d x(k) + \mu(k)
\end{aligned}
\tag{6.1}
$$

where $\varepsilon_x(k)$ is chosen to represent the unmodeled dynamics and $\mu(k)$ denotes the measurement noise. $M_{ex}(k)$ is an external moment term acting on the PAWEC float, and it can be treated as an unknown input term of system (6.1). Thereby, to assume the discrete-time dynamics of the WEM (Nguyen and Tona, 2017b) as:

$$
M_{ex}(k+1) = M_{ex}(k) + \varepsilon_m(k)
\tag{6.2}
$$

where $\varepsilon_m(k)$ means a Gaussian distributed random variable. In general, the next value of WEM will conduct a random step away from the present value after a sampling time, and all moving steps are considered independent. $M_{ex}(k)$ can be considered as a new system state and then be estimated through optimal state estimation by a Kalman filter. Then, the related augmented system can be defined as a Random Walk system as:

$$\begin{aligned}
\bar{x}(k+1) &= \bar{A}\bar{x}(k) + \bar{B}u(k) + \varepsilon(k) \\
y(k) &= \bar{C}\bar{x}(k) + \mu(k)
\end{aligned} \tag{6.3}$$

where $\bar{A} = \begin{bmatrix} A_d & B_d \\ \mathbf{0}_{1\times4} & 1 \end{bmatrix}$, $\bar{x} = \begin{bmatrix} x \\ M_{ex} \end{bmatrix}$, $\bar{B} = \begin{bmatrix} B_d \\ 0 \end{bmatrix}$, $\bar{C} = \begin{bmatrix} C_d & \mathbf{0}_{2\times1} \end{bmatrix}$,

$\varepsilon(k) = \begin{bmatrix} \varepsilon_x(k) \\ \varepsilon_m(k) \end{bmatrix}$. The dimensions of system matrices are $\bar{A} \in \mathfrak{R}^{5\times5}$, $\bar{B} \in \mathfrak{R}^{5\times1}$, $\bar{C} \in \mathfrak{R}^{2\times5}$. $\varepsilon(k)$ and $\mu(k)$ are uncorrelated zero-mean white noise processes with covariance matrices Q_f and R_f.

Hence, the prediction update equations (Nguyen and Tona, 2017b) of the Kalman filter are:

$$\begin{aligned}
\hat{\bar{x}}(k|k-1) &= \bar{A}\hat{\bar{x}}(k-1|k-1) + \bar{B}u(k-1) \\
P_f(k|k-1) &= \bar{A}P_f(k-1|k-1)\bar{A}^T + Q_f
\end{aligned}$$

The correction update equations (Nguyen and Tona, 2017b) of the Kalman filter are:

$$\begin{aligned}
K_f(k) &= P_f(k|k-1)\bar{C}^T(\bar{C}P_f(k|k-1)\bar{C}^T + R_f)^{-1} \\
\hat{\bar{x}}(k|k) &= \hat{\bar{x}}(k|k-1) + K_f(k)(y(k) - \bar{C}\hat{\bar{x}}(k|k-1)) \\
P_f(k|k) &= (I - K_f(k)\bar{C})P_f(k|k-1)
\end{aligned}$$

The estimated $\hat{M}_{ex}$ will be acquired after the optimal estimation of state vector $\hat{\bar{x}}$ is known. Note the following:

$\hat{\bar{x}}(k|k-1)$ is a predicted priori state estimate given the observations at time $k-1$.

$P_f(k|k-1)$ is a predicted priori covariance matrix given the observations at time $k-1$.

$\hat{\bar{x}}(k|k)$ is an updated posteriori state estimate given the observations at time k.

$P_f(k|k)$ is an updated posteriori covariance matrix given the observations at time k.

6.4 Model-predictive tracking control with short-term forecasting

The proposed new MPC approach (Li and Patton, 2023a) considers to add the velocity error signal into its quadratic objective function for the purpose of tracking. On the other hand, the sequences of future $\hat{M}_{ex}$ and future reference velocity $\dot{\theta}_{ref}$ are also required, and they will be predicted in the short term by two uncorrelated GP models. As outlined in Section 6.1, the required reference velocity can be computed using an EKF. Furthermore, it is necessary to choose the forecasting time carefully due to a trade-off between computation burden and prediction accuracy.

6.4.1 Model-predictive tracking control design

To define $v = \dot{\theta}$ and with $C_v = \begin{bmatrix} 0 & 1 & 0 & 0 \end{bmatrix}$, and set the angular velocity $\dot{\theta}$ as the PAWEC system output, then a discrete-time state space model has the form of:

$$
\begin{aligned}
x(k+1) &= A_d x(k) + B_d u(k) + B_d \hat{M}_{ex}(k) \\
v(k) &= C_v x(k)
\end{aligned}
\tag{6.4}
$$

After applying the iteration process to model (6.4), with the prediction horizon N, a prediction model (Li and Patton, 2023a) can be obtained as below:

$$
V_N = S_{av} x(k) + S_{bv} u_N + S_{bv} M_{ex,N}
\tag{6.5}
$$

with $V_N = \begin{bmatrix} v(k+1) \\ v(k+2) \\ \dots \\ v(k+N) \end{bmatrix}, S_{av} = \begin{bmatrix} C_v A_d \\ C_v A_d^2 \\ \dots \\ C_v A_d^N \end{bmatrix}, M_{ex,N} = \begin{bmatrix} \hat{M}_{ex}(k) \\ \hat{M}_{ex}(k+1) \\ \dots \\ \hat{M}_{ex}(k+N-1) \end{bmatrix}$

$$
u_N = \begin{bmatrix} u(k) \\ u(k+1) \\ \dots \\ u(k+N-1) \end{bmatrix}, S_{bv} = \begin{bmatrix} C_v B_d & 0 & 0 & \cdots & 0 \\ C_v A_d B_d & C_v B_d & 0 & \cdots & 0 \\ \vdots & \vdots & \vdots & \ddots & \vdots \\ C_v A_d^{N-1} B_d & C_v A_d^{N-2} B_d & \cdots & C_v A_d B_d & C_v B_d \end{bmatrix}.
$$

These stacked predictions are involved in the MPC objective function of the next optimization problem.

By defining $v_{ref} = \dot{\theta}_{ref}$, Then, the constrained optimization problem about velocity

tracking can be represented (Oscar Mauricio Agudelo Mañozca, 2017) as follows:

$$\min_{\substack{V_N, u_N \\ M_{ex,N}}} \sum_{i=1}^{N} [v(k+i) - v_{ref}(k+i)]^T Q_v [v(k+i) - v_{ref}(k+i)] + \sum_{i=0}^{N-1} [u(k+i)]^T R_v u(k+i)$$

(6.6)

$$subject\ to \quad |u(k+i)| \leq u_{max} \tag{6.7}$$

According to Equations (6.5) and (6.6), the objective function can be chosen as:

$$J_m = \frac{1}{2} V_N^T \bar{Q} V_N - v_{ref,N}^T \bar{Q} V_N + \frac{1}{2} v_{ref,N}^T \bar{Q} v_{ref,N} + \frac{1}{2} u_N^T \bar{R} u_N \tag{6.8}$$

where $\bar{Q} = \begin{pmatrix} Q_v & 0 & \cdots & 0 \\ 0 & \dfrac{N-1}{N} Q_v & \cdots & 0 \\ \vdots & \vdots & \ddots & \vdots \\ 0 & 0 & \cdots & \dfrac{1}{N} Q_v \end{pmatrix}, \bar{R} = \begin{pmatrix} R_v & 0 & \cdots & 0 \\ 0 & \dfrac{N-1}{N} R_v & \cdots & 0 \\ \vdots & \vdots & \ddots & \vdots \\ 0 & 0 & \cdots & \dfrac{1}{N} R_v \end{pmatrix},$

$v_{ref,N} = \begin{pmatrix} v_{ref}(k+1) \\ \vdots \\ v_{ref}(k+N) \end{pmatrix}.$

Then, on substituting Equations (6.5) into (6.8), the objective function (Li and Patton, 2023a) will be transformed into:

$$J_m = \frac{1}{2} (S_{av} x(k) + S_{bv} u_N + S_{bv} M_{ex,N})^T \bar{Q} (S_{av} x(k) + S_{bv} u_N + S_{bv} M_{ex,N}) + \frac{1}{2} u_N^T \bar{R} u_N$$
$$- v_{ref,N}^T \bar{Q} S_{av} x(k) - v_{ref,N}^T \bar{Q} S_{bv} u_N - v_{ref,N}^T \bar{Q} S_{bv} M_{ex,N} + \frac{1}{2} v_{ref,N}^T \bar{Q} v_{ref,N}$$

(6.9)

In terms of the velocity tracking and dropping some bias terms, the quadratic form of the above objective function J_m will be as follows:

$$J_m = \frac{1}{2} u_N^T H_m u_N + f_m^T u_N \tag{6.10}$$

where $H_m = S_{bv}^T \bar{Q} S_{bv} + \bar{R}$, $f_m^T = x^T(k) S_{av}^T \bar{Q} S_{bv} + M_{ex,N}^T S_{bv}^T \bar{Q} S_{bv} - v_{ref,N}^T \bar{Q} v_{ref,N}$.

Hence, the purpose of the MPC velocity tracking has been transformed into a Quadratic Programming (QP) optimization process (Li and Patton, 2023a), and the energy maximization can be achieved when the Wavestar-prototype device does the velocity tracking work across a range of irregular waves. To solve the QP optimization of the designed new MPC method, the qpOASES QP solver (Ferreau et al., 2014) is selected

and it has an advantage of being well-suited to the applications of MPC that require fast and reliable computation. As for the $M_{ex,N}$ and $v_{ref,N}$, these sequences can be obtained by a short-term forecasting from two GP models, respectively.

6.4.2 Gaussian Process model design

An *a priori* expression of a GP model $f(a)$ is usually expressed by a mean function $m(a)$ and covariance function $k(a,a^*)$ (Williams and Rasmussen, 2006) as follows:

$$
\begin{aligned}
f(a) &\sim \mathcal{GP}(m(a),k(a,a^*)) \\
m(a) &= \mathbb{E}[f(a)] \\
k(a,a^*) &= cov(f(a),f(a^*))
\end{aligned}
\tag{6.11}
$$

where $a \in \Re^{\mathcal{D}}$ is a vector of the dynamics inputs with dimension $\mathcal{D}$, and the random Gaussian scalar variables $f(a)$ and $f(a^*)$ (Liu et al., 2022) are indexed by input a and a^*. The $k(a,a^*)$ is a kernel function which is usually parametrized by the specific hyperparameters.

Next, define a training set $\mathfrak{D} = (\boldsymbol{a},\boldsymbol{z})$, where $\boldsymbol{a} = [a_1,a_2,\cdots,a_n]$ is a input vector, and $\boldsymbol{z} = [z_1,z_2,\cdots,z_n]$ is a corresponding vector with all scalar outputs. Thereby, to express a GP *a posterior* model as the form of

$$
z_i = f(a_i) + \varepsilon_i \quad \varepsilon_i \sim \mathcal{N}(0,\sigma^2)
\tag{6.12}
$$

where z_i are the values of observed output, $f(a_i)$ denote the GP model values, and ε_i represent zero mean white Gaussian noise.

Here, a spectral mixture (SM) kernel is chosen as the covariance function of a GP model, to perform the forecasting computation work for generating future WEM or future reference velocity sequences. The form of SM kernel is given by (Wilson and Adams, 2013):

$$
k_{SM}(\bar{\tau}) = \sum_{s=1}^{S} w_s cos(2\pi \bar{\tau}^T \mu_s) \prod_{o=1}^{O} \exp(-2\pi^2 \tau_o^2 v_s^{(o)})
\tag{6.13}
$$

where the one-dimensional input $O = 1$, S is the number of the total wave frequency components, and $\bar{\tau}$ denotes the distance between two arbitrary input points a_i and a_j.

In terms of the concept of wave reconstruction (Shi, 2021), the three elements in the SM kernel hyperparameter vector $\Theta = (\mu_s, w_s, v_s)^T$ represent the period, amplitude and evolutionary-scale of each wave component, respectively. In other words, the SM kernel is suitable to be used as the covariance function of a GP model to do the short term wave forecasting (Shi et al., 2018) due to its automatic discovery capability (Wilson and Adams, 2013).

The hyperparameters of Θ in the SM kernel can be obtained by optimizing its *log* marginal likelihood function (Williams and Rasmussen, 2006) as follows:

$$log\, p(\mathbf{z}|\mathbf{a},\Theta) = -\frac{1}{2}log|K + \sigma^2 I| - \frac{1}{2}\mathbf{z}^T(K + \sigma^2 I)^{-1}\mathbf{z} - \frac{n}{2}log(2\pi) \qquad (6.14)$$

Note that there are advantages of choosing the initial hyperparameters with highly suitable values before the training process (Shi, 2021), such as the promotion on the convergence rate of optimization and to avoid reaching an unsatisfactory local optimum.

After finishing the training process, the *a posterior* joint distribution of the prediction f^* with given input vector $\mathbf{a}^*$ takes the following form:

$$\begin{bmatrix} f^* \\ \mathbf{z} \end{bmatrix} \sim \left(\begin{bmatrix} m(\mathbf{a}^*) \\ m(\mathbf{a}) \end{bmatrix}, \begin{bmatrix} k(\mathbf{a}^*,\mathbf{a}^*) & k(\mathbf{a}^*,\mathbf{a}) \\ k(\mathbf{a},\mathbf{a}^*) & K + \sigma^2 I \end{bmatrix} \right) \qquad (6.15)$$

with $k(\mathbf{a}^*,\mathbf{a}) = k(\mathbf{a},\mathbf{a}^*) = [k(\mathbf{a}_1,\mathbf{a}^*), \cdots, k(\mathbf{a}_N,\mathbf{a}^*)]$. Then, based on the Joint Gaussian Distribution Theorem, the predicted result about f^* can be described as:

$$\begin{aligned} \mu(f^*) &= m(\mathbf{a}^*) + k(\mathbf{a}^*,\mathbf{a})[K + \sigma^2 I]^{-1}(\mathbf{z} - m(\mathbf{a})) \\ \sigma(f^*) &= k(\mathbf{a}^*,\mathbf{a}^*) - k(\mathbf{a}^*,\mathbf{a})[K + \sigma^2 I]^{-1}k(\mathbf{a},\mathbf{a}^*) \end{aligned} \qquad (6.16)$$

The Gaussian Process for Machine Learning (GPML) package (Williams and Rasmussen, 2006) is then applied to design the GP model and perform the training and test prediction work.

6.5 Simulation results

The main simulation results include GP modelling for short-term forecasting and MPC velocity tracking for testing on a WEC-Sim model of the Wavestar-prototype device considering irregular waves. As mentioned in Section 6.2, all of algorithms used in this Chapter is designed in discrete version simulation with sampling rate (simulation

step) 0.05s. The discussion and analysis of extracted energy, generated instantaneous power, and PTO moment are also given, respectively. More testing and comparison works between model-following robust control and MPC methods are described in Chapter 7.

The related simulation parameters for this Chapter are listed in Table 6.1 and as for the Wavestar modelling parameters, given in Table 3.2. A fixed-step size ode8 (Dormand-Prince) solver is selected to conduct the simulation works for the WEC-Sim numerical model in Matlab/Simulink software.

Table 6.1: The simulation parameters.

Parameters	Values
Simulation sampling time T_s	0.05s
KF coefficient Q_f	diag(0.01, 0.1, 0.01, 0.01, 200)
KF coefficient R_f	diag(0.01, 0.01)
EKF initial state x_e	$[1,1,5]^T$
EKF coefficient Q_e	diag(0.2, 0.2, 0.001)
EKF coefficient R_e	0.1
Angular displacement limit θ_{lim}	0.4 rad
Control limit u_{max}	± 12 Nm
GP coefficient S	12/14

As mentioned in Chapter 3, the JONSWAP wave Spectrum is still used here to generate three irregular waves: Seastate 4, 5 and 6. The MPC prediction horizon N_p and MPC coefficients Q_v and R_v are shown in Table 6.2.

Table 6.2: The irregular wave information and MPC coefficients.

Case	N_p	Q_v	R_v
Seastate4	20	0.5	2×10^{-3}
Seastate5	30	0.5	5×10^{-4}
Seastate6	40	0.5	2×10^{-4}

The predicted results of WEM and reference velocity from two GP models under three sea states are shown in Figure 6.2. The future sequences of WEM and reference velocity are required in the objective function of MPC tracking design.

(a) Sea State 4.

(a) Sea State 4.

(b) Sea State 5.

(b) Sea State 5.

(c) Sea State 6.
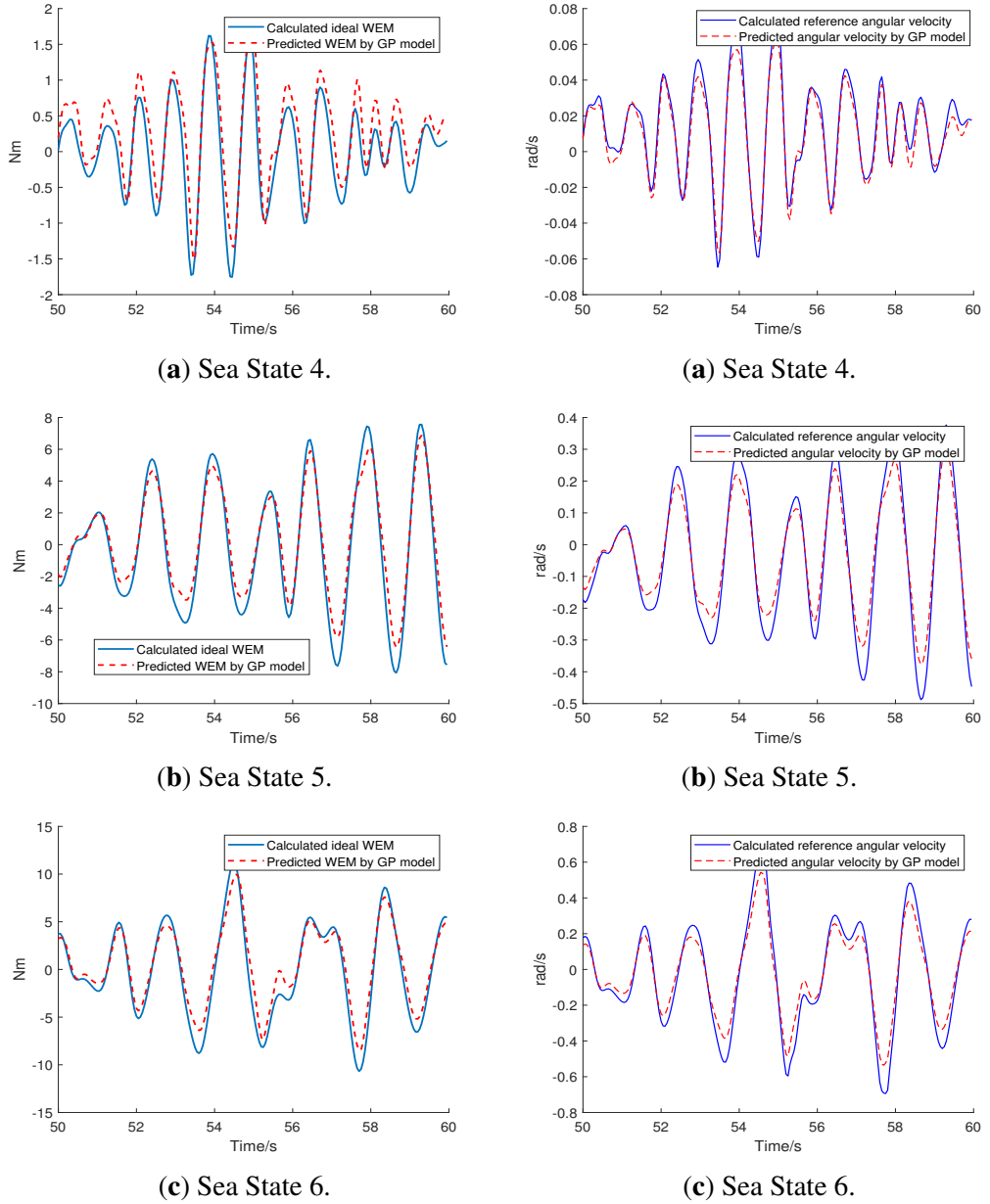
(c) Sea State 6.

Figure 6.2: Predicted WEM and reference velocity by GP models (three sea states).

From the Figure 6.2, it is clear that the predicted WEM is matched well with the ideal WEM computed by formula (3.25). The GP modelling presents a high accuracy of WEM prediction with good learning smoothness. In addition, as long as suitable hyperparameters are chosen in advance before the training process, there is no extra need to update the GP hyperparameters during the forecasting work. According to the Equation (4.28), it can be determined that the wave excitation moment $\hat{M}_{ex}$ and reference velocity $\dot{\theta}_{ref}$ share the same phase but with different amplitude if the velocity tracking work has been achieved correctly through the PAWEC system MPC approach. This

shows clearly that the predicted velocity reference is able to generate similar trends to the predicted WEM.

(**a**) Sea State 4. (**a**) Sea State 4.

(**b**) Sea State 5. (**b**) Sea State 5.

(**c**) Sea State 6. (**c**) Sea State 6.
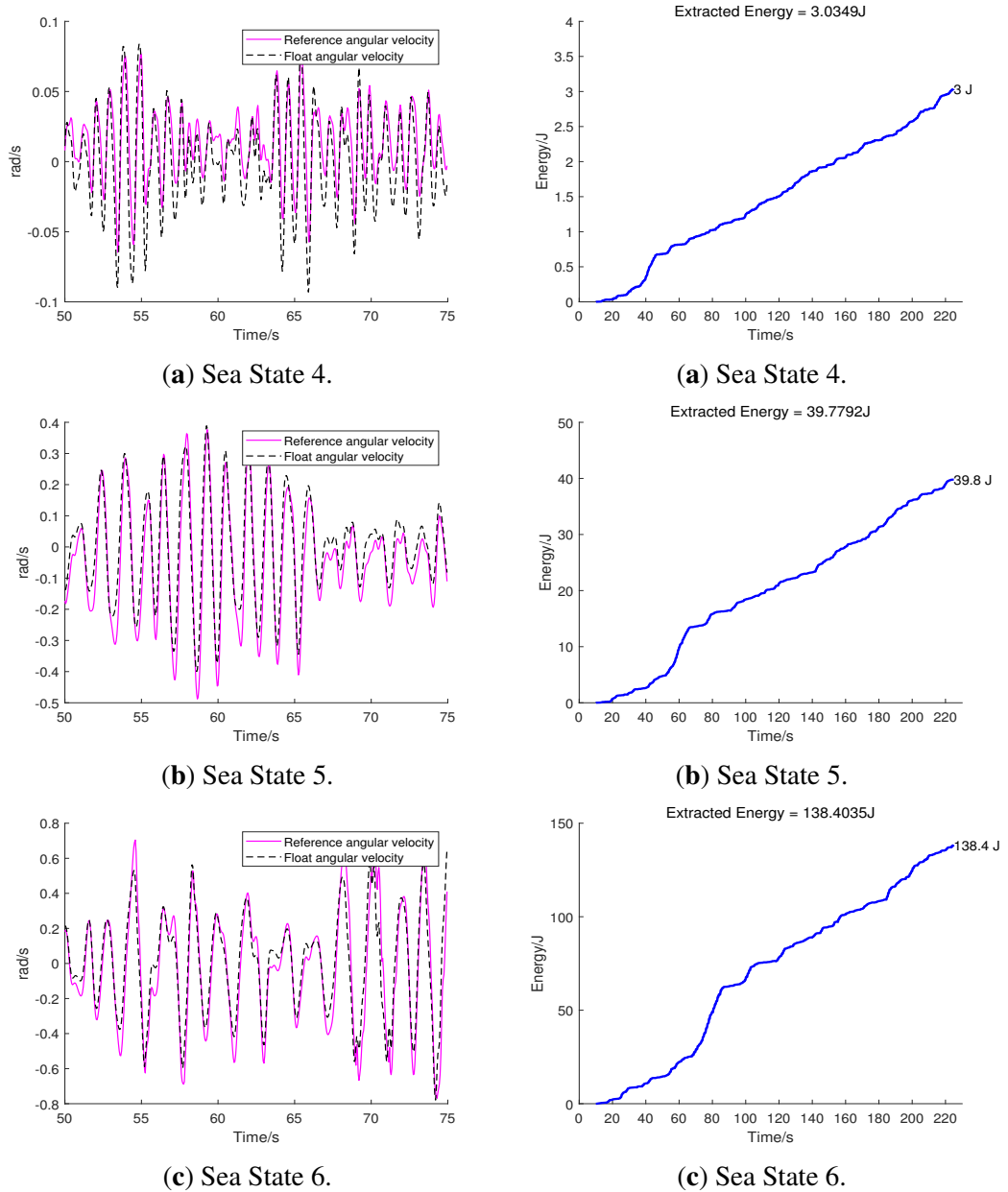
Figure 6.3: MPC velocity tracking and corresponding extracted energy (three sea states).

The MPC tracking results and the corresponding extracted energy from three sea states are shown in Figure 6.3. The overall tracking performance of MPC is good, even though the float angular velocity $\dot{\theta}$ has a few amplitude differences with the reference velocity $\dot{\theta}_{ref}$ occasionally. But the tracking errors are small and acceptable between

$\dot{\theta}$ and $\dot{\theta}_{ref}$. Besides they share approximately same phase most of time. The significance of this that a near-resonance operation for the PAWEC device has been achieved along with good energy maximization. In other words, the PAWEC system follows the incident waves by using the tracking MPC controller to reach its tracking mission. In summary, although the MPC tracking system may lack some robustness, it yields very small PAWEC tracking errors.

(a) Sea State 4. (a) Sea State 4.

(b) Sea State 5. (b) Sea State 5.

(c) Sea State 6. (c) Sea State 6.
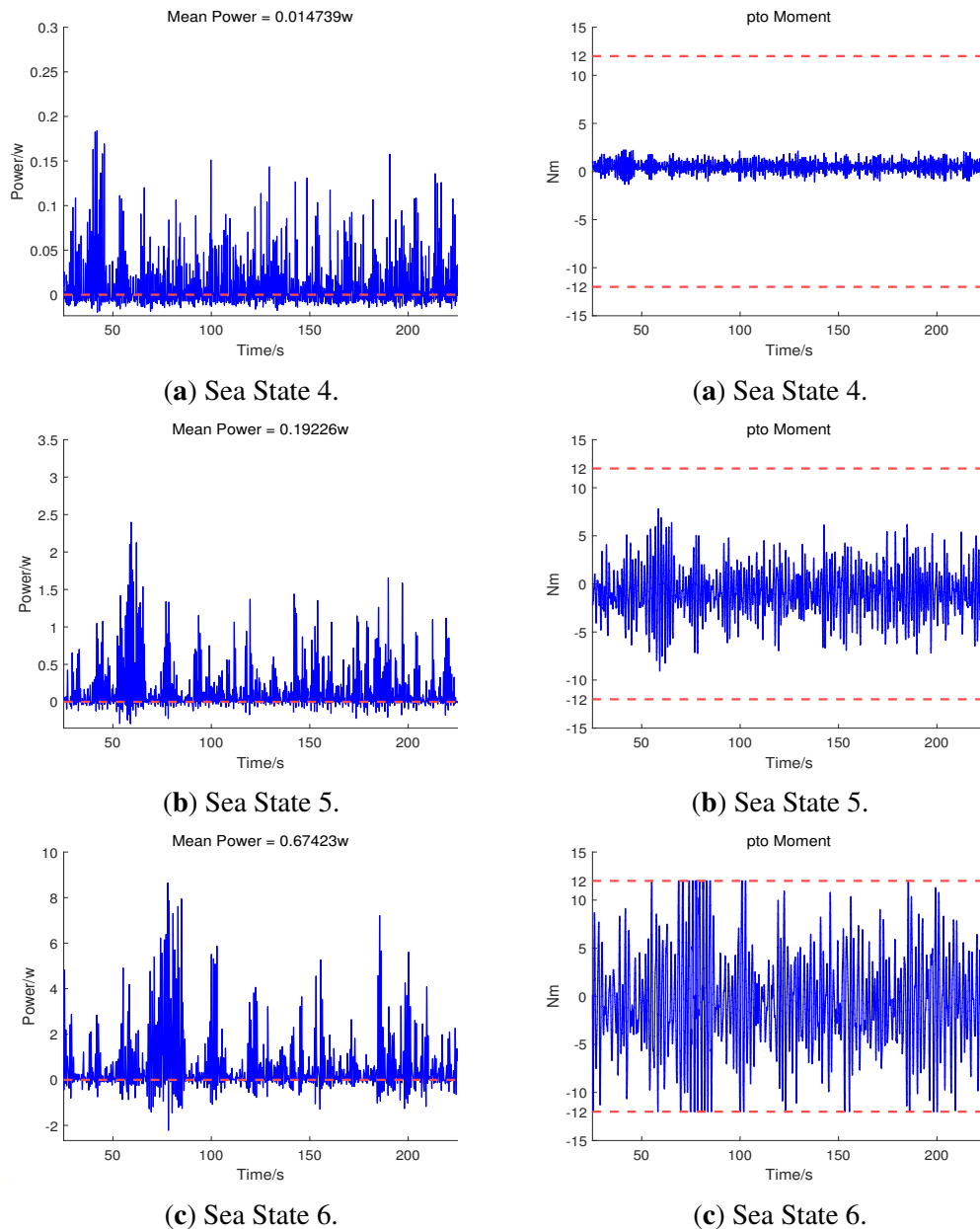
Figure 6.4: Generated instantaneous power and PTO moment (three sea states).

The generated instantaneous power and PTO moment from three sea states are given in

Figure 6.4. It is clear that the MPC approach proposed in this Chapter introduces very few negative power PTO excursions. This offers a significant advantage for reducing energy loss over currently discussed MPC methods, which has good advantages in solving the bi-directional flow problem in a PTO system. Thereby reducing the energy loss when the PTO system works in motor mode.

On the other hand, from the Figure 6.4, the input maximum limits of the PTO moment are $\pm 12 Nm$, shown as the red lines and the MPC control input is satisfied by the constraint conditions. In general, the MPC tracking performance can be improved when the coefficient R_v is decreased, but this results in a large PTO moment. Conversely, the control input can be small if a large R_v is selected, which reduces the MPC tracking performance.

The proposed MPC tracking approach of this Chapter can be compared with Model-following robust control methods (Chapter 5), and more comparisons will be given in (Chapter 7).

6.6   Summary

This Chapter concentrates on the design of an MPC tracking controller based on the hierarchical structure described in Chapter 1. The goal is to achieve energy maximization extraction for a 1:20 scaled Wavestar-prototype device built in the WEC-Sim benchmark. The first part of the system structure comprises a Kalman filter to provide a WEM signal, necessary for PAWEC control. An EKF is used to compute the instantaneous WEM amplitude and frequency for determining the required reference velocity. The second part of the overall structure includes MPC tracking control design incorporating GP models. Two GP models are chosen to perform WEM prediction instead of the familiar and simplistic AR prediction strategy. The future WEM and future reference velocity, are both required in the MPC objective function for optimization solving. The simulation results show the low-level MPC controller can provide good velocity tracking performance with samll errors and enable the PAWEC system to reach a near-resonance condition for good energy-maximization. The MPC tracking system is able to deal with input contraint and is shown to generate very few negative power excursions, avoiding significant bi-directional power flow in the PTO system.

The MPC and model-following robust control approaches will be compared in Chapter 7 under irregular wave conditions, in terms of metrics such as the disturbance testing, absorbed energy, extracted energy, extracted power, and the Wavestar model PTO moment, etc.

Chapter 7

Comparison Study between MPC, Robust Mixed LQR/H-infinity Control and SMC for PAWEC Energy Maximisation Control Analysis

7.1 Introduction

The aim of this chapter is to carry out a comparison study between the MPC and robust control approaches in order to give some discussions about the characteristics of these methods on energy maximization and do robustness analysis for the scaled Wavestar-like device modelled in WEC-Sim. Generally, MPC has been widely studied in the wave energy field (Faedo et al., 2017) for maximisation of energy capture by the point absorber wave energy converters (PAWECs). As described in Chapter 6, the main purpose of basic MPC method is to maximize the absorbed mechanical energy (Guerrero-Fernández et al., 2020) by solving an optimization problem. And MPC could reach the optimal solution (Li and Belmont, 2014) for energy extraction and deal with PAWEC system physical constraints elegantly. A significant number of references in the PAWEC literature e.g. (Cretel et al., 2011; Soltani et al., 2014; Richter et al., 2014) provide more covering the design of an MPC system.

The robust energy-maximizing control can be designed in a tracking control strategy, based on a hierarchical structure (Fusco and Ringwood, 2014a) as mentioned in Chapter 5, which guides the PAWEC system into a near-resonance operation for energy

maximization generation with strong robustness against the system uncertainty. Usually, there is a gap in discussing the MPC and robust control together. After all, lots of researchers only did their work based on MPC but not in a tracking control way, making its not straightforward to compare MPC and robust control design. However, the MPC tracking strategy has been proposed in Chapter 6 of this thesis that creates a bridge in doing a comparison study between MPC and robust control strategies.

The popular design of MPC used in wave energy field is derived in Section 7.2. It is considered to select the average absorbed mechanical power as the control objective and to do an optimization procedure for the purpose of energy maximization. Section 7.3 shows the comparison results between:

- **Case 1:** MPC only includes power term (no tracking purpose),

- **Case 2:** MPC has both power term and input penalty term (no tracking purpose),

- **Case 3:** MPC velocity tracking based on GP model,

- **Case 4:** Model-following mixed LQR/H_∞ tracking control, and

- **Case 5:** Model-following sliding mode control.

According to some contents such as velocity tracking results between cases 3, 4, and 5, disturbance tests, absorbed energy, extracted energy, extracted power, PTO moment, etc. Finally, the Summary is given in Section 7.4.

7.2   Frequently used MPC design

MPC formulation

The first step of MPC design is to start from the discretized system of the state space model (3.26), as given by:

$$x(k+1) = A_d x(k) + B_d u(k) + B_d \hat{M}_{ex}(k)$$
$$y(k) = C_d x(k)$$

(7.1)

where $\hat{M}_{ex}$ is the estimated excitation moment obtained by a Kalman filter with random walk, and the details can be found in Chapter 6. u is the control input calculated from the designed controller.

The prediction model of Equation (7.1) can be built after iterations (Soltani et al., 2014), as shown:

$$x_N = \Omega x(k) + \Phi u_N + \Phi M_{ex,N} \tag{7.2}$$

with $x_N = \begin{bmatrix} x(k+1) \\ x(k+2) \\ \cdots \\ x(k+N) \end{bmatrix}$, $\Omega = \begin{bmatrix} A_d \\ A_d^2 \\ \cdots \\ A_d^N \end{bmatrix}$, $u_N = \begin{bmatrix} u(k) \\ u(k+1) \\ \cdots \\ u(k+N-1) \end{bmatrix}$,

$M_{ex,N} = \begin{bmatrix} \hat{M}_{ex}(k) \\ \hat{M}_{ex}(k+1) \\ \cdots \\ \hat{M}_{ex}(k+N-1) \end{bmatrix}$, $\Phi = \begin{bmatrix} B_d & 0 & 0 & \cdots & 0 \\ A_d B_d & B_d & 0 & \cdots & 0 \\ \vdots & \vdots & \vdots & \ddots & \vdots \\ A_d^{N-1} B_d & A_d^{N-2} B_d & \cdots & A_d B_d & B_d \end{bmatrix}$.

where N is the selected prediction horizon, $M_{ex,N}$ is the predicted sequence of the $\hat{M}_{ex}$ provided by a Gaussian Process model through a short-term forecasting. More details are given in Chapter 6.

Objective function

The absorbed mechanical energy E_{abs} by a PTO system can be calculated over a time horizon T_l (Soltani et al., 2014) as follows:

$$E_{abs} = \int_0^{T_l} P_a(t) dt \tag{7.3}$$

where $P_a(t)$ is the instantaneous absorbed mechanical power, defined by:

$$P_a(t) = -M_{PTO}(t)\dot{\theta}(t) = u(t)\dot{\theta}(t) \tag{7.4}$$

The control objective of MPC can be set to maximize the E_{abs} (Guerrero-Fernández et al., 2020) for the PAWEC system. It means that to minimise the average absorbed mechanical power $\bar{P}_a$ during a desired time interval T_l as there is a negative multiplying factor in P_a.

Based on this, the optimization problem follows the form:

$$\bar{P}_a = \frac{1}{T_l} \int_0^{T_l} P_a(t) dt \tag{7.5}$$

The integral in Equation (7.5) can be formulated into a discrete form (Soltani et al., 2014) as:

$$\bar{P}_a \approx \frac{T_s}{T_l} \sum_{i=k}^{k+T_l/T_s} x^T(i) s_1 u(i) \tag{7.6}$$

where T_s is the sampling time selected in the simulation, $s_1 = \begin{bmatrix} 0 & 1 & 0 & 0 \end{bmatrix}^T$.

The MPC objective function can be defined as:

$$J_s = x_N^T \bar{S} u_N + u_N^T R_s u_N \tag{7.7}$$

where $x_N^T \bar{S} u_N$ is the power term and $u_N^T R_s u_N$ is the penalty term on the control input.

$$\bar{S} = \begin{pmatrix} s_1 & 0 & \cdots & 0 \\ 0 & \frac{N-1}{N} s_1 & \cdots & 0 \\ \vdots & \vdots & \ddots & \vdots \\ 0 & 0 & \cdots & \frac{1}{N} s_1 \end{pmatrix}, R_s = \begin{pmatrix} r_s & 0 & \cdots & 0 \\ 0 & \frac{N-1}{N} r_s & \cdots & 0 \\ \vdots & \vdots & \ddots & \vdots \\ 0 & 0 & \cdots & \frac{1}{N} r_s \end{pmatrix}.$$

On subsituting Equation (7.2) into the objective function (7.7) can have

$$J_s = (\Omega x(k) + \Phi u_N + \Phi M_{ex,N})^T \bar{S} u_N + u_N^T R_s u_N \tag{7.8}$$

Then the objective function can be converted into a quadratic form:

$$J_s = \frac{1}{2} u_N^T H_s u_N + f_s^T u_N \tag{7.9}$$

where $H_s = 2(\Phi^T \bar{S} + R_s)$, $f_s^T = x^T(k)\Omega^T \bar{S} + M_{ex,N}^T \Phi^T \bar{S}$.

This means that the energy maximization problem for PAWEC system is transformed into a QP optimization problem (Nocedal and Wright, 1999).

When removing the penalty term in Equation (7.7), the objective function becomes:

$$J_s = x_N^T \bar{S} u_N \tag{7.10}$$

(7.10) only includes the power term and the matrix H_s will be changed with $H_s = 2\Phi^T \bar{S}$.

Additionally, the PAWEC system has the control input constraint due to the limitation of the PTO and it can be handled in an MPC optimization procedure at each sampling instant (Soltani et al., 2014) according to the following description:

$$\begin{aligned} minimise \quad & \frac{1}{2} u_N^T H_s u_N + f_s^T u_N \\ subject\ to \quad & u_{N,min} \leq u \leq u_{N,max} \end{aligned} \tag{7.11}$$

where $u_{N,min} = [u_{min}\, u_{min} \cdots u_{min}]^T$, $u_{N,min} \in \mathfrak{R}^N$ and $u_{N,max} = [u_{max}\, u_{max} \cdots u_{max}]^T$, $u_{N,max} \in \mathfrak{R}^N$.

The qpOASES QP solver is used to do the QP optimization (as used in Chapter 6).

7.3   Simulation results

A comparison study is conducted between the frequently used MPC design, the model-following mixed LQR/H_∞ control and SMC approaches (described in Chapter 5) and MPC tracking method proposed in Chapter 6. The simulation results are expanded around the below contents:

- MPC case 1 only includes power term (with no tracking purpose).

$$J_s = x_N^T \bar{S} u_N$$

- MPC case 2 has power term and input penalty term (with no tracking purpose).

$$J_s = x_N^T \bar{S} u_N + u_N^T R_s u_N$$

- MPC velocity-tracking, based on GP model (Chapter 6).

- Model-following mixed LQR/H_∞ tracking control (Chapter 5).

- Model-following sliding mode tracking control (Chapter 5).

The comparison metrics: velocity tracking results, disturbance test, absorbed energy, extracted energy, extracted power, PTO moment, etc.

Test 1: Seastate 5

The absorbed mechanical energy E_{abs} corresponding to the five methods is shown in Figure 7.1. The MPC case 1 produces the largest energy absorption approximately 77.8 J. The other four methods generate almost the same absorbed energy, around 50 J, and the mixed LQR/H_∞ control method provides the least absorbed energy about 47.5 J.
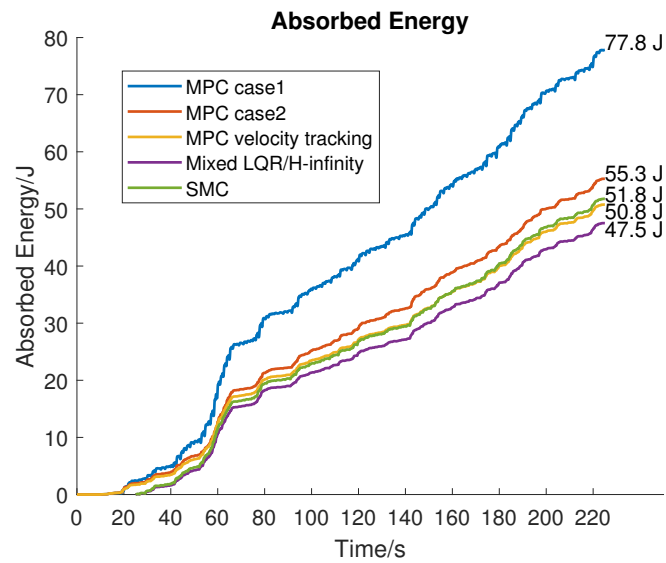
Figure 7.1: Absorbed energy from all methods (Seastate 5).
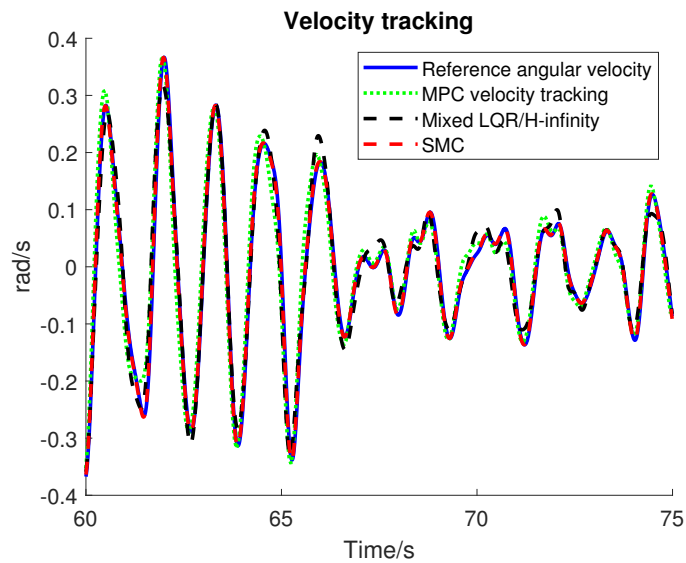
Figure 7.2: Velocity tracking results: (i) MPC, (ii) Mixed LQR/H_∞ control and (iii) Model-following SMC approaches (Seastate 5).

The simulation results for: (i) MPC velocity tracking, (ii) Mixed LQR/H_∞ tracking control and, (iii) SMC tracking are shown in Figure 7.2, where the MPC Case 1 and MPC Case 2 do not include a tracking function.

It can be seen that all of the three tracking strategies are able to perform very good tracking with low tracking phase errors, even if there are amplitude errors. In general, the purpose of energy-maximising is largely satisfied when the velocity tracking is achieved based on the hierarchical tracking strucuture (suboptimal solution), to reach a

near-resonance condition and ensure the float angular velocity $\dot{\theta}$ remains close in phase with the excitation moment M_{ex}.
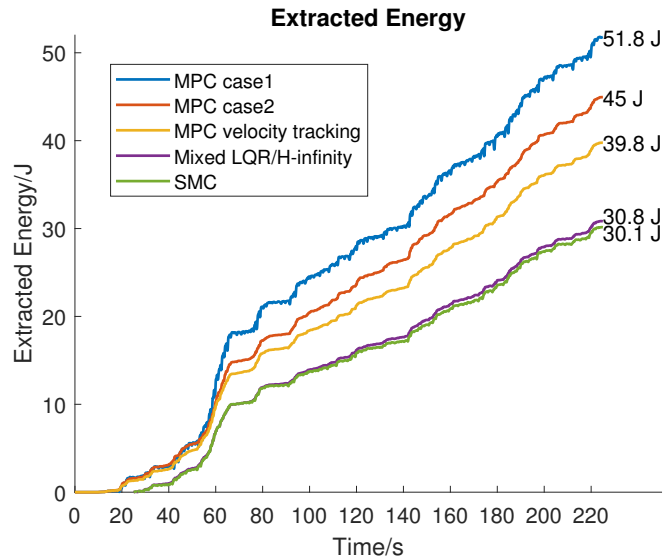
Figure 7.3: Extracted energy from all methods (Seastate 5).

Consider the PTO system conversion efficiency Γ, the extracted energy E_e from all five approaches is given in Figure 7.3. The MPC case 1 still has the largest extracted energy 51.8 J compared with the other four methods since it is the optimal solution for energy maximization. This is different from the MPC case 2 which has a penalty term in objective function and has an extracted energy of about 45 J. Furthermore, it is clear that the E_e from MPC velocity tracking method equals to 39.8 J, which is larger than the E_e from model-following mixed LQR/H_∞ control and model-following SMC.

The reason for this is that the MPC tracking approach only has a small amount of negative power excursions in the extracted power, in contrast to mixed LQR/H_∞ control and SMC methods, as shown in Figure 7.4.
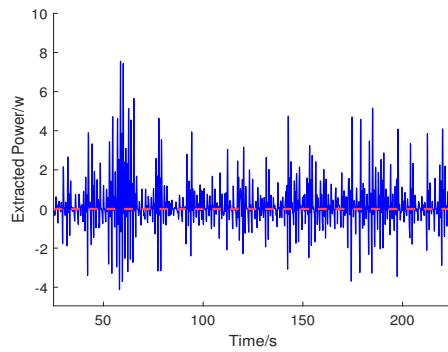
(a) MPC case1 extracted power.
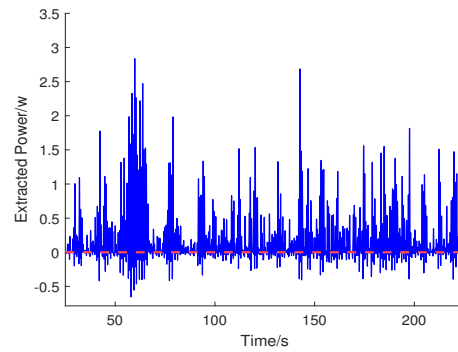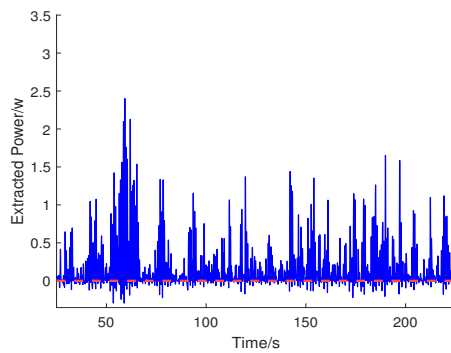
(b) MPC case 2 extracted power.

(c) MPC velocity tracking extracted power. (d) Mixed LQR/H_∞ control extracted power.
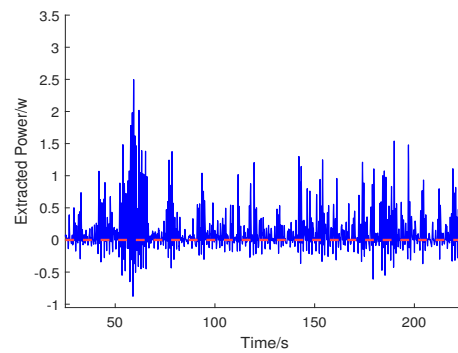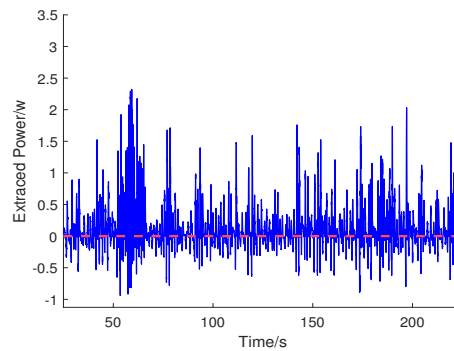
(e) Sliding mode control extracted power.

Figure 7.4: Extracted power of all methods (Seastate 5).

The control input M_{PTO} of all approches is given in Figure 7.5. It is clear that the input constraint (red line) of the PAWEC PTO system is satisfied by all methods, under Seastate 5!

(**a**) MPC case 1 PTO moment.

(**b**) MPC case 2 PTO moment.

(**c**) MPC velocity tracking PTO moment.

(**d**) Mixed LQR/H_∞ control PTO moment.

(**e**) Sliding mode control PTO moment.
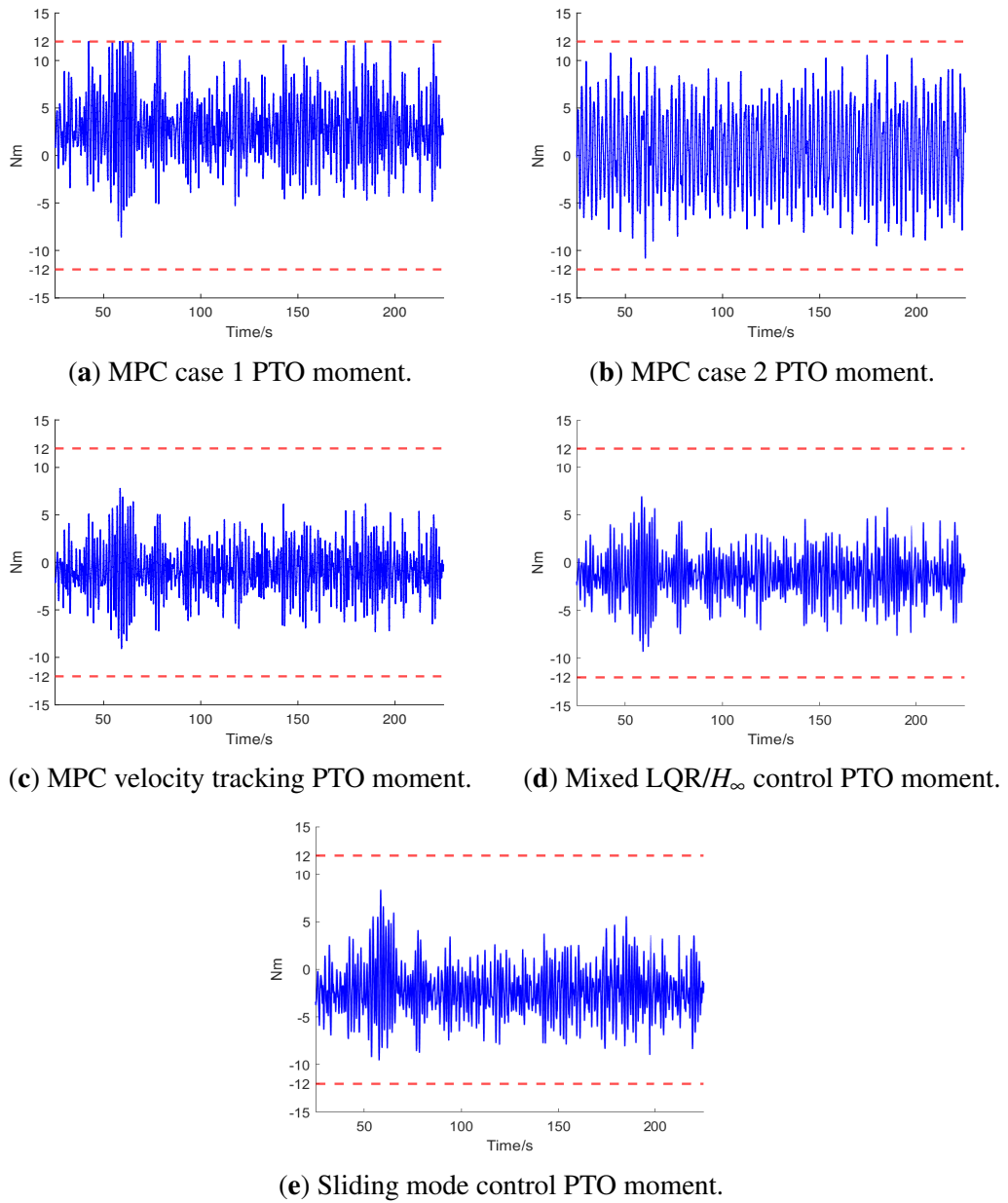
Figure 7.5: PTO moment of all methods (Seastate 5).

Regarding the robustness testing of each of the methods, the matched disturbance $B_e \cdot d_m = \frac{1}{J_t}(4sin(3t + \frac{\pi}{4}) - sin(2t + \frac{\pi}{3}))$ used in Section 5.4 is added into the PAWEC system to check its effects on extracted energy and velocity tracking results. Figure 7.6 gives the extracted energy with added matched disturbance corresponding to all methods. It is clear that the MPC Case 1 is affected largely by the matched disturbance and gives rise to a non-convex problem due to its lack of robustness. Furthermore, the E_e is even driven to be negative -28.7 J. Apart from this, MPC Case 2 is also significantly influenced by the matched disturbance, and the E_e is decreased to 8.1 J. This falling

phenomenon of E_e is similar to MPC Case 1 but Case 2 shows evidence of stronger robustness than Case 1. Additionally, the E_e from the MPC tracking strategy has dropped somewhat to 24.4 J when compared with "no added matched disturbance" test shown in Figure 7.3. However, both the model-following mixed LQR/H_∞ control and SMC only demonstrate low energy-loss between the no disturbance and the matched disturbance tests, which means that these two robust methods shows fairly strong robustness.
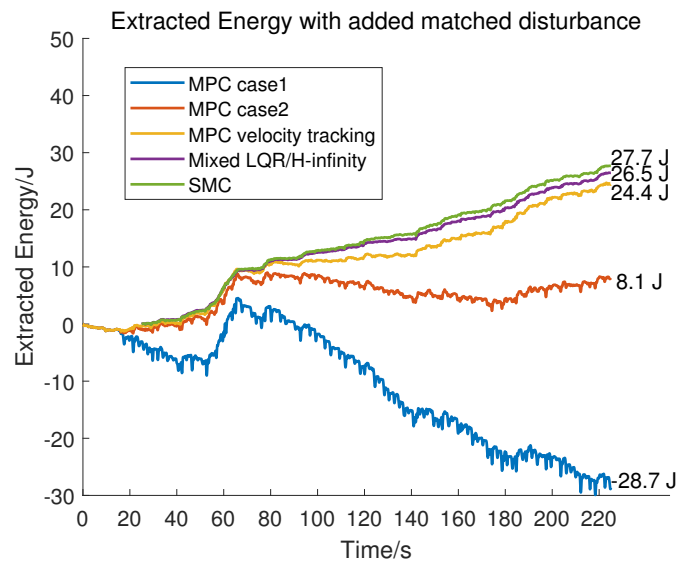
Figure 7.6: Extracted energy with added matched disturbance from all methods (Seastate 5).
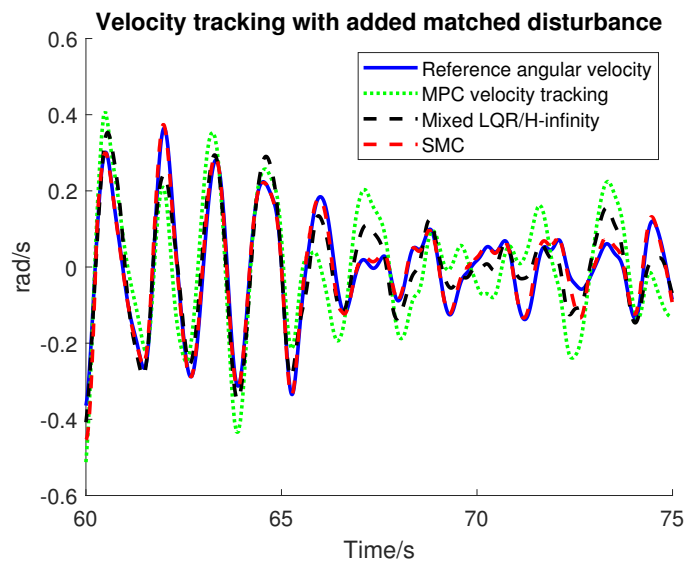
Figure 7.7: MPC velocity tracking, Model-following mixed LQR/H_∞ control and SMC with matched disturbance (Seastate 5).

The velocity tracking results with matched disturbance under Seastate 5 are given in Figure 7.7. It can be seen that the MPC velocity tracking error becomes larger to some extent, when the matched disturbance being added on the PAWEC device. The mixed LQR/H_∞ control and SMC have strong robustness with low tracking errors. But SMC shows best velocity tracking performance.

Test 2: Seastate 6
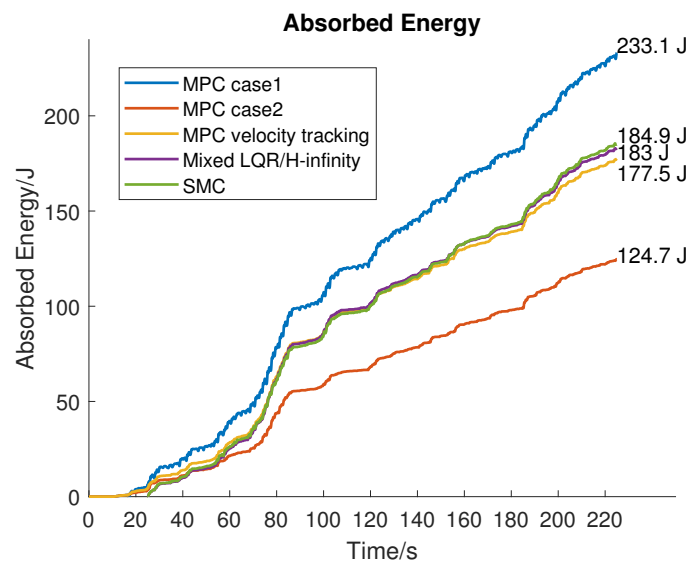
Figure 7.8: Absorbed energy from all methods (Seastate 6).

Figure 7.8 shows the absorbed energy E_{abs} for all five methods under Seastate 6. There is no doubt that the MPC Case 1 still has the largest energy absorption 233.1 J. However, there are some changes in the ranking of E_{abs} under Seastate 6 compared with the ranking of Seastate 5 in Figure 7.1. The Model-following SMC produces the second largest E_{abs} of 184.9J. The E_{abs} from Model-following mixed LQR/H_∞ control becomes larger than for the MPC velocity tracking and MPC case 2 methods.
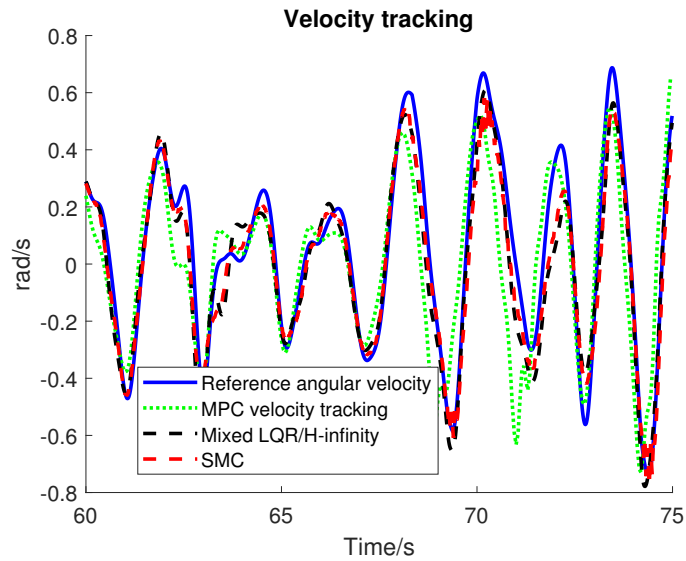
Figure 7.9: Velocity tracking results: (i) MPC, (ii) Mixed LQR/H_∞ control and (iii) SMC approaches (Seastate 6).
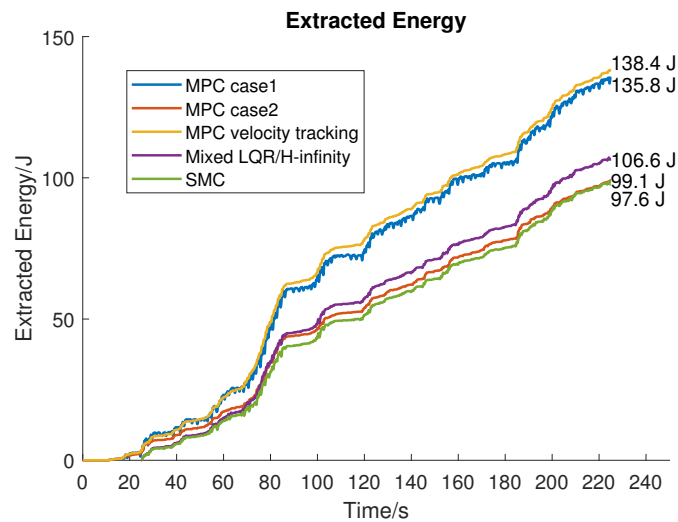
Figure 7.10: Extracted energy from all methods (Seastate 6).

The velocity tracking results of MPC, mixed LQR/H_∞ control and SMC approaches under Seastate 6 are shown in Figure 7.9. All of three methods are able to bring good control performance with low tracking errors, but the tracking result gets a bit worse compared with the simulation result under Seastate 5 in Figure 7.2. The reason for this is the excitation moment M_{ex} is an external moment, regarded as a large disturbance onto the PAWEC device to do oscillation. The amplitude of incoming irregular waves based on Seastate 6 is bigger than the amplitude of irregular waves from Seastate 5. In other words, the M_{ex} (external disturbance) generated by Seastate 6 is larger than the

one produced by Seastate 5, to see the details in Chapter 4 the M_{ex} estimation work.

Figure 7.10 gives the extracted energy E_e from all methods under Seastate 6. It is clear that the MPC velocity tracking method has the largest E_e that approaches to 138.4J and the MPC case 1 drops to second place in the ranking of E_e that equals to 135.8J. In addition, the E_e of mixed LQR/H_∞ control becomes larger than the SMC and MPC case 2 which is another change with the E_e obtained from Seastate 5 in Figure 7.3.

(a) MPC case 1 extracted power.

(b) MPC case 2 extracted power.

(c) MPC velocity tracking extracted power.

(d) Mixed LQR/H_∞ control extracted power.

(e) Sliding mode control extracted power.
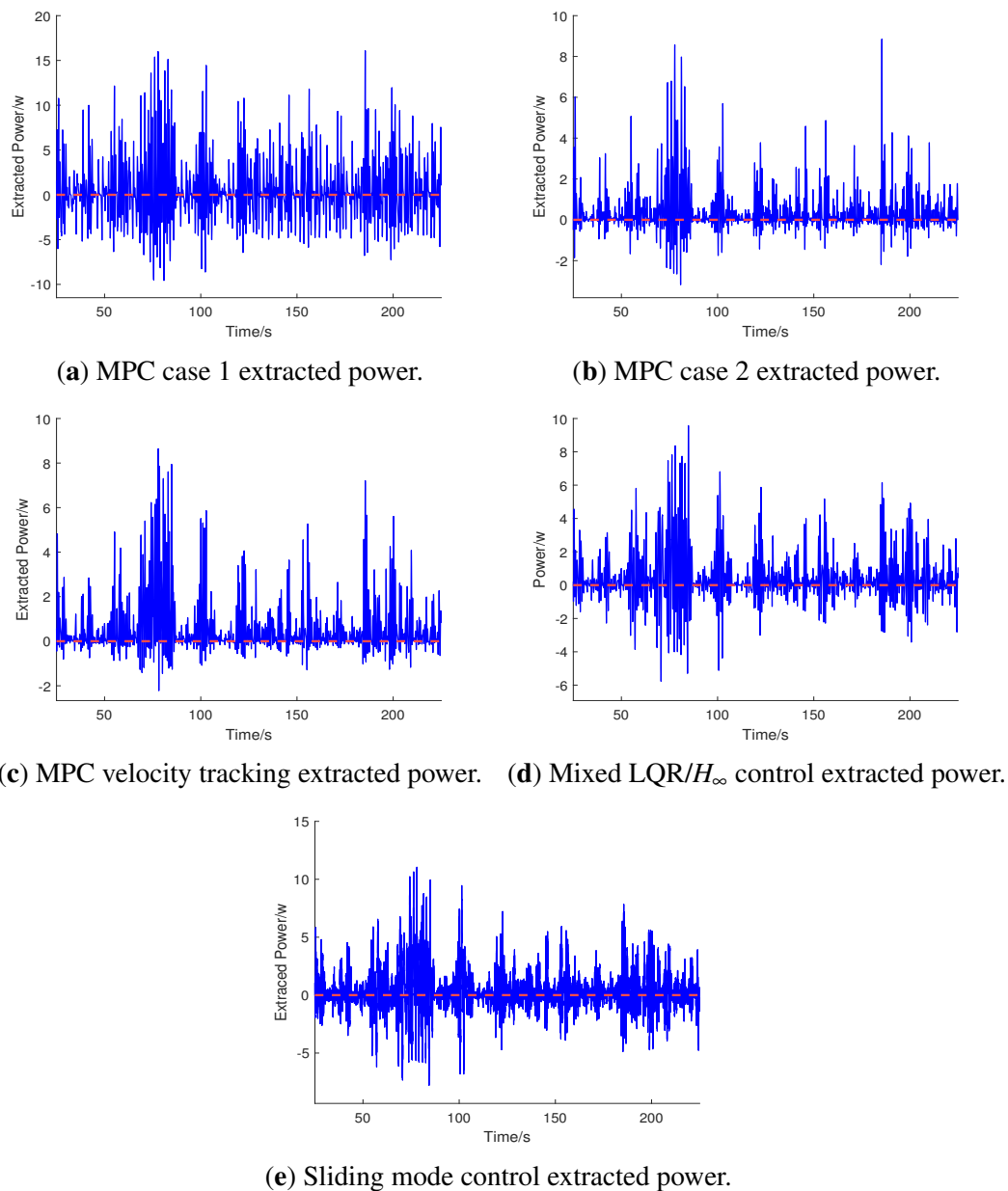
Figure 7.11: Extracted power of all methods (Seastate 6).

The extracted power of five methods is shown in Figure 7.11. It can be seen that only

MPC velocity tracking and MPC case 2 methods have few negative power, which is a good advantage in energy conversion in PTO system. On the contrary, the other three methods, MPC case 1, model-following mixed LQR/H_∞ control and SMC approaches have lots of large negative power which is bad for PTO system. In this situation, the massive bi-directional power flow will cause huge burden on PTO system and lead to energy loss.

(a) MPC case 1 PTO moment.

(b) MPC case 2 PTO moment.

(c) MPC velocity tracking PTO moment.

(d) Mixed LQR/H_∞ control PTO moment.

(e) Sliding mode control PTO moment.
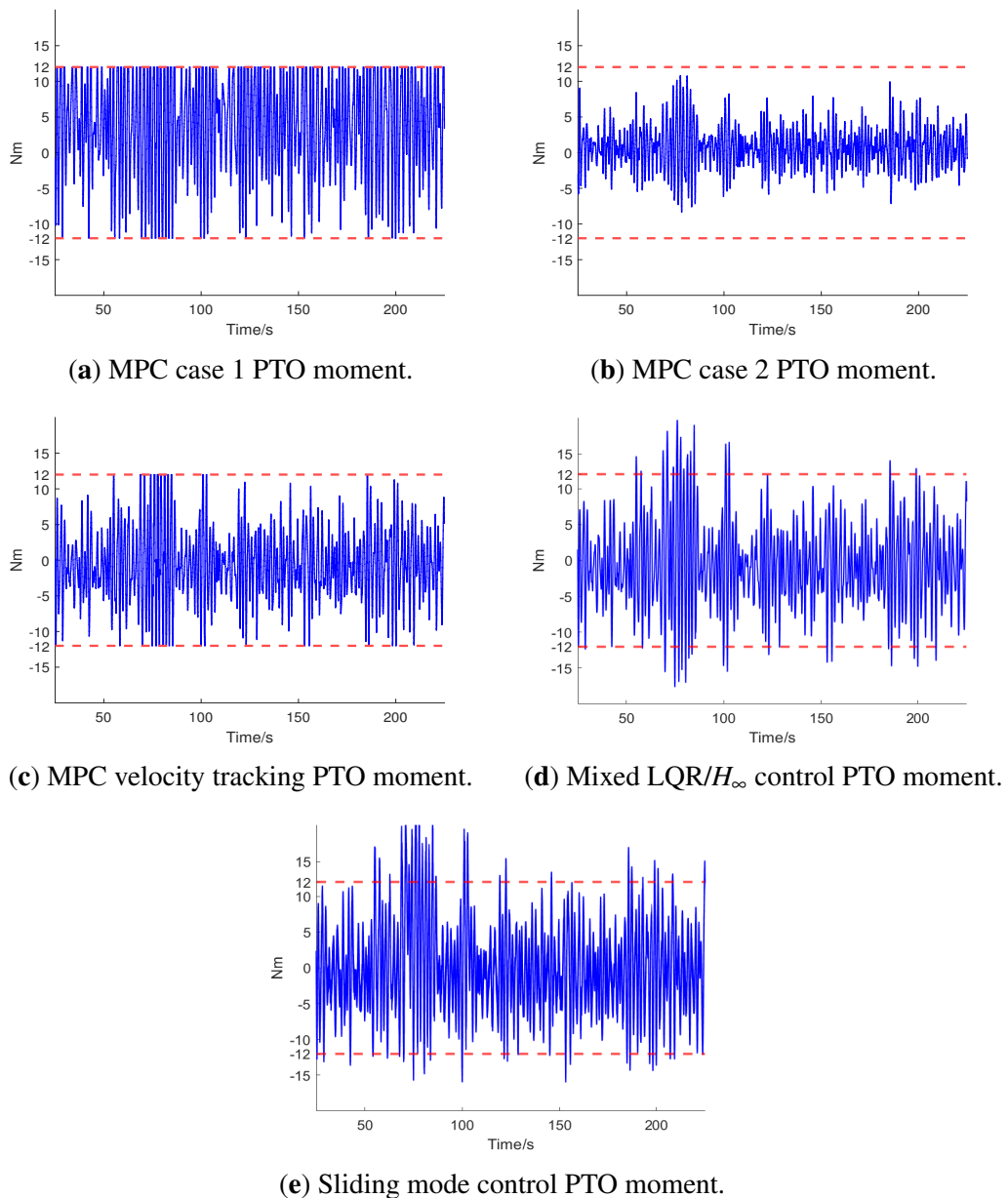
Figure 7.12: PTO moment of all methods (Seastate 6).

The PTO moment (control input) of all strategies are given in Figure 7.12. It can be

seen that three MPC methods have the advantages in coping with the input constraint of PAWEC system. But the input limitation (red line) is not satisfied by the model-following mixed LQR/H_∞ control and SMC approaches.

Figure 7.13 gives the extracted energy E_e of all methods by adding the matched disturbance to WEC-Sim numerical model under Seastate 6. The E_e of MPC case 1 gets a relatively large decline again but not serious like the E_e from Seastate 5. Correspondingly, the E_e of MPC case 2 drops some but not large as Seastate 5 as well. Additionally, the E_e of both mixed LQR/H_∞ control and SMC approaches have a few decrease. However, the MPC velocity tracking strategy can work properly under Seastate 6 with the matched disturbance. This is different from the Seastate 5 matched disturbance test.
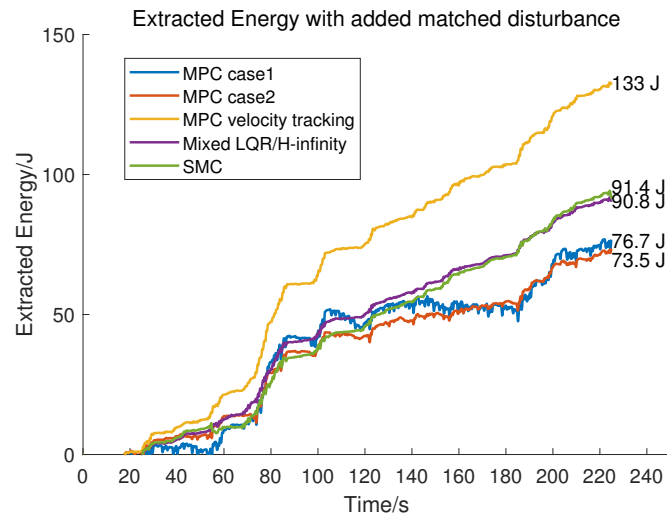
Figure 7.13: Extracted energy with added matched disturbance from all methods (Seastate 6).

Figure 7.14 shows the velocity tracking results of MPC, mixed LQR/H_∞ control and SMC approaches with matched disturbance under Seastate 6. Actually, there are two disturbance terms in WEC-Sim numerical model. One is the added matched disturbance and another is the M_{ex} treated as the external disturbance. Here, it is different from the velocity tracking result of Seastate 5. Only model-following mixed LQR/H_∞ control can provide good tracking performance in Seastate 6 condition. The MPC velocity tracking result gets a bit worse but it is still reasonable. However, there is a serious problem appeared in SMC tracking result. The SMC can not always satisfy the matching condition in sliding mode under Seastate 6 which produces large amplitude M_{ex}.
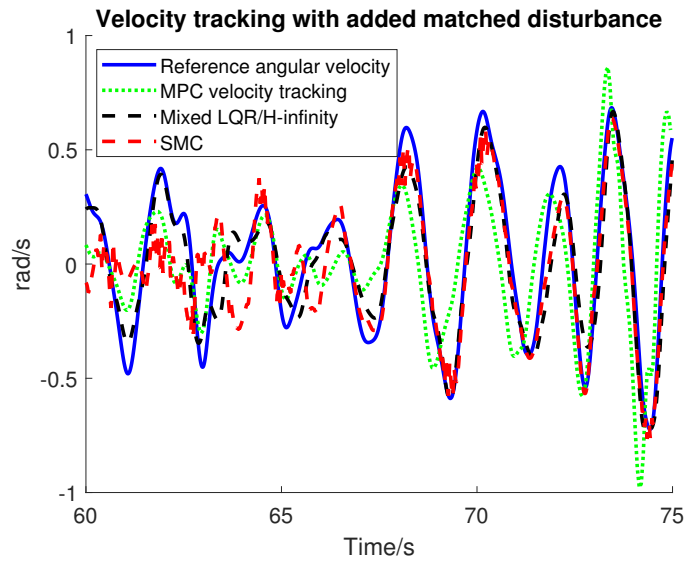
Figure 7.14: MPC velocity tracking, Model-following mixed LQR/H_∞ control and SMC with matched disturbance (Seastate 6).

7.4   Summary

This Chapter provides a comparison study between the MPC and robust methods to test the robustness of PAWEC control systems and analyse the energy maximization extraction. Five cases are considered based on the frequently used MPC methods, MPC velocity tracking based on GP model presented in this thesis Chapter 6, and Model-following mixed LQR/H_∞ control and SMC control proposed in this thesis Chapter 5. In general, the common MPC approach brings an optimal solution but it may lack robustness if the PAWEC system has large disturbance or uncertainty. Both model-following mixed LQR/H_∞ control and SMC are suboptimal solutions for energy-maximising control design for PAWEC system. Furthermore, model-following mixed LQR/H_∞ control has applicability in Seastate 5 and 6, compared with SMC with strong robustness. The SMC method is a method that can work well with best tracking performace under Seastate 5 but it may need to be redefined in design under the large amplitude incident waves like Seastate 6. In total, the MPC velocity tracking strategy is the best one which has good robustness and largest energy production during the disturbance tests under Seastate 5 and 6.

Chapter 8

Concluding Discussion and Future Work

8.1 Concluding Discussion

Specific to the Aim and Objectives of this thesis, a 1:20 scaled Wavestar-like WEC device in WEC-Sim benchmark (Tom et al., 2018) has been selected to design advanced control strategies. The purpose is to maximize the energy conversion and robustness enhancement (to modelling uncertainty). To date control systems have been usefully employed in PAWEC research for improving the energy maximization objective and reducing the damage by handling system physical constraints. Thereby, in terms of the two themes of robustness and optimality, the model-following robust control strategies (Chapter 5) and model-predictive tracking control method (Chapter 6) (Li and Patton, 2023a) are proposed, respectively based on a hierarchical tracking structure, with a special two-level approach. The most significant contribution of this PhD study is to compare and discuss these approaches, in Chapter 7. Although both robust control and MPC are the most studied and important topics in the current wave energy community, some issues about the combination of robustness and efficient power conversion remain as unsolved issues in the literature.

Wave energy researchers tend to focus only on one aspect of MPC, generally its main function of predictive control optimization. But a few researchers study the issues under which MPC can be made robust to uncertainty. It is clear from the literature that there is a utilization gap between MPC and robust control. Few studies have successfully brought MPC and robust control together to understand what can be involved in

designing robust MPC systems (Zhan et al., 2017; Jama et al., 2018). However, one of the frequently used MPC strategies (Soltani et al., 2014), whilst not considering tracking, nevertheless does choose the average absorbed mechanical power as its objective function, to calculate the optimal PTO force by using quadratic programming optimization. This thesis has shown that the tracking structure should be considered that for most of standard robust control approaches if they are chosen to maximize energy production. This also provides a powerful framework for developing robust MPC in wave energy and PAWEC.

Inspired by the hierarchical tracking structure first proposed by (Fusco and Ringwood, 2014a), various control methods could be used with MPC being one. In order to make a comparison with the use of MPC Chapter 5 describes two different robust control methods to combine robustness with tracking control as follows:

- A mixed LQR/H_∞ control (Zhu and Li, 2021a) and

- Sliding Mode Control (Lan et al., 2017b)

At the low hierarchical level these methods use the model-following tracking control concept (Section 5.3). In the contribution in this thesis, the PAWEC system is forced to follow a reference model and perform both position and velocity tracking robustly. A near-resonance condition for the purpose of energy maximization can be reached when the PAWEC tracking is achieved. Both of the model-following LQR/H_∞ and SMC approaches have strong robustness, against the added matched disturbance (see Section 5.4 for definition). The robustness is manifest without much absorbed energy being lost during the energy production under irregular waves. In this work SMC tracking shows promise in bringing good robustness to the PAWEC device and hydrodynamic parameter uncertainty. The robustness is achieved by suppressing the affects induced by the matched disturbance. This "matched disturbance robustness" is a well-known feature and property of the sliding mode. Certainly, the LQR/H_∞ tracking also demonstrates good disturbance rejection performance. But these robust control approaches are unlike the MPC methods that can solve the system control input and physical constraints elegantly.

Again at the low-level (Chapter 6), the MPC is designed into a velocity tracking mode, treated as a bridge to the comparison study between robust control and MPC methods. Actually, the tracking form can give more freedom for the controller design and also increase the robustness of the MPC system. Furthermore, two GP models are adopted

to perform short-term forcasting to generate the predictions of the future WEM and future reference velocity values. These are required in the objective function of the model-predictive tracking control. The predictions of GP models present good learning smoothness.

Considering the high-level part of the selected hierarchical structure, this must be considered as the preliminary work before doing the energy-maximising controller design. An important function at this high-level is the WEM estimation and the determination of the optimal reference signal. In Section 4.2, four robust methods are selected to design the WEM estimators with simple and effective structure. The comparison study demonstrates the robustness and response speed of both the UIO (Zhu and Li, 2021b) and LO (Du et al., 2015). The robust designs are attempted, based on H_∞ performance which are limited due to the LMI feasibility problem that introduces a side effect in calculating observer gain. The problem is that the LMI search could be infeasible, so that the performance of the WEM estimation may not appear to be satisfactory. In contrast to using LMI, the proposed LO method using pole-placement (PP) design has the simplest solution structure and shows very attractive estimation performance, which may be a suitable approach for a number of PAWEC applications. The adaptive sliding mode observer (ASMO) of (Lan et al., 2017a) is not only a nonlinear approach but provides the best WEM estimation performance, providing a potentially new strategy for application problems involving PAWEC systems. Both LO with PP and the ASMO designs are the new contributions tested on the a 1:20 scaled Wavestar-like WEC device, and show promise for future studies based on real PAWEC applications.

In contrast to this the optimal reference generation is based on an EKF. The result in Section 4.4 shows that the EKF can perform well in computing the estimated instantaneous amplitude and frequency of WEM, although it needs long convergence time and lacks robustness. Some new methods for the optimal reference determination can be a focus of future work.

The two-level system comparison results (Chapter 7) indicate that among all methods considered, the frequently used MPC method (with no tracking purpose) can give an optimal solution towards to absorbed energy, when considering irregular waves. However, the basic MPC method tends to generate large negative power when the objective function does not include a penalty term to restrain the control input. If the penalty term is considered, the generated negative power is reduced, but the absorbed energy is also reduced. This shows up a certain degree of quadratic trade-off between control

input restraint and absorbed energy. Furthermore, the frequently used MPC lacks robustness, when the PAWEC system involves the added matched disturbance, and also tends to give rise to persistent negative energy.

Chapter 7 also indicates that the input constraint is satisfied by the MPC methods. On the other hand, it is shown that the two robust tracking methods (LQR/H_∞ and SMC) generate significant negative power, which compromises the overall extracted energy. However, the model-predictive tracking control only produces a small amount of negative power and demonstrates good energy conversion efficiency between absorbed energy and extracted energy with/without the added matched disturbance arising in the PAWEC system. Recall that the model-predictive tracking approach is designed by a combination of the tracking structure scheme and the MPC methodology, which provides the PAWEC system with sufficient robustness, whilst extracting as much energy as possible. So, the robustness of the MPC can be enhanced using the optimal velocity tracking. Then optimality can be ensured by the MPC optimization procedure. Nevertheless, the two Gaussian Learning predictors (GP models) are needed in this model-predictive tracking method that involves the prediction errors to the PAWEC control system. Both basic MPC and MPC velocity tracking methods have considerable real-time computation burdens, especially because of the QP optimization. In contrast the robust tracking approaches demonstrate much faster real-time performance. Overall, the MPC tracking system demonstrates the best solution in terms of expected LCoE, among all control approaches in this thesis work.

8.2 Future work

- **Optimal reference generation:** As described in Chapter 4, the WEM signal is assumed as a narrow-band process in a harmonic model form (4.23) and can be further expressed to a single cyclical component (4.24), based on the Harvey's structural model (Fusco and Ringwood, 2014a). Then the non-linear time-varying model can be used in an EKF to estimate the instantaneous WEM amplitude and frequency, in order to calculate the optimal reference signal.

    The EKF might be replaced by the other methods, which have shorter convergence times and hopefully stronger robustness. Two other methods can be considered to obtain (a) the WEM instantaneous amplitude and frequency and

from this (b) calculate the optimal reference signal. These are: The Hilbert-Huang transform (HHT) (Garcia-Rosa et al., 2017), Teager Energy Operator (TEO) (Maragos et al., 1993). Another attractive possibility is to just choose a Fourier pseudo-spectral method, to compute the optimal trajectories directly (Auger et al., 2018).

- **The improvement of reducing negative power and extracted energy:** The robust control methods should be redefined in order to reduce negative power generated in PAWEC control system and extract much more energy from the irregular waves. A logistic conceptual model (8.1) with suitable damping ratio ζ and damped natural frequency ω_n will be considered as a reference model, which can cover all key physical features of the PAWEC system.

$$G(s) = \frac{C(s)}{R(s)} = \frac{\omega_n^2 s_0}{(s+s_0)(s^2 + 2\zeta\omega_n s + \omega_n^2)} \tag{8.1}$$

Then, the model-following robust control methods will be improved in energy production. In general, robust control is superior in coping with system disturbances, unmodeled dynamics, and quickly varying parameters. Furthermore, the model reference adaptive control (Nguyen and Nguyen, 2018) can be tested based on it. Adaptive control has benefits in coping with some uncertainties or slow-varying parameters.

- **Robustness enhancing MPC:** Tube-MPC method (Mayne et al., 2011) could be considered to do velocity tracking work but with stronger robustness compared with the MPC methods discussed in Chapter 7. The tube-MPC is a hot research topic that has attracted attention of many researchers (Mesbah, 2016; Lopez et al., 2019; Fleming et al., 2014) due to it has strong robustness compared with the basic MPC methods. The main idea of tube-MPC (Langson et al., 2004) is to keep the system actual state staying in an invariant (bounded) "tube" around a desired trajectory. It ensures that the deviation remains bounded by an ancillary feedback controller when the system involves modelling uncertainty and disturbance.

- **Energy-maximising control for PAWEC arrays:** When the PAWECs are deployed in large arrays (Peña-Sanchez, 2020), the LCoE per device will be reduced and the total cost of the generated electricity will also decrease. Therefore, it would be better to consider the overall PAWEC array, and perform the energy-maximising control work on it as a network of PAWECs. Certainly, the

WEF/WEM estimation should be computed before the control. Relative to a single PAWEC device application, the PAWEC arrays have much more complex hydrodynamics (Penalba et al., 2017a) and should be considered carefully. In addition, the spatial propagation of waves and the interactions coupling (Yang et al., 2022) between PAWEC devices need to be considered. The work developed in this thesis can provide good input to work on PAWEC arrays.

References

Abas, N., Kalair, A., and Khan, N. (2015). Review of fossil fuels and future energy technologies. *Futures*, 69:31–49.

Abdelkhalik, O., Zou, S., Robinett, R., Bacelli, G., and Wilson, D. (2017). Estimation of excitation forces for wave energy converters control using pressure measurements. *International Journal of Control*, 90(8):1793–1805.

Abdelrahman, M. (2019). *Wave Excitation Force Estimation and Robust Control Approaches for A Wave Energy Converter*. PhD thesis, University of Hull, Hull (England).

Abdelrahman, M. and Patton, R. (2017). Robust control of a wave energy converter with soft sensing of wave excitation force. In *Proc. 12th Eur. wave tidal energy conf*, pages 974–1.

Abdelrahman, M. and Patton, R. (2019). Observer-based unknown input estimator of wave excitation force for a wave energy converter. *IEEE Transactions on Control Systems Technology*, 28(6):2665–2672.

Abdelrahman, M., Patton, R., Guo, B., and Lan, J. (2016). Estimation of wave excitation force for wave energy converters. In *2016 3rd Conference on Control and Fault-Tolerant Systems (SysTol)*, pages 654–659. IEEE.

Abraham, E. and Kerrigan, E. C. (2012). Optimal active control and optimization of a wave energy converter. *IEEE Transactions on Sustainable Energy*, 4(2):324–332.

Aggidis, G. and Taylor, C. (2017). Overview of wave energy converter devices and the development of a new multi-axis laboratory prototype. *IFAC-PapersOnLine*, 50(1):15651–15656.

Anaconda (2023). Available at `https://energy.soton.ac.uk/anaconda-wave-energy-converter-concept/`. [accessed 15.08.23].

Anderlini, E., Forehand, D., Bannon, E., Xiao, Q., and Abusara, M. (2018). Reactive control of a two-body point absorber using reinforcement learning. *Ocean Engineering*, 148:650–658.

Anderlini, E., Forehand, D. I., Bannon, E., and Abusara, M. (2017). Control of a realistic wave energy converter model using least-squares policy iteration. *IEEE Transactions on Sustainable Energy*, 8(4):1618–1628.

Anderlini, E., Forehand, D. I., Stansell, P., Xiao, Q., and Abusara, M. (2016). Control of a point absorber using reinforcement learning. *IEEE Transactions on Sustainable Energy*, 7(4):1681–1690.

Anderlini, E., Husain, S., Parker, G. G., Abusara, M., and Thomas, G. (2020). Towards real-time reinforcement learning control of a wave energy converter. *Journal of Marine Science and Engineering*, 8(11):845.

Artal-Sevil, J., Domínguez, J., El-Shalakany, H., and Dufo, R. (2018). Modeling and simulation of a wave energy converter system. case study: Point absorber. In *2018 Thirteenth International Conference on Ecological Vehicles and Renewable Energies (EVER)*, pages 1–7. IEEE.

ASSEL, K. (2014). Theoretical and practical aspects of control strategies for wave energy converters of the point absorber type.

Auger, C., Mérigaud, A., and Ringwood, J. V. (2018). Receding-horizon pseudo-spectral control of wave energy converters using periodic basis functions. *IEEE Transactions on Sustainable Energy*, 10(4):1644–1652.

Babarit, A. (2017). *Ocean wave energy conversion: resource, technologies and performance*. Elsevier.

Babarit, A., Duclos, G., and Clément, A. H. (2004). Comparison of latching control strategies for a heaving wave energy device in random sea. *Applied Ocean Research*, 26(5):227–238.

Babarit, A., Guglielmi, M., and Clément, A. H. (2009). Declutching control of a wave energy converter. *Ocean engineering*, 36(12-13):1015–1024.

Babarit, A., Hals, J., Muliawan, M. J., Kurniawan, A., Moan, T., and Krokstad, J. (2012). Numerical benchmarking study of a selection of wave energy converters. *Renewable energy*, 41:44–63.

Bacelli, G. and Ringwood, J. (2011). A geometrical interpretation of force and position constraints in the optimal control of wave energy devices. In *Proceedings of the 9th European Wave and Tidal Energy Conference (EWTEC)*. School of Civil Engineering and the Environment, University of Southampton.

Bacelli, G. and Ringwood, J. V. (2014). Nonlinear optimal wave energy converter control with application to a flap-type device. *IFAC Proceedings Volumes*, 47(3):7696–7701.

Bacelli, G., Spencer, S. J., Patterson, D. C., and Coe, R. G. (2019). Wave tank and bench-top control testing of a wave energy converter. *Applied Ocean Research*, 86:351–366.

Boyd, S., El Ghaoui, L., Feron, E., and Balakrishnan, V. (1994). *Linear matrix inequalities in system and control theory*. SIAM.

Bruzzone, L., Fanghella, P., and Berselli, G. (2020). Reinforcement learning control of an onshore oscillating arm wave energy converter. *Ocean Engineering*, 206:107346.

Budar, K. and Falnes, J. (1975). A resonant point absorber of ocean-wave power. *Nature*, 256(5517):478–479.

Burgaç, A. and Yavuz, H. (2019). Fuzzy logic based hybrid type control implementation of a heaving wave energy converter. *Energy*, 170:1202–1214.

Cameron, L., Doherty, R., Henry, A., Doherty, K., Van't Hoff, J., Kaye, D., Naylor, D., Bourdier, S., and Whittaker, T. (2010). Design of the next generation of the Oyster wave energy converter. In *3rd international conference on ocean energy*, volume 6, page 1e12. ICOE Bilbao, Spain.

Cantarellas, A. M., Remon, D., and Rodriguez, P. (2017). Adaptive vector control of wave energy converters. *IEEE Transactions on Industry Applications*, 53(3):2382–2391.

Chang, G., Jones, C. A., Roberts, J. D., and Neary, V. S. (2018). A comprehensive evaluation of factors affecting the levelized cost of wave energy conversion projects. *Renewable energy*, 127:344–354.

Coe, R. G., Bacelli, G., Wilson, D. G., Abdelkhalik, O., Korde, U. A., and Robinett III, R. D. (2017). A comparison of control strategies for wave energy converters. *International journal of marine energy*, 20:45–63.

Crassidis, J. L. and Junkins, J. L. (2004). *Optimal estimation of dynamic systems*. Chapman and Hall/CRC.

Cretel, J. A., Lightbody, G., Thomas, G. P., and Lewis, A. W. (2011). Maximisation of energy capture by a wave-energy point absorber using model predictive control. *IFAC Proceedings Volumes*, 44(1):3714–3721.

Cummins, W. et al. (1962). The impulse response function and ship motions.

Czech, B. and Bauer, P. (2012). Wave energy converter concepts: Design challenges and classification. *IEEE Industrial Electronics Magazine*, 6(2):4–16.

Dallman, A., Jenne, D. S., Neary, V., Driscoll, F., Thresher, R., and Gunawan, B. (2018). Evaluation of performance metrics for the wave energy prize converters tested at 1/20th scale. *Renewable and Sustainable Energy Reviews*, 98:79–91.

Davidson, J., Genest, R., and Ringwood, J. V. (2018). Adaptive control of a wave energy converter. *IEEE Transactions on Sustainable Energy*, 9(4):1588–1595.

Davidson, J., Giorgi, S., and Ringwood, J. V. (2015). Linear parametric hydrodynamic models for ocean wave energy converters identified from numerical wave tank experiments. *Ocean Engineering*, 103:31–39.

De Chowdhury, S., Nader, J.-R., Sanchez, A. M., Fleming, A., Winship, B., Illesinghe, S., Toffoli, A., Babanin, A., Penesis, I., and Manasseh, R. (2015). A review of hydrodynamic investigations into arrays of ocean wave energy converters. *arXiv preprint arXiv:1508.00866*.

Delmonte, N., Barater, D., Giuliani, F., Cova, P., and Buticchi, G. (2014). Oscillating water column power conversion: A technology review. In *2014 IEEE Energy Conversion Congress and Exposition (ECCE)*, pages 1852–1859. IEEE.

Driscoll, F. R., Weber, J. W., Jenne, D. S., Thresher, R. W., Fingersh, L. J., Bull, D., Dallman, A., Gunawan, B., Ruehl, K., Newborn, D., et al. (2018). Methodology to calculate the ACE and HPQ metrics used in the Wave Energy Prize. Technical report, National Renewable Energy Lab.(NREL), Golden, CO (United States).

Du, H., Li, W., and Zhang, Y. (2015). Tracking control of wheel slip ratio with velocity estimation for vehicle anti-lock braking system. In *The 27th Chinese control and decision conference (2015 CCDC)*, pages 1900–1905. IEEE.

Durham, W. (1989). *Contributions to model following control theory*. PhD thesis, Virginia Polytechnic Institute and State University.

Edwards, C. and Spurgeon, S. (1998). *Sliding mode control: theory and applications*. CRC Press.

Ellabban, O., Abu-Rub, H., and Blaabjerg, F. (2014). Renewable energy resources: Current status, future prospects and their enabling technology. *Renewable and sustainable energy reviews*, 39:748–764.

Erzberger, H. (1967). Analysis and design of model following control systems by state space techniques. In *Joint Autom. Control Conf.*, number NASA-TM-X-61189.

Faedo, N., Olaya, S., and Ringwood, J. V. (2017). Optimal control, MPC and MPC-like algorithms for wave energy systems: An overview. *IFAC Journal of Systems and Control*, 1:37–56.

Faedo, N., Scarciotti, G., Astolfi, A., and Ringwood, J. V. (2018). Energy-maximising control of wave energy converters using a moment-domain representation. *Control Engineering Practice*, 81:85–96.

Faedo, N., Scarciotti, G., Astolfi, A., and Ringwood, J. V. (2021). Nonlinear energy-maximizing optimal control of wave energy systems: A moment-based approach. *IEEE Transactions on Control Systems Technology*, 29(6):2533–2547.

Faizal, M., Ahmed, M. R., and Lee, Y.-H. (2014). A design outline for floating point absorber wave energy converters. *Advances in Mechanical Engineering*, 6:846097.

Falnes, J. (1995). On non-causal impulse response functions related to propagating water waves. *Applied Ocean Research*, 17(6):379–389.

Falnes, J. (2007). A review of wave-energy extraction. *Marine structures*, 20(4):185–201.

Falnes, J. and Kurniawan, A. (2020). *Ocean waves and oscillating systems: linear interactions including wave-energy extraction*, volume 8. Cambridge university press.

Farrok, O., Ahmed, K., Tahlil, A. D., Farah, M. M., Kiran, M. R., and Islam, M. R. (2020). Electrical power generation from the oceanic wave for sustainable advancement in renewable energy technologies. *Sustainability*, 12(6):2178.

Feng, Z. and Kerrigan, E. C. (2015). Latching-declutching control of wave energy converters using derivative-free optimization. *IEEE Transactions on Sustainable Energy*, 6(3):773–780.

Ferreau, H. J., Kirches, C., Potschka, A., Bock, H. G., and Diehl, M. (2014). qpOASES: A parametric active-set algorithm for quadratic programming. *Mathematical Programming Computation*, 6:327–363.

Fleming, J., Kouvaritakis, B., and Cannon, M. (2014). Robust tube mpc for linear systems with multiplicative uncertainty. *IEEE Transactions on Automatic Control*, 60(4):1087–1092.

Fusco, F. (2012). *Real-time forecasting and control for oscillating wave energy devices*. PhD thesis, National University of Ireland Maynooth.

Fusco, F. and Ringwood, J. V. (2010). Short-term wave forecasting for real-time control of wave energy converters. *IEEE Transactions on sustainable energy*, 1(2):99–106.

Fusco, F. and Ringwood, J. V. (2014a). Hierarchical robust control of oscillating wave energy converters with uncertain dynamics. *IEEE Transactions on Sustainable Energy*, 5(3):958–966.

Fusco, F. and Ringwood, J. V. (2014b). Robust control of wave energy converters. In *2014 IEEE Conference on Control Applications (CCA)*, pages 292–297. IEEE.

Garcia-Abril, M., Paparella, F., and Ringwood, J. V. (2017). Excitation force estimation and forecasting for wave energy applications. *IFAC-PapersOnLine*, 50(1):14692–14697.

Garcia-Rosa, P. B., Kulia, G., Ringwood, J. V., and Molinas, M. (2017). Real-time passive control of wave energy converters using the Hilbert-Huang transform. *IFAC-PapersOnLine*, 50(1):14705–14710.

Garcia-Rosa, P. B. and Ringwood, J. V. (2015). On the sensitivity of optimal wave energy device geometry to the energy maximizing control system. *IEEE Transactions on Sustainable Energy*, 7(1):419–426.

García-Violini, D., Faedo, N., Jaramillo-Lopez, F., and Ringwood, J. V. (2020a). Simple controllers for wave energy devices compared. *Journal of Marine Science and Engineering*, 8(10):793.

García-Violini, D., Peña-Sanchez, Y., Faedo, N., Ferri, F., and Ringwood, J. V. (2023). A broadband time-varying energy maximising control for wave energy systems (LiTe-Con+): Framework and experimental assessment. *IEEE Transactions on Sustainable Energy*.

García-Violini, D., Peña-Sanchez, Y., Faedo, N., and Ringwood, J. V. (2020b). An energy-maximising linear time invariant controller (LiTe-Con) for wave energy devices. *IEEE Transactions on Sustainable Energy*, 11(4):2713–2721.

Genest, R. and Ringwood, J. V. (2016). Receding horizon pseudospectral control for energy maximization with application to wave energy devices. *IEEE Transactions on Control Systems Technology*, 25(1):29–38.

Giorcelli, F., Sirigu, S. A., Basile, D., et al. (2023). Relevance of robustness and uncertainties analysis in the optimal design of wave energy converters. In *Proceedings of the European Wave and Tidal Energy Conference*, volume 15.

Guerrero-Fernández, J., González-Villarreal, O. J., Rossiter, J. A., and Jones, B. (2020). Model predictive control for wave energy converters: A moving window blocking approach. *IFAC-PapersOnLine*, 53(2):12815–12821.

Guerrero-Fernandez, J. L., González-Villarreal, O. J., and Rossiter, J. A. (2023). Efficiency-aware nonlinear model-predictive control with real-time iteration scheme for wave energy converters. *International Journal of Control*, 96(8):1909–1921.

Gunn, K. and Stock-Williams, C. (2012). Quantifying the global wave power resource. *Renewable energy*, 44:296–304.

Guo, B. (2017). *Study of scale modelling, verification and control of a heaving point absorber wave energy converter*. PhD thesis, University of Hull.

Guo, B., Patton, R., and Jin, S. (2017). Identification and validation of excitation force for a heaving point absorber wave energy convertor. *Proc. EWTEC*, pages 1–9.

Guo, B., Patton, R. J., Jin, S., and Lan, J. (2018). Numerical and experimental studies of excitation force approximation for wave energy conversion. *Renewable energy*, 125:877–889.

Guo, B. and Ringwood, J. (2021). A review of wave energy technology from a research and commercial perspective. *IET Renewable Power Generation*, 15(14):3065–3090.

Guo, B., Wang, T., Jin, S., Duan, S., Yang, K., and Zhao, Y. (2022). A review of point absorber wave energy converters. *Journal of Marine Science and Engineering*, 10(10):1534.

Hall, M. (2015). Moordyn user's guide. *Department of Mechanical Engineering, University of Maine: Orono, ME, USA*, 15.

Harvey, A. C. (1990). Forecasting, structural time series models and the Kalman Filter.

Hasselmann, K., Barnett, T. P., Bouws, E., Carlson, H., Cartwright, D. E., Enke, K., Ewing, J., Gienapp, A., Hasselmann, D., Kruseman, P., et al. (1973). Measurements of wind-wave growth and swell decay during the Joint North Sea Wave Project (JONSWAP). *Ergaenzungsheft zur Deutschen Hydrographischen Zeitschrift, Reihe A*.

Heath, T., Whittaker, T. J., and Boake, C. (2001). The design, construction and operation of the LIMPET wave energy converter (Islay, Scotland)[Land Installed Marine Powered Energy Transformer].

Heller, V., Chaplin, J., Farley, F., Hann, M., Hearn, G., et al. (2000). Physical model tests of the Anaconda wave energy converter. In *Proc. 1st IAHR European Congress*.

Hendrikx, R., Leth, J., Andersen, P., and Heemels, W. (2017). Optimal control of a wave energy converter. In *2017 IEEE Conference on Control Technology and Applications (CCTA)*, pages 779–786. IEEE.

Herber, D. R. and Allison, J. T. (2013). Wave energy extraction maximization in irregular ocean waves using pseudospectral methods. In *International Design Engineering Technical Conferences and Computers and Information in Engineering Conference*, volume 55881, page V03AT03A018. American Society of Mechanical Engineers.

Hillis, A., Yardley, J., Plummer, A., and Brask, A. (2020). Model predictive control of a multi-degree-of-freedom wave energy converter with model mismatch and prediction errors. *Ocean Engineering*, 212:107724.

IEA (2020). Electricity Information Overview 2020 Edition. Technical report.

IRENA (2020). Innovation outlook Ocean Energy Technologies. Technical report.

Isurugi, Y. (1990). *Model following control for nonlinear systems*. PhD thesis, INRIA.

Jama, M., Wahyudie, A., and Noura, H. (2018). Robust predictive control for heaving wave energy converters. *Control Engineering Practice*, 77:138–149.

Jin, S. and Greaves, D. (2021). Wave energy in the UK: Status review and future perspectives. *Renewable and Sustainable Energy Reviews*, 143:110932.

Karthikeyan, A., Previsic, M., Scruggs, J., and Chertok, A. (2019). Non-linear model predictive control of wave energy converters with realistic power take-off configurations and loss model. In *2019 IEEE Conference on Control Technology and Applications (CCTA)*, pages 270–277. IEEE.

Kofoed, J. P., Frigaard, P., Friis-Madsen, E., and Sørensen, H. C. (2006). Prototype testing of the wave energy converter wave dragon. *Renewable energy*, 31(2):181–189.

Kramer, M., Marquis, L., and Frigaard, P. (2011). Performance evaluation of the wavestar prototype. In *9th EWTEC 2011: Proceedings of the 9th European Wave and Tidal Conference, Southampton, UK, 5th-9th September 2011*. University of Southampton.

Kung, S.-Y. (1978). A new identification and model reduction algorithm via singular value decomposition. In *Proc. 12th Asilomar Conf. on Circuits, Systems and Computer*, pages 705–714.

Lan, J. and Patton, R. J. (2017). Integrated fault estimation and fault-tolerant control for uncertain Lipschitz nonlinear systems. *International Journal of Robust and Nonlinear Control*, 27(5):761–780.

Lan, J., Patton, R. J., and Punta, E. (2017a). Fault-tolerant tracking control for a 3-dof helicopter with actuator faults and saturation. *IFAC-PapersOnLine*, 50(1):5250–5255.

Lan, J., Patton, R. J., and Zhu, X. (2017b). Integrated fault-tolerant control for a 3-dof helicopter with actuator faults and saturation. *IET Control Theory & Applications*, 11(14):2232–2241.

Langson, W., Chryssochoos, I., Raković, S., and Mayne, D. Q. (2004). Robust model predictive control using tubes. *Automatica*, 40(1):125–133.

Lao, Y. and Scruggs, J. T. (2020). Robust control of wave energy converters using unstructured uncertainty. In *2020 American Control Conference (ACC)*, pages 4237–4244. IEEE.

Laub, A. and Wette, M. (1984). Algorithms and software for pole assignment and observers. Technical report, California Univ., Santa Barbara (USA). Dept. of Electrical and Computer Engineering.

Lawson, M., Yu, Y.-H., Nelessen, A., Ruehl, K., and Michelen, C. (2014a). Implementing nonlinear buoyancy and excitation forces in the wec-sim wave energy converter modeling tool. In *International Conference on Offshore Mechanics and Arctic Engineering*, volume 45547, page V09BT09A043. American Society of Mechanical Engineers.

Lawson, M., Yu, Y.-H., Ruehl, K., Michelen, C., et al. (2014b). Development and demonstration of the wec-sim wave energy converter simulation tool.

Li, D. and Patton, R. (2023a). Model predictive energy-maximising tracking control for a wavestar-prototype wave energy converter. *Journal of Marine Science and Engineering*, 11(7):1289.

Li, D. and Patton, R. J. (2023b). Model following robust control of a wavestar-prototype wave energy converter: Part 1 control. *IFAC-PapersOnLine*, 56(2):10892–10897.

Li, D. and Patton, R. J. (2023c). Model following robust control of a wavestar-prototype wave energy converter: Part 2 estimation and optimal reference computation. *IFAC-PapersOnLine*, 56(2):11729–11734.

Li, G. (2017). Nonlinear model predictive control of a wave energy converter based on differential flatness parameterisation. *International Journal of Control*, 90(1):68–77.

Li, G. and Belmont, M. R. (2014). Model predictive control of sea wave energy converters–Part I: A convex approach for the case of a single device. *Renewable Energy*, 69:453–463.

Li, G., Weiss, G., Mueller, M., Townley, S., and Belmont, M. R. (2012). Wave energy converter control by wave prediction and dynamic programming. *Renewable energy*, 48:392–403.

Li, Y., Ma, X., Tang, T., Zha, F., Chen, Z., Liu, H., and Sun, L. (2022). High-efficient built-in wave energy harvesting technology: From laboratory to open ocean test. *Applied Energy*, 322:119498.

Ling, B. A. (2015). Real-time estimation and prediction of wave excitation forces for wave energy control applications.

Ling, B. A., Bosma, B., and Brekken, T. K. (2019). Experimental validation of model predictive control applied to the azura wave energy converter. *IEEE Transactions on Sustainable Energy*, 11(4):2284–2293.

Liu, Y., Shi, S., Zhang, Z., Di, Z., and Babayomi, O. (2022). Data-driven model predictive control for wave energy converters using gaussian process. *Symmetry*, 14(7):1284.

Liu, Y., Zhu, X., Zhang, H., and Basin, M. (2018). Improved robust speed tracking controller design for an integrated motor-transmission powertrain system over controller area network. *IEEE/ASME Transactions on Mechatronics*, 23(3):1404–1414.

Lopez, B. T., Slotine, J.-J. E., and How, J. P. (2019). Dynamic tube MPC for nonlinear systems. In *2019 American Control Conference (ACC)*, pages 1655–1662. IEEE.

López, I., Andreu, J., Ceballos, S., De Alegría, I. M., and Kortabarria, I. (2013). Review of wave energy technologies and the necessary power-equipment. *Renewable and sustainable energy reviews*, 27:413–434.

Maragos, P., Kaiser, J. F., and Quatieri, T. F. (1993). Energy separation in signal modulations with application to speech analysis. *IEEE transactions on signal processing*, 41(10):3024–3051.

Maria-Arenas, A., Garrido, A. J., Rusu, E., and Garrido, I. (2019). Control strategies applied to wave energy converters: State of the art. *Energies*, 12(16):3115.

Martin, D., Li, X., Chen, C.-A., Thiagarajan, K., Ngo, K., Parker, R., and Zuo, L. (2020). Numerical analysis and wave tank validation on the optimal design of a two-body wave energy converter. *Renewable Energy*, 145:632–641.

Mayne, D. Q., Kerrigan, E. C., Van Wyk, E., and Falugi, P. (2011). Tube-based robust nonlinear model predictive control. *International journal of robust and nonlinear control*, 21(11):1341–1353.

McCabe, A., Bradshaw, A., Meadowcroft, J., and Aggidis, G. (2006). Developments in the design of the PS Frog Mk 5 wave energy converter. *Renewable Energy*, 31(2):141–151.

Mérigaud, A. (2018). *A harmonic balance framework for the numerical simulation of non-linear wave energy converter models in random seas*. PhD thesis, National University of Ireland, Maynooth (Ireland).

Mérigaud, A. and Ringwood, J. V. (2016). Condition-based maintenance methods for marine renewable energy. *Renewable and Sustainable Energy Reviews*, 66:53–78.

Mesbah, A. (2016). Stochastic model predictive control: An overview and perspectives for future research. *IEEE Control Systems Magazine*, 36(6):30–44.

Mocean, B. X. (2023). Available at `https://www.mocean.energy/`. [accessed 29.11.19].

Moens de Haste, D., Pasta, E., Faedo, N., and Ringwood, J. (2021). Towards efficient extremum-seeking control of wave energy systems: possibilities and pitfalls.

Mwasilu, F. and Jung, J.-W. (2019). Potential for power generation from ocean wave renewable energy source: a comprehensive review on state-of-the-art technology and future prospects. *IET Renewable Power Generation*, 13(3):363–375.

Na, J., Wang, B., Li, G., Zhan, S., and He, W. (2018). Nonlinear constrained optimal control of wave energy converters with adaptive dynamic programming. *IEEE Transactions on Industrial Electronics*, 66(10):7904–7915.

Newell, R., Raimi, D., and Aldana, G. (2019). Global energy outlook 2019: the next generation of energy. *Resources for the Future*, 1:8–19.

Nguyen, H.-N., Sabiron, G., Tona, P., Kramer, M. M., and Vidal Sanchez, E. (2016). Experimental validation of a nonlinear MPC strategy for a wave energy converter prototype. In *International conference on offshore mechanics and arctic engineering*, volume 49972, page V006T09A019. American Society of Mechanical Engineers.

Nguyen, H.-N. and Tona, P. (2017a). Continuously adaptive PI control of wave energy converters under irregular sea-state conditions. In *12th European Wave and Tidal Energy Conference 2017*.

Nguyen, H.-N. and Tona, P. (2017b). Wave excitation force estimation for wave energy converters of the point-absorber type. *IEEE Transactions on Control Systems Technology*, 26(6):2173–2181.

Nguyen, N. T. and Nguyen, N. T. (2018). *Model-reference adaptive control*. Springer.

Nguyen, P. Q. P. et al. (2019). Ocean Energy-A Clean Energy Source. *European Journal of Engineering and Technology Research*, 4(1):5–11.

Nocedal, J. and Wright, S. J. (1999). *Numerical optimization*. Springer.

NREL and Sandia (2014). Wec-sim (wave energy converter simulator). Available at `https://wec-sim.github.io/WEC-Sim/master/index.html`. [accessed 19. August.23].

Ogilvie, T. F. (1964). Recent progress toward the understanding and prediction of ship motions. In *David W. Taylor Model Basin, Washington DC, USA, Presented at: Proceedings of the 5th Symposium on Naval Hydrodynamics, Bergen, Norway, pp. 3-80.*

Oscar Mauricio Agudelo Mañozca, B. D. M. (2017). Introduction to Model Predictive Control (MPC). Technical report, Katholieke Universiteit Leuven., Leuven, (Belgium). Electrical Engineering Department (ESAT).

Oyster (2012). Available at `https://www.oleoinc.com/case-studies/view/2023/10/oyster-wave-energy-converter`. [accessed 1.05.12].

Parrinello, L., Dafnakis, P., Pasta, E., Bracco, G., Naseradinmousavi, P., Mattiazzo, G., and Bhalla, A. P. S. (2020). An adaptive and energy-maximizing control optimization of wave energy converters using an extremum-seeking approach. *Physics of Fluids*, 32(11).

Pastor, J. and Liu, Y. (2014). Frequency and time domain modeling and power output for a heaving point absorber wave energy converter. *International Journal of Energy and Environmental Engineering*, 5:1–13.

Pecher, A. and Kofoed, J. P. (2017). *Handbook of ocean wave energy*. Springer Nature.

Peña-Sanchez, Y. (2020). *Hydrodynamic excitation force estimation and forecasting for wave energy applications*. PhD thesis, National University of Ireland, Maynooth (Ireland).

Peña-Sanchez, Y., Windt, C., Davidson, J., and Ringwood, J. V. (2019). A critical comparison of excitation force estimators for wave-energy devices. *IEEE Transactions on Control Systems Technology*, 28(6):2263–2275.

Penalba, M. (2018). *Design, validation and application of wave-to-wire models for heaving point absorber wave energy converters*. PhD thesis, National University of Ireland, Maynooth (Ireland).

Penalba, M., Giorgi, G., and Ringwood, J. V. (2017a). Mathematical modelling of wave energy converters: A review of nonlinear approaches. *Renewable and Sustainable Energy Reviews*, 78:1188–1207.

Penalba, M., Kelly, T., and Ringwood, J. (2017b). Using NEMOH for modelling wave energy converters: A comparative study with WAMIT.

Penguin, W. (2022). Available at `https://wello.eu/the-penguin-2/`. [accessed 10.11.22].

Pozzi, N. et al. (2018). Numerical modeling and experimental testing of a pendulum wave energy converter (PeWEC). *Politecnico di Torino, Torino, Italy*.

Prasad, K. A., Chand, A. A., Kumar, N. M., Narayan, S., and Mamun, K. A. (2022). A critical review of power take-off wave energy technology leading to the conceptual design of a novel wave-plus-photon energy harvester for island/coastal communities' energy needs. *Sustainability*, 14(4):2354.

Rafiee, A. and Fiévez, J. (2015). Numerical prediction of extreme loads on the CETO wave energy converter. In *Proceedings of the 11th European Wave and Tidal Energy Conference, Nantes, France*, number 09A1-2.

Reguero, B., Losada, I., and Méndez, F. (2015). A global wave power resource and its seasonal, interannual and long-term variability. *Applied Energy*, 148:366–380.

Richter, M., Magana, M. E., Sawodny, O., and Brekken, T. K. (2012). Nonlinear model predictive control of a point absorber wave energy converter. *IEEE Transactions on Sustainable Energy*, 4(1):118–126.

Richter, M., Magaña, M. E., Sawodny, O., and Brekken, T. K. (2014). Power optimisation of a point absorber wave energy converter by means of linear model predictive control. *IET Renewable Power Generation*, 8(2):203–215.

Ringwood, J., Ferri, F., Ruehl, K. M., Yu, Y.-H., Coe, R. G., Bacelli, G., Weber, J., and Kramer, M. (2017). A competition for wec control systems. In *Proceedings of the 12th European Wave and Tidal Energy Conference 27th Aug-1st Sept 2017*, pages 1–9. European Wave and Tidal Energy Conference 2017.

Ringwood, J., Ferri, F., Tom, N., Ruehl, K., Faedo, N., Bacelli, G., Yu, Y.-H., and Coe, R. G. (2019). The wave energy converter control competition: Overview. In *International conference on offshore mechanics and arctic engineering*, volume 58899, page V010T09A035. American Society of Mechanical Engineers.

Ringwood, J. V., Bacelli, G., and Fusco, F. (2014). Energy-maximizing control of wave-energy converters: The development of control system technology to optimize their operation. *IEEE control systems magazine*, 34(5):30–55.

Ringwood, J. V., Merigaud, A., Faedo, N., and Fusco, F. (2018). Wave energy control systems: robustness issues. *IFAC-PapersOnLine*, 51(29):62–67.

Ringwood, J. V., Tom, N., Ferri, F., Yu, Y.-H., Coe, R. G., Ruehl, K., Bacelli, G., Shi, S., Patton, R. J., Tona, P., et al. (2023a). The wave energy converter control competition (WECCCOMP): Wave energy control algorithms compared in both simulation and tank testing. *Applied Ocean Research*, 138:103653.

Ringwood, J. V., Zhan, S., and Faedo, N. (2023b). Empowering wave energy with control technology: Possibilities and pitfalls. *Annual Reviews in Control*.

Ross, D. (1995). Power from the waves. *Oxford University Press*.

Safonov, M. and Chiang, R. (1988). A Schur method for balanced model reduction. In *1988 American Control Conference*, pages 1036–1040. IEEE.

Scharmen, W. (2016). Wave energy prize-1/20th testing-harvest wave energy oscillating wave surge converter. Technical report, Marine and Hydrokinetic Data Repository (MHKDR); Ricardo Detroit Technical Center.

Scruggs, J., Lattanzio, S., Taflanidis, A., and Cassidy, I. (2013). Optimal causal control of a wave energy converter in a random sea. *Applied Ocean Research*, 42:1–15.

Sheng, S., Wang, K., Lin, H., Zhang, Y., You, Y., Wang, Z., Chen, A., Jiang, J., Wang, W., and Ye, Y. (2017). Model research and open sea tests of 100 kW wave energy convertor Sharp Eagle Wanshan. *Renewable Energy*, 113:587–595.

Sheng, W. (2019). Wave energy conversion and hydrodynamics modelling technologies: A review. *Renewable and Sustainable Energy Reviews*, 109:482–498.

Sheng, W., Alcorn, R., and Lewis, A. (2015). On improving wave energy conversion, part II: Development of latching control technologies. *Renewable Energy*, 75:935–944.

Sheng, W., Tapoglou, E., Ma, X., Taylor, C. J., Dorrell, R., Parsons, D. R., and Aggidis, G. (2022a). Time-domain implementation and analyses of multi-motion modes of floating structures. *Journal of Marine Science and Engineering*, 10(5):662.

Sheng, W., Tapoglou, E., Ma, X., Taylor, C. J., Dorrell, R. M., Parsons, D. R., and Aggidis, G. (2022b). Hydrodynamic studies of floating structures: Comparison of wave-structure interaction modelling. *Ocean Engineering*, 249:110878.

Shi, S. (2021). *Robust machine learning control for wave energy converters*. PhD thesis, University of Hull, Hull (England).

Shi, S., Patton, R. J., Abdelrahman, M., and Liu, Y. (2019). Learning a predictionless resonating controller for wave energy converters. In *International Conference on Offshore Mechanics and Arctic Engineering*, volume 58899, page V010T09A037. American Society of Mechanical Engineers.

Shi, S., Patton, R. J., and Liu, Y. (2018). Short-term wave forecasting using gaussian process for optimal control of wave energy converters. *IFAC-PapersOnLine*, 51(29):44–49.

Siegel, F. R. (2019). *Adaptations of coastal cities to global warming, sea level rise, climate change and endemic hazards*. Springer.

Soltani, M. N., Sichani, M. T., and Mirzaei, M. (2014). Model predictive control of buoy type wave energy converter. *IFAC Proceedings Volumes*, 47(3):11159–11164.

Spurgeon, S. K., Edwards, C., and Foster, N. P. (1996). Robust model reference control using a sliding mode controller/observer scheme with application to a helicopter problem. In *Proceedings. 1996 IEEE International Workshop on Variable Structure Systems.-VSS'96-*, pages 36–41. IEEE.

Stratigaki, V., Troch, P., Stallard, T., Forehand, D., Kofoed, J. P., Folley, M., Benoit, M., Babarit, A., and Kirkegaard, J. (2014). Wave basin experiments with large wave energy converter arrays to study interactions between the converters and effects on other users in the sea and the coastal area. *Energies*, 7(2):701–734.

Sun, T. and Nielsen, S. R. (2018). Stochastic optimal control of a heave point wave energy converter based on a modified LQG approach. *Ocean Engineering*, 154:357–366.

Sun, Z., Zhao, A., Zhu, L., Lu, K., Wu, W., and Blaabjerg, F. (2018). Extremum-seeking control of wave energy converters using two-objective flower pollination algorithm. In *2018 IEEE International Power Electronics and Application Conference and Exposition (PEAC)*, pages 1–5. IEEE.

Svoboda, J. A. and Dorf, R. C. (2013). *Introduction to electric circuits*. John Wiley & Sons.

Taylor, C. J., Bradshaw, A., Chaplin, R., French, M., and Widden, M. B. (2002). Wave Energy Research at Lancaster University: PS Frog and Frond. In *World Renewable Energy Congress VII*.

Titah-Benbouzid, H. and Benbouzid, M. (2015). An up-to-date technologies review and evaluation of wave energy converters. *International review of electrical engineering-IREE*, 10(1):52–61.

Tom, N., Ruehl, K., and Ferri, F. (2018). Numerical model development and validation for the WECCCOMP control competition. In *International Conference on Offshore Mechanics and Arctic Engineering*, volume 51319, page V010T09A042. American Society of Mechanical Engineers.

Tom, N. and Yeung, R. W. (2014). Nonlinear model predictive control applied to a generic ocean-wave energy extractor. *Journal of Offshore Mechanics and Arctic Engineering*, 136(4):041901.

Tona, P., Nguyen, H.-N., Sabiron, G., and Creff, Y. (2015). An efficiency-aware model predictive control strategy for a heaving buoy wave energy converter. In *11th European wave and tidal energy conference-EWTEC 2015*.

Tona, P., Sabiron, G., and Nguyen, H.-N. (2019). An energy-maximising MPC solution to the WEC control competition. In *International Conference on Offshore Mechanics and Arctic Engineering*, volume 58899, page V010T09A034. American Society of Mechanical Engineers.

Utkin, V. I. (2013). *Sliding modes in control and optimization*. Springer Science & Business Media.

Vicinanza, D., Margheritini, L., Kofoed, J. P., and Buccino, M. (2012). The SSG wave energy converter: Performance, status and recent developments. *Energies*, 5(2):193–226.

Wahyudie, A., Jama, M., Saeed, O., Noura, H., Assi, A., and Harib, K. (2015). Robust and low computational cost controller for improving captured power in heaving wave energy converters. *Renewable Energy*, 82:114–124.

WavePlane (2008). Available at `http://www.waveplane.com/`. [accessed 21.11.21].

Welch, G., Bishop, G., et al. (1995). An introduction to the Kalman Filter.

Westwood, A. (2004). Ocean power: Wave and tidal energy review. *Refocus*, 5(5):50–55.

Williams, C. K. and Rasmussen, C. E. (2006). *Gaussian processes for machine learning*, volume 2. MIT press Cambridge, MA.

Wilson, A. and Adams, R. (2013). Gaussian process kernels for pattern discovery and extrapolation. In *International conference on machine learning*, pages 1067–1075. PMLR.

Windt, C., Faedo, N., García-Violini, D., Peña-Sanchez, Y., Davidson, J., Ferri, F., and Ringwood, J. V. (2020). Validation of a CFD-based numerical wave tank model of the 1/20th scale wavestar wave energy converter. *Fluids*, 5(3):112.

Yang, B., Wu, S., Zhang, H., Liu, B., Shu, H., Shan, J., Ren, Y., and Yao, W. (2022). Wave energy converter array layout optimization: A critical and comprehensive overview. *Renewable and Sustainable Energy Reviews*, 167:112668.

Yi-Hsiang Yu, M. L., Kelley Ruehl, C. M., et al. (2014). Wec-sim repository. Available at `https://github.com/WEC-Sim/WEC-Sim`. [accessed 10.02.19].

Yong, S. Z., Zhu, M., and Frazzoli, E. (2016). A unified filter for simultaneous input and state estimation of linear discrete-time stochastic systems. *Automatica*, 63:321–329.

Zadeh, L. G., Haider, A. S., and Brekken, T. K. (2022). Bayesian actor-critic wave energy converter control with modeling errors. *IEEE Transactions on Sustainable Energy*, 14(1):3–11.

Zhan, S., He, W., and Li, G. (2017). Robust feedback model predictive control of sea wave energy converters. *IFAC-PapersOnLine*, 50(1):141–146.

Zhan, S., Huijberts, H., Na, J., and Li, G. (2016). Optimal controller design and constraints analysis of a sea wave energy converter. In *2016 UKACC 11th International Conference on Control (CONTROL)*, pages 1–6. IEEE.

Zhan, S., Wang, B., Na, J., and Li, G. (2018). Adaptive optimal control of wave energy converters. *IFAC-PapersOnLine*, 51(29):38–43.

Zhang, Y. and Li, G. (2019). Non-causal linear optimal control of wave energy converters with enhanced robustness by sliding mode control. *IEEE Transactions on Sustainable Energy*, 11(4):2201–2209.

Zhang, Y. and Li, G. (2022). Robust tube-based model predictive control for wave energy converters. *IEEE Transactions on Sustainable Energy*, 14(1):65–74.

Zhang, Y., Zeng, T., and Li, G. (2019). Robust excitation force estimation and prediction for wave energy converter m4 based on adaptive sliding-mode observer. *IEEE Transactions on Industrial Informatics*, 16(2):1163–1171.

Zhang, Y., Zhao, Y., Sun, W., and Li, J. (2021). Ocean wave energy converters: Technical principle, device realization, and performance evaluation. *Renewable and Sustainable Energy Reviews*, 141:110764.

Zhong, Q. and Yeung, R. W. (2019). Model-predictive control strategy for an array of wave-energy converters. *Journal of Marine Science and Application*, 18:26–37.

Zhu, X. and Li, D. (2021a). Robust attitude control of a 3-DOF helicopter considering actuator saturation. *Mechanical Systems and Signal Processing*, 149:107209.

Zhu, X. and Li, D. (2021b). Robust fault estimation for a 3-DOF helicopter considering actuator saturation. *Mechanical Systems and Signal Processing*, 155:107624.

Zou, S., Abdelkhalik, O., Robinett, R., Korde, U., Bacelli, G., Wilson, D., and Coe, R. (2017). Model predictive control of parametric excited pitch-surge modes in wave energy converters. *International journal of marine energy*, 19:32–46.

Zou, S., Song, J., and Abdelkhalik, O. (2023). A sliding mode control for wave energy converters in presence of unknown noise and nonlinearities. *Renewable Energy*, 202:432–441.

Zou, S., Zhou, X., Khan, I., Weaver, W. W., and Rahman, S. (2022). Optimization of the electricity generation of a wave energy converter using deep reinforcement learning. *Ocean Engineering*, 244:110363.

Zurkinden, A. S., Ferri, F., Beatty, S., Kofoed, J. P., and Kramer, M. (2014). Nonlinear numerical modeling and experimental testing of a point absorber wave energy converter. *Ocean Engineering*, 78:11–21.